Stochastic many-particle systems far from equilibrium coupled to bulk reservoirs

Dissertation

zur

Erlangung des Doktorgrades (Dr. rer. nat.)

der

Mathematisch-Naturwissenschaftlichen Fakultät

der

Rheinischen Friedrich-Wilhelms-Universität Bonn

vorgelegt

von

Richard Daniel Willmann

aus

Bonn

2004

Anfertigung mit Genehmigung der Mathematisch-Naturwissenschaftlichen Fakultät der Rheinischen Friedrich-Wilhelms-Universität Bonn.

1. Referent: PD Dr. G. M. Schütz
2. Referent: Prof. Dr. U.-G. Meißner
Tag der Promotion:

Contents

Chapter 1

Preface

Complex systems containing a large number of interacting particles could in principle be described by equations of motion such as the Schrödinger or Hamilton equation. Still, the solution of those equations, if available, contains not much useful information, which has instead to be extracted using a statistical treatment.
In equilibrium, the stationary distribution of an interacting particle system can be constructed from the Hamiltonian H by using the Gibbs measure $\exp(-\beta H)$. Although theoretically the free energy of a system, and from it all relevant quantities, can be obtained using this equilibrium measure, an exact treatment is in practice only possible in rare cases. Powerful approximation schemes have been devised to overcome these difficulties (see e.g. [1, 2]). Especially, the renormalization group theory, dealing with the behavior of statistical systems close to a critical point, is used successfully to compute critical exponents and scaling laws. It also lays the foundation for understanding the concept of universality classes: The critical behavior of statistical systems does not depend on all details of the occurring interactions but only on the dimensionality of the order parameter and the symmetries and dimension of the system. Thus, studying simple toy models suffices to understand the critical behavior of the whole universality class.
The understanding of non-equilibrium systems is in a much earlier stage. In principle there are two kinds of non-equilibrium systems: Systems relaxing towards an equilibrium steady state and systems which are by construction far from equilibrium. The latter kind of non-equilibrium systems is treated in this work.
Many-particle systems can be kept far from equilibrium by applying a constant driving force, leading to a current of a conserved quantity. Such classical systems are known as driven diffusive systems. Examples include conductors in an electric field and fluids flowing due to a pressure gradient.
The existence of an absorbing state, i.e. a state that can be reached by the system dynamics but never left is another cause for a system to be far from equilibrium by construction.
In contrast to the equilibrium case, no general theoretical framework exists for systems far from equilibrium. It is hoped that by studying individually a large variety of models some common features can be found and non-equilibrium universality classes be defined.
Contrary to equilibrium processes, systems far from equilibrium show phase transitions even in one dimension, where it is easiest to treat them analytically. Due to a wealth of exact results and many applications, the Asymmetric Simple Exclusion Process (ASEP) constitutes the paradigmatic model of one-dimensional driven diffusive systems with a single conserved particle species [3]. The most interesting results are obtained when the model is

treated with open boundary conditions, where particles perform a directed motion between two boundary reservoirs. The phase diagram, which is known exactly, can be understood from regarding the motion of shocks and density fluctuation, i.e. collective degrees of freedom.
Driven diffusive systems with two conserved particle species were studied intensely in recent years [4]. These systems have been demonstrated to show such interesting phenomena as phase separation and spontaneous symmetry breaking even in one dimension.
The paradigmatic model of phase transitions into an absorbing state is directed percolation [5]. The transition constitutes an example of a non-equilibrium critical phenomenon. Lacking an analytical solution, it is studied by renormalization group methods, series expansions and Monte Carlo simulations. Especially, it is attempted to define criteria for models belonging to the non-equilibrium universality class of directed percolation.

The aim of this work is to study the influence of *bulk reservoirs* on lattice models for both driven diffusive systems and absorbing phase transitions. The effect of these reservoirs is, depending on their coupling to the system, the spontaneous creation or annihilation of particles at any lattice site. This work consists of two parts contrasting models far from equilibrium with and without bulk reservoirs:
Part I treats systems without bulk reservoirs. It contains both a review of known results and two new contributions concerning spontaneous symmetry breaking and phase separation in driven diffusive systems with two species of particles.
In part II, the systems treated in the first part are considered again, this time under the influence of a bulk reservoir. This part contains new results on single species driven models with bulk reservoirs, spontaneous symmetry breaking in a two species non-conserving model and directed percolation as well as the pair contact process in an external field.
Although the ASEP as the simplest driven diffusive system has been solved exactly, exact solutions are very difficult to obtain for more complicated systems as regarded in this work. Especially there exists no generally applicable solution method. Instead of trying to find an exact solution for a specific single species model without bulk conservation, in part II of this work a hydrodynamic equation is formulated, which allows for obtaining the phase diagrams and stationary solutions for a whole class of models. For the two-species models, effective treatments are used. These comprise mapping the effective dynamics to simpler, analytically tractable models, as well as considering collective modes such as localized density shocks and the motion

of particle waves. Although such mappings are usually not exact, they are intended to capture the essential behavior of the system under consideration for large times and system sizes. Furthermore the findings are supported by Monte Carlo simulations and mean field calculations. For directed percolation and the pair contact process no exact solution exists below the upper critical dimension. Therefore we revert to Monte Carlo simulations. Above the upper critical dimension mean field treatments are applied.
The focus of this work is on exploring which kinds of phenomena are principally observable in models far from equilibrium with and without coupling to a bulk reservoir. Therefore not much room is given to possible experimental realizations. Applications are briefly mentioned in the introductory chapters of parts I and II.

In chapter 2 a brief review of known results on single species driven diffusive systems is given. Furthermore, existing results on the phenomena of spontaneous symmetry breaking and phase separation in two-species models are discussed. For both of these topics, open questions are identified which are addressed in the two subsequent chapters. The chapter also contains a brief introduction to the directed percolation universality class.
A two species model with periodic boundary conditions showing a novel kind of phase separation is presented in chapter 3. Above a critical density, this model shows a phase separation transition that is formally analogous to Bose-Einstein condensation.
The dynamics of a two species system with open boundaries exhibiting spontaneous symmetry breaking is the topic of chapter 4. By considering the approach to the steady state, the phase diagram of this model can be constructed. Especially, it is possible to prove the existence of a symmetry broken state without further assumptions on the rates.
Part II starts with an illustration of the bulk reservoir concept for both driven diffusive systems and absorbing phase transitions in chapter 5. It also contains a review of results on the ASEP coupled to a bulk reservoir.
In chapter 6 driven diffusive systems with open boundaries coupled to a bulk reservoir are considered. A hydrodynamic equation is proposed that allows to construct the density profiles if the coupling strength to the bulk reservoir scales with the inverse system size. A driven system with the novel features of a localized downward shock as well as a localized double shock is introduced.
The effect of a bulk reservoir on single species driven systems with periodic boundaries in the case of weak coupling is studied in chapter 7. The impossibility of phase separation in this case is demonstrated. The existence

of phase transitions between uniform steady states as well as hysteresis and spontaneous symmetry breaking in these systems are demonstrated.
A toy model for a limit order market is presented in chapter 8. Due to a mapping of this model to the ASEP with bulk reservoir the Hurst exponent can be determined exactly. For the first time a crossover from overdiffusive to diffusive behavior of a marked particle is demonstrated in a limit order market model that is analytically tractable.
The discussion of spontaneous symmetry breaking in two-species models with open boundaries started in chapter 4 is resumed in chapter 9. Here, the influence of a bulk reservoir is studied, which leads to a rich phase diagram. Some of the phase transitions can be understood by regarding the positions of shocks which are localized due to the action of the bulk reservoir. The model shows the novel feature of localized induced shocks.
Finally, in chapter 10 the influence of a unidirectionally coupled bulk reservoir on models from the directed percolation universality class is studied. The action of the bulk reservoir is equivalent to an external field coupled to the order parameter. The scaling functions of directed site percolation are determined numerically on lattices from one to five dimensions. Furthermore, for the first time the pair contact process, a model with infinitely many absorbing states, is considered in an external field.

The results presented in chapters 3, 6, 8, 9 and 10 were published in refs. [6–11] prior to submission of this work. The names of the respective collaborators in these works are indicated in the introductory section of each chapter.

Part I

Non-equilibrium many-particle models

Chapter 2

Introduction

2.1 Single-species driven diffusive systems

In one-dimensional driven diffusive systems particles perform a directed motion along a discrete chain. Treated with either open or periodic boundary conditions, this directed motion gives rise to a particle current in the steady state, which means that these systems are by construction far from equilibrium.
The simplest one-dimensional driven diffusive system, as outlined in the next subsection, is the TASEP, which was introduced as a model for the directed movement of ribosomes along a messenger RNA [12]. Here, the mutual exclusion of the ribosomes leads to the collective effect of a jamming which yields a slowing down of the ribosome velocity. Another situation of directed motion of interacting particles which lends itself to modeling by driven diffusive systems in one dimension is traffic flow [13, 14]. Apart from that also the shape of an interface, growing according to the dynamics of the Kardar-Parisi-Zhang equation, can be mapped to a one-dimensional driven diffusive system (see ref. [15] for a review). For further references to applications see e.g. refs. [3, 4].
One-dimensional driven diffusive systems with a single species of particles and conserving bulk dynamics are largely understood. The following three subsections briefly review known results as far as they are relevant for this work. For a detailed review see ref. [3]. These results should be mainly seen in contrast to the phenomena which occur when non-conserving bulk dynamics by coupling to a reservoir is introduced in part II of this work.

2.1.1 The Totally Asymmetric Simple Exclusion Process

The simplest and best understood driven diffusive system is the Totally Asymmetric Simple Exclusion Process (TASEP) [3, 16]. In the case of open boundaries, the model is defined on a one-dimensional lattice of length L. Sites can either be occupied by a single particle or empty (exclusion interaction). In the interior of the lattice, particles hop to the adjacent site to the right with unit rate, provided the target site is empty. If site 1 is empty, a particle is created with rate α. If site L is occupied, the particle is annihilated with rate β. These processes can be also described in terms of *boundary reservoirs*. The creation process at site 1 is equivalent to a hopping process as in the bulk from a reservoir of constant density $\rho_- = \alpha$. Similarly, the annihilation at site L is equivalent to hopping with unit rate into a reservoir of constant density $\rho_+ = 1 - \beta$.
When treated with periodic boundary conditions without reservoirs, the sys-

tem settles into a steady state with a product measure of density ρ and current-density relation $j(\rho) = \rho(1-\rho)$.
In spite of its simplicity, the TASEP with boundary reservoirs shows a variety of very interesting features: The phase diagram and the stationary states of the TASEP are known exactly [17, 18]:
Low density phase: For $1-\rho_+ > \rho_-$ and $\rho_- < 1/2$, the bulk density is given by ρ_-. At the right end, a boundary layer exhibiting an exponential decay with finite localization length ξ interpolates between the bulk density and the boundary density of ρ_+.
High density phase: For $1-\rho_+ < \rho_-$ and $\rho_+ > 1/2$, the bulk density is given by ρ_+. A boundary layer as in the low density phase connects the bulk density to the left boundary density of ρ_-.
Maximal current phase: For $\rho_- > 1/2$ and $\rho_+ < 1/2$, the system resides in a phase of bulk density $1/2$, which is connected to the boundary densities by algebraically decaying boundary layers.
The transition from the high-density as well as the low-density phase to the maximal-current phase is of second order, where the localization length ξ diverges. The transition from the low-density to the high-density phase at $\rho_- = 1-\rho_+ < 1/2$ is of first order. Here, the system shows phase coexistence in the sense of the existence of a microscopically sharp shock in the density profile, connecting a region of density ρ_- on the left side and a region of density ρ_+ on the right side. The dynamics of this shock will be addressed below.

2.1.2 The Katz-Lebowitz-Spohn model

The non-equilibrium kinetic Ising model by Katz, Lebowitz and Spohn (KLS model) was introduced as a model for superionic conductors [19]. In the totally asymmetric, one-dimensional case it can be viewed as a variant of the TASEP with next-nearest neighbor interaction. Using the parameters δ and ϵ, both having an absolute value smaller than one, the bulk hopping processes are defined as follows:

$$\begin{aligned} 0100 &\to 0010 \quad \text{with rate} \quad 1+\delta \\ 1100 &\to 1010 \quad \text{with rate} \quad 1+\epsilon \\ 0101 &\to 0011 \quad \text{with rate} \quad 1-\epsilon \\ 1101 &\to 1011 \quad \text{with rate} \quad 1-\delta \end{aligned} \tag{2.1}$$

At the boundaries, injection and ejection of particles from boundary reservoirs are possible as in the TASEP. The current-density relation for the periodic system can be computed exactly using the fact that the stationary

measure is as for a one-dimensional Ising model [20]. For a certain range of parameters, the current-density relation exhibits two maxima. In that case, the phase diagram comprises seven phases [20].
Sometimes, the KLS model is termed the 'standard model' of driven diffusive systems. It has been studied intensely, also in higher dimensions [21].

2.1.3 Steady-state selection in driven models

Due to the coupling of the bulk to boundary reservoirs, the question arises which steady state density a driven diffusive system will attain. Being intrinsically far from equilibrium, this question can not be answered by considering a general thermodynamic potential for this class of models. Still, for the case of single species driven models, an extremal principle was formulated [22, 23] that does not refer to specific details of the model under consideration, but just to the current-density relation $j(\rho)$:
For single species models, the steady state is selected according to

$$j = \begin{cases} \max j(\rho), \text{ where } \rho \in [\rho_+, \rho_-], \text{ if } \rho_- > \rho_+ \\ \min j(\rho), \text{ where } \rho \in [\rho_-, \rho_+], \text{ if } \rho_- < \rho_+. \end{cases} \tag{2.2}$$

The physics of this steady state selection can be understood from a dynamical perspective by considering the drift and diffusion of shocks as well as localized density waves [20, 22, 23]. The *shock velocity* is given by

$$v_s = \frac{j_l - j_r}{\rho_l - \rho_r}, \tag{2.3}$$

where $j_{l/r}$ and $\rho_{l/r}$ are the currents and densities to the left and right of the shock, respectively. The center of mass of a density perturbation travels with the *collective velocity*

$$v_c = \frac{\partial j}{\partial \rho} \tag{2.4}$$

on a homogeneous background density ρ. A shock is stable if

$$v_c^l > v_s > v_c^r. \tag{2.5}$$

For details see refs. [20, 22, 23] and the review [3].

2.2 Two-species driven diffusive systems

In contrast to single species driven models with bulk conservation, which are largely understood, two-species models show phenomena that are a matter of

current research, such as spontaneous symmetry breaking and phase separation (see [4] for a review). In this section a brief overview over known results is given, leading to questions that yield new results presented in chapters 3 and 4.
A review of known results on phase separation is given in the following subsection, leading to the conclusion that so far no model for soft phase separation exists. In chapter 3 a two-species driven model showing this novel type of phase separation is introduced.
An existing model showing spontaneous symmetry breaking (SSB) is described in subsection 2.2.2. Here, the dynamics of symmetry breaking remains unclear except in the limiting case of some vanishing rate. The variant of the model introduced in chapter 4 allows for a proof of symmetry breaking without assumptions on the rates by considering the dynamics of SSB.
The discussion of spontaneous symmetry breaking is resumed in chapter 9, where SSB in a non-conserving model is studied.

2.2.1 Phase separation

In equilibrium, phase separation is a phenomenon that is observed in many experimental situations (see e.g. [1]). However, it is restricted to dimensions $d \geq 2$. In one dimension, due to missing line tension, there is no mechanism that restricts the growth of a domain of say phase A, within phase B, leading to the formation of a single, homogeneous phase.
Far from equilibrium, there are a number of driven diffusive systems that exhibit phase separation. We concentrate in this work on one-dimensional driven systems with periodic boundary conditions and two species of particles. For a review of situations that might lead to phase separation in single species driven diffusive systems, see ref. [4]. In two-species driven diffusive systems there are in fact two different kinds of phase separation:

- *Strong phase separation:* The system phase separates into three phases, each of them being pure, i.e. containing only one particle species or vacancies, respectively. The current through a domain decreases to zero exponentially with the system size. The phase separated state exists at any particle density.

- *Soft phase separation:* The system phase separates into two phases, each of them containing both species of particles. One of the phases is devoid of vacancies. The current through a domain decreases algebraically with the system size to a finite value. There is a critical particle density that has to be exceeded for phase separation to take

place. This behavior is similar to Bose-Einstein condensation. Therefore, the vacancy-free phase is termed *condensed phase* and the phase transition from a homogeneous to a phase separated state a *condensation transition*.

The AHR model

The first translationally invariant two-species model that was reported to show soft phase separation is the AHR model [24]. It is defined on a ring with L sites. The rates of the model are as follows:

$$+\,0 \xrightarrow{\alpha} 0\,+ \qquad 0\,- \xrightarrow{\alpha} -\,0 \qquad +\,- \underset{1}{\overset{q}{\rightleftarrows}} -\,+ \tag{2.6}$$

Clearly, a domain wall between a phase consisting only of vacancies, which is to the left of a phase consisting only of plus-particles is stable. This is because + and 0 behave as particles and vacancies in the ASEP, where an upward shock in the density is stable. An analogous argument holds for the stability of a pure phase of minus-particles to the left of a phase of only vacancies. If the parameter q is smaller than 1, the bias of plus-particles relative to minus-particles is such that also a shock front between a plus-phase to the left of a minus-phase is stable. In this case, the system has a steady state which is strongly phase separated (see fig. 2.1). For $L \to \infty$ there is no current in the system. Note the finite fluctuation width of the interface between the plus and minus-phase in fig. 2.1.

For $q > 1$, the stability argument for the + to − domain wall fails and the system is in a disordered state, where the particle densities are homogeneous throughout the system.

For $q \approx 1$ the authors of ref. [24] observed in computer simulations a third regime, in which a scenario occurs that has been described as soft phase separation above. In this regime, a high density condensate is fluctuating in a background of low particle density (see fig. 2.1).

Using the matrix product ansatz, the stationary distribution of the AHR model was calculated in a grand canonical ensemble [25, 26]. It turned out that the authors of ref. [24] were mislead by their simulation results and that the model does not exhibit soft phase separation. In fact, around $q \approx 1$, the correlation length of the model shows a steep increase over several orders of magnitude but without diverging. Lattices of size 10^{70} would be needed to see the full distribution of domain sizes, implying that in any feasible computer simulation the impression of soft phase separation arises. Unfortunately, not all models can be treated exactly. This makes it even more desirable to have a criterion at hand which allows without direct simulation to decide whether a system phase separates or not.

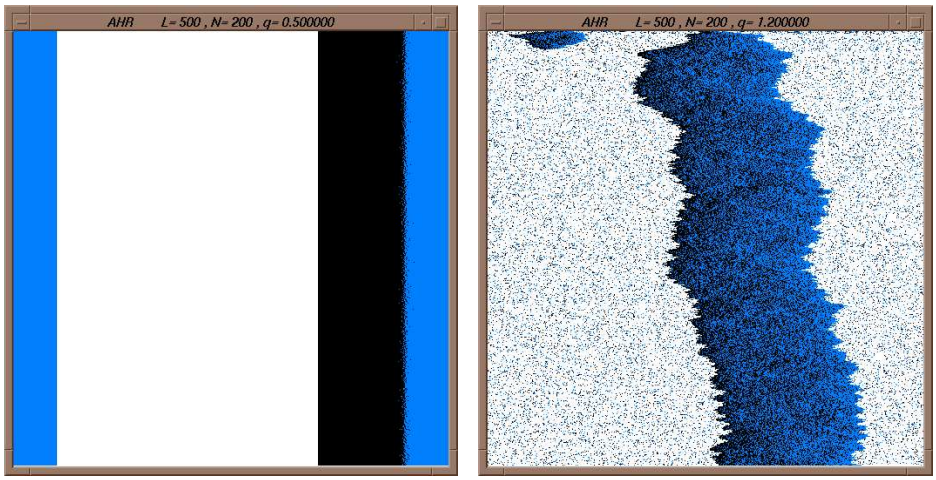

Figure 2.1: Left: Strongly phase separated phase of the AHR model at $q = 0.5$. The system has a length of $L = 500$ with 100 particles of each species. Vacancies are white, + particles black and − particles grey. Time is running top-down, space from left to right. Right: Disordered phase of the AHR model at $q = 1.2$. Due to the large correlation length the system appears to be softly phase separated.

Criterion for phase separation

In ref. [27] a general criterion for the possibility of phase separation in one-dimensional driven diffusive systems was formulated. Let an uninterrupted sequence of particles of either kind be called a domain. In order to achieve a phase separated state, a coarsening process of these domains has to take place. This means that the rate, at which a large domain looses particles has to be smaller than for a small domain. The criterion is based on the following conjecture:
The rate at which a domain of size n looses particles is given by the steady state current J_n flowing through it. Here, domains are regarded like single species driven models with open boundaries.
This conjecture uses two assumptions:

- The domains are long-lived enough to equilibrate.
- The domains are independent.

Based on this conjecture, phase separation takes place if

$$\text{Case A:} \qquad J_n \to 0 \text{ as } n \to \infty. \tag{2.7}$$

$$\text{Case B:} \quad J_n \sim J_\infty(1 + b/n^\sigma) \text{ for either } \sigma < 1, \text{ or } \sigma = 1 \text{ and } b > 2. \tag{2.8}$$

Here, case A refers to strong phase separation and case B to soft phase separation. In case A, phase separation occurs at any density. This is also true in case B, provided that $\sigma < 1$. If $\sigma = 1$ and $b > 2$ in case B, the system phase separates above a critical density.
The origin of the criterion lies in the observation that driven systems can be mapped to zero range processes, which show a condensation transition under certain conditions (see section 3.2).
The criterion makes it possible to decide on the existence of phase separation without a direct simulation of the model in question. A candidate for soft phase separation just has to be tested with respect to the finite size corrections of the current through a domain. Thus it is sufficient to simulate a single domain, which is essentially a single species driven model with open boundaries. This is of course much easier than simulating the whole model, as the single domain just has to be large enough to extract the first order finite size correction to the current.
In case of the AHR model, the dynamics of a single domain corresponds to an ASEP with open boundaries. For this model J_n is known exactly and shows that $b = 3/2 < 2$. Therefore, the result of the analytical solution [25, 26] can be understood in the framework of the criterion for phase separation [27]. On the basis of the criterion, the existence of phase separation in a two-lane driven model [28] could be refuted [27]. For this model, no exact solution exists.

In chapter 3 a two-species driven model with soft phase separation is introduced. In contrast to all previous models, it has finite size corrections to the currents through the domains with $b > 2$, thus fulfilling the requirement of the criterion for phase separation stated above.

2.2.2 Spontaneous symmetry breaking

It is well known that symmetries are a vital ingredient in many physical theories, such as Landau theory of phase transitions and the standard model of particle physics. In many experimental situations, these symmetries are hidden: An Ising ferromagnet below the curie temperature shows a finite magnetization, i.e. the majority of spins organized themselves into a specific direction. Thus, the Z_2 symmetry of the Ising Hamiltonian (i.e. invariance under flipping of all spins) is hidden or *spontaneously broken*.
Likewise, in Landau theory of superconductivity the $U(1)$ symmetry of the Hamiltonian is spontaneously broken leading to a finite absolute value of the complex order parameter, which means that a finite fraction of the electrons in the system is in the superconducting state.

Spontaneous symmetry breaking is also at the heart of the Higgs mechanism of the standard model of elementary particles, where the breaking of the $U(1)$ symmetry leads to the gauge bosons of the weak interaction acquiring a finite mass [29].

Spontaneous symmetry breaking far from equilibrium

Models far from equilibrium are not defined by a Hamiltonian, but by their transition rates. Spontaneous symmetry breaking in this situation means that a symmetry of the rates is hidden in the stationary states of the system. As there is no free energy functional to be minimized, the symmetry breaking must be explained solely on dynamical grounds.
The first driven diffusive model with symmetry broken steady states was proposed by Evans et. al. in 1995 [30, 31]. It is a two-species driven model in one dimension with open boundaries. The rates are defined as follows (see fig. 2.2): In the bulk, the following processes take place:

$$+0 \xrightarrow{1} 0+ \qquad\qquad +- \xrightarrow{q} -+ \qquad\qquad 0- \xrightarrow{1} -0\ . \tag{2.9}$$

At the boundaries particles may be introduced and removed. At the left boundary, site $i = 1$, positive particles are introduced and negative particles are removed with rates

$$0 \xrightarrow{\alpha} + \qquad\qquad - \xrightarrow{\beta} 0 \qquad\qquad (i = 1)\ , \tag{2.10}$$

while at the right boundary, $i = N$, negative particles are introduced and positive particles are removed with rates

$$0 \xrightarrow{\alpha} - \qquad\qquad + \xrightarrow{\beta} 0 \qquad\qquad (i = N)\ . \tag{2.11}$$

The processes at the boundaries can *not* be described in terms of reservoirs [32]. Note that all rates are CP-symmetric, namely symmetric under the subsequent exchange of positive-negative charges and left-right directions. As the system resembles a road bridge with narrow entries, it is in the following termed 'bridge model'. The structure of the phase diagram in this model could not be clarified exactly. In a mean field approximation, four phases are found [31]:

A In the *power-law symmetric phase* both species of particles are in a state as for the power law phase of the ASEP, with bulk density 1/2 each.

B In the *low-density symmetric phase* the density of both species is at the same bulk value below 1/2, as in the low density phase of the ASEP.

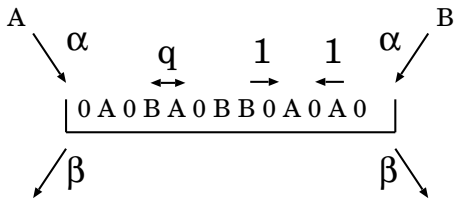

Figure 2.2: Illustration of the hopping processes in the bridge model.

C In the *low-density asymmetric phase* both species have bulk densities below 1/2. In contrast to phase B, the bulk densities are different.

D In the *high-low asymmetric phase* the density of one species is above 1/2 as in the high density phase of the ASEP, while the other one has a bulk density below 1/2.

Phases A,B and D could be observed in Monte Carlo simulations. The existence of spontaneous symmetry breaking in phase D was proven rigorously in the limit of $\beta \to 0$ [33].
The existence of phase C is disputed. It covers only a tiny region in the mean-field phase diagram. In Monte Carlo simulations its existence could not be clearly demonstrated. In [34] it was attempted to refute the existence of phase C by employing a non-equilibrium free-energy functional. It was suggested that a first-order phase transition between phases B and D takes place. This attempt was criticized due to its ad hoc use of an order parameter (difference between the bulk densities), which makes the detection of phase C by Monte Carlo simulations very difficult.

Chapter 4 covers a variant of the bridge model with deterministic hopping in the bulk. This model allows for a proof of symmetry breaking without further assumptions on the rates. Especially, the dynamics of symmetry breaking in this model is clarified.
In chapter 9, a variant of the bridge model with non-conserving rates in the bulk is considered.

2.3 Directed percolation

Apart from driven diffusive systems, models with absorbing phase transitions are a second largely studied subgroup of intrinsically non-equilibrium models. In these models, there are states which can be reached by the system

dynamics, but never left. These states are called *absorbing*. Absorbing states always result from the irreversibility of some microscopic processes and thus violate detailed balance by construction.
Generally, in models for absorbing phase transitions an agent X (such as particles, viruses, chemicals etc.) can undergo two kinds of reactions: proliferation and absorption. In the proliferation process, the agent gives rise to one or several offsprings.

$$X \to n\,X \quad \text{where } n > 1$$

In the annihilation process, the number of agents is reduced:

$$n\,X \to m\,X \quad \text{where } n > m$$

Depending on which process dominates, the system either falls into the absorbing state (annihilation dominated), or attains an active state with a density of the agent that is larger than zero (proliferation dominated). An often cited example for an absorbing phase transition is the spreading of a disease within a population.
The study of absorbing phase transitions is an active research field, see e.g. ref. [5] for a review. The numerous models showing non-equilibrium critical phenomena are attempted to be grouped into universality classes. In the remainder of this section a brief introduction to one of these classes, *directed percolation*, is given. The treatment of directed percolation is resumed in part II, where these models are investigated under the action of an external field, which plays a similar role as an external field in a ferromagnet (see chapter 10).

Directed percolation is the most studied class of absorbing phase transitions. It bears its name due to the resemblance to isotropic percolation [35]. Isotropic percolation models the connectivity in porous media. In isotropic percolation all space directions are treated equivalently. Directed percolation in contrast has one distinct direction in space along which the connectivity of the pores is directed. Consider e.g. the figure 2.3 sketching how a fluid percolates in a medium in presence of gravity (neglecting capillary effects).

Instead of regarding directed percolation as a spreading phenomenon in $D+1$ dimensions, it can be also seen from a dynamical perspective as a process in D dimensions, the directed dimension now being the time.
Let $s_i(t)$ denote the state of a site. $s_i(t) = 1$ represents a wet site, $s_i(t) = 0$ a dry one. Then the time evolution of the s_i for $D = 1$ can be phrased as

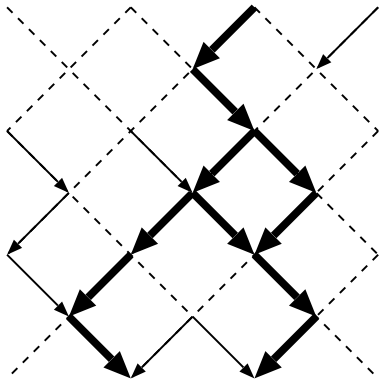

Figure 2.3: Sketch of directed percolation as a geometrical spreading phenomenon. Arrows indicate open connections between pores. The flow of a liquid inserted at the top is indicated by thick arrows.

follows [5]:

$$s_i(t+1) = \begin{cases} 1 \text{ with probability } p_1 \text{ if either } s_{i-1}(t) = 1 \text{ or } s_{i+1}(t) = 1 \\ 1 \text{ with probability } p_2 \text{ if } s_{i-1}(t) = 1 \text{ and } s_{i+1}(t) = 1 \\ 0 \text{ otherwise.} \end{cases} \tag{2.12}$$

The example of fluid-flow can be modeled by choosing $p_1 = p$ and $p_2 = p(2-p)$, where p corresponds to the mutually independent probability to find an open connection between pores. Using this dynamical definition of the model, which is called *directed bond percolation*, it becomes clear that the competing processes of proliferation and annihilation mentioned in the previous subsection govern its behavior.
Another commonly studied choice is $p_1 = p_2 = p$, which is called *directed site percolation*. In both cases, depending on the probability p which acts as a control parameter, a phase transition takes place. The order parameter of this transition is the density of active particles (wet sites) ρ_a, which characterizes the absorbing state $\rho_a = 0$ and the active state with $\rho_a > 0$. Approaching the critical p from above, ρ_a continuously decreases to zero. The phase transition of directed percolation can be regarded as a non-equilibrium critical phenomenon.
Clearly, space and timelike directions are different in these models. In fact, in the scaling theory for directed percolation (see subsection 10.1.2) two correlation lengths $\xi_\parallel$ and $\xi_\perp$ are defined, which both diverge at the critical point

with associated exponents $\nu_\parallel$ and $\nu_\perp$:

$$\xi_\parallel \sim (p - p_c)^{\nu_\parallel} , \quad \xi_\perp \sim (p - p_c)^{\nu_\perp}. \tag{2.13}$$

Critical phenomena in equilibrium can be grouped into universality classes sharing the same critical exponents and universal scaling functions (see [36] for a recent review). The foundations of universality in equilibrium can be understood from Wilson's renormalization group treatment [37, 38].
In contrast to equilibrium critical phenomena less is known in the case of non-equilibrium phase transitions. This is due to the fact that a generalized treatment is not possible, lacking an analog to the equilibrium free energy. The rich and often surprising variety of phenomena has to be studied for each system individually.
The scaling behavior of directed percolation (DP) as studied in section 10.1 is recognized as the paradigm of the critical behavior of several non-equilibrium systems which exhibit a continuous phase transition from an active to an absorbing state (see e.g. [5]). According to the universality hypothesis of Janssen and Grassberger [39, 40] a model belongs to the universality class of directed percolation provided the following conditions are fulfilled [5]:

- The model exhibits a continuous phase transition from a fluctuating active phase into a unique absorbing state.
- The model has a one-component order parameter.
- All interactions are short ranged.
- There are no additional symmetries or quenched randomness in the model.

Note that this includes the examples of directed bond and site percolation given above.
Different universality classes are expected to occur in the presence of additional symmetries, like particle conservation [41], particle-hole symmetry (compact directed percolation) [42], or parity conservation (e.g. branching annihilating random walks with an even number of offsprings [43]). Other model details, such as e.g. the geometry or shape of a lattice, are expected to have no influence on the scaling behavior in the vicinity of the critical point. The universality hypothesis still awaits a rigorous proof. In fact, at present there even seems to be no definite statement of the hypothesis. The conditions given above according to ref. [5] are just a subset of the sufficient conditions for models to be in the DP universality class.
Amazingly, numerous simulations suggest that the DP universality class is

even larger than expected. For instance, the pair contact process (PCP) considered in section 10.2 is one of the simplest models with infinitely many absorbing states exhibiting a continuous phase transition [44]. It was shown that the critical scaling behavior of the one-dimensional PCP is characterized by the same critical exponents as DP [44, 45] . This numerical evidence confirms a corresponding RG-conjecture [46]. These findings are at odds with a recently performed RG analysis conjecturing a different scaling behavior of both models in higher dimensions [47]. In section 10.2 we therefore consider the universal scaling behavior of the PCP in comparison with DP both for $D = 1$ and above the upper critical dimension.
Despite the apparent simplicity of the models, even in $1 + 1$ dimension no exact solutions for directed percolation are known. Therefore investigations have to rely either on approximation techniques such as series expansions [48] and RG schemes [49, 50] or on simulations as presented in sections 10.1 and 10.2.
So far no experimental realization of the DP universality class is known [5]. This is at first very surprising, given the theoretical robustness of the class as expressed in the universality hypothesis. In an experimental situation, two main problems arise: The failure to realize a truly non-fluctuating absorbing state and the presence of quenched randomness. Both ingredients are necessary for the DP universality class.

Chapter 3

Soft phase separation in driven diffusive systems

3.1 Introduction

The criterion of ref. [27] (see eq. (2.7) in subsection 2.2.1) predicts one-dimensional driven models to show phase separation provided the steady state current through a domain J_n shows the following behavior:

Type A: $J_n \to 0$ as $n \to \infty$.

Type B: $J_n \sim J_\infty(1 + b/n^\sigma)$ for either $\sigma < 1$, or $\sigma = 1$ and $b > 2$.

So far, all one-dimensional models found to phase separate are of type A [24, 51–55], and thus they exhibit strong phase separation at any density. In these models more than one species of particles is involved. For the AHR model introduced in subsection 2.2.1 it was suggested, based on numerical simulations, that the model exhibits a *condensed* phase separated state, where the particle densities fluctuate in the interior of the coexisting domains, and not just at the domain boundaries. In this state, a region with a high density of particles of both species coexists with a low density region. Moreover, the model has non-vanishing currents even in the thermodynamic limit. As in equilibrium phase separation it has been suggested that this state exists only at sufficiently high densities. However, a subsequent exact solution of the model [25, 26] shows that what numerically seems like a condensed state is in fact homogeneous, with a very large but finite correlation length. Further analysis of this model, in the light of the criterion suggested in [27] shows that the currents J_n corresponding to this model are given by the form B (see eq. 2.8), with $\sigma = 1$ and $b = 3/2$ [27]. Therefore, according to the criterion, no phase separation takes place.

Another example of a model which was suggested to exhibit phase separation into a fluctuating macroscopically inhomogeneous state is the two-lane model introduced by Korniss *et. al.* [28, 56]. While numerical studies of the model indicate that such a phase exists in the model, studies of the current J_n of finite domains suggests that it is of type B with $\sigma = 1$ and $b \simeq 0.8$ [27], indicating, again, that no phase separation exists in this model. Thus the question of whether a phase separation of type B exists remains an intriguing open question.

In this chapter we introduce a class of models which are demonstrated to be of type B, with $\sigma = 1$ and $b > 2$. According to the criterion conjectured in [27] this class is expected to exhibit a phase transition to a phase separated *condensed* state. Thus at high densities these models exhibit a novel type of phase separation with non-vanishing currents in the thermodynamic limit, and bulk fluctuations which are not restricted to the vicinity of the domain boundaries. To our knowledge, this is the first example of a genuine transition

of this type in one-dimensional driven systems.
In the following section we review the connection between the zero range process and driven systems, which is essential for understanding the origin of the criterion of ref. [27]. Section 3.3 contains the definition of our model. The application of the criterion is demonstrated in section 3.4. Finally, the nature of the phase transition is discussed in section 3.5.
The work presented in this section was done in collaboration with Y. Kafri, E. Levine and D. Mukamel and published in ref. [6].

3.2 Condensation transition in the zero range process

The formulation of the criterion for phase-separation is based on the analysis of the condensation transition in the zero-range process (ZRP) [57] considered below. This process constitutes a generic model for domain dynamics in one dimension. One-dimensional driven models can be mapped into corresponding ZRPs, although the mapping is generally not exact.
The translationally invariant symmetric one-dimensional ZRP is defined as follows: Let a lattice of size M with periodic boundary conditions contain N particles, where multiple occupancy of the lattice sites is allowed. The occupation number of site i is denoted as n_i. The dynamics is defined as random sequential update. Provided the chosen site is occupied, a single particle is moved to either of the neighboring sites with rate u_n. Generally, the stationary state of a translationally invariant ZRP is given by

$$P(\{n_\mu\}) = \frac{1}{Z(M,N)} \prod_{\mu=1}^{M} f(n_\mu), \tag{3.1}$$

where

$$f(n) = \prod_{m=1}^{n} \frac{1}{u_m} \tag{3.2}$$

if $n > 0$ and $f(0) = 0$. Here, $Z(M,N)$ plays the role of a partition sum, constrained to a fixed number of particles N:

$$Z(M,N) = \sum_{n_1,n_2 \ldots n_M} \delta(\sum_\mu n_\mu - N) \prod_{\mu=1}^{M} f(n_\mu). \tag{3.3}$$

Using the integral representation of the δ-function, this expression can be written as

$$Z(M,N) = \oint \frac{dz}{2\pi i}\, z^{-(N+1)} \prod_{\mu=1}^{M} F(z), \tag{3.4}$$

where

$$F(z) = \sum_{n=0}^{\infty} \prod_{m=1}^{n} \left[\frac{z}{u(m)}\right]. \tag{3.5}$$

The expression for $F(z)$ only converges, if $z < z_c = \lim_{m\to\infty} u(m)$.
For large M, N eq. (3.4) is dominated by the saddle point of the integral. Using $\Phi = N/M$:

$$\phi = \frac{zF'(z)}{F(z)}. \tag{3.6}$$

z plays the role of the fugacity, fixing the number of particles in the system. $F(z)$ is monotonically increasing, but z is bounded from above by z_c. Thus, if

$$\lim_{z\to z_c} \frac{F'(z)}{F(z)} < \infty, \tag{3.7}$$

a condensation transition may occur as then there is a critical density above which no solution for z can be obtained. This is analogous to Bose-Einstein condensation. For the specific choice of hopping rates

$$u_n = u_\infty \left(1 + \frac{b}{n_i}\right), \tag{3.8}$$

condensation occurs above a critical density if $b > 2$ [57].
In case of Bose-Einstein condensation, all energy levels apart from the ground state are occupied according to Bose-Einstein statistics with the critical value for the fugacity, while the excess particles macroscopically occupy the ground state.
In case of the ZRP with the given choice of hopping rates, the distribution of single site occupations is given by [27, 57]

$$P(k) \sim \frac{1}{k^b} \exp(-k/\xi) \qquad \xi = \frac{1}{|\ln(z/u_\infty)|}, \tag{3.9}$$

provided that $\rho < \rho_c$. At the critical density, the fugacity takes the value $z = u_\infty$ and the occupation probability becomes a power law with negative slope b. Above the critical density, this occupation probability remains, the particles on these sites form the low density phase. All excess particles gather at a single, spontaneously chosen site that becomes macroscopically occupied even in the thermodynamic limit and forms the condensed phase.

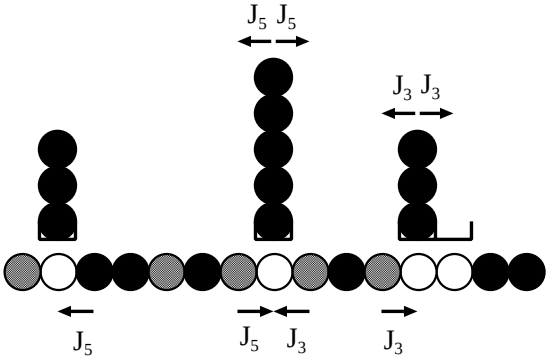

Figure 3.1: Illustration of the mapping of a driven diffusive system to a ZRP.

Mapping a driven model to a ZRP

In order to use the knowledge about the condensation transition for the ZRP also for driven diffusive systems, the latter ones have to be mapped into corresponding ZRPs. Consider a configuration of a driven diffusive two species system. Let the number of vacancies in the driven model be M and all vacancies be labeled from 1 to M. The number of lattice sites of the corresponding ZRP is identical to the number of vacancies in the driven model, i.e. M. Site i of the ZRP carries as many particles as there are particles between vacancies $i-1$ and i in the driven model (see fig. 3.1). Thus every site of the ZRP corresponds to a domain in the driven model (this domain may have length 0). The hopping rate u_n from one ZRP lattice site to its neighbors thus corresponds to the rate of particle flow out of a domain, which is according to the criterion stated above, given by the steady state current out of a domain of length n with open boundaries:

$$u_n = J_n. \tag{3.10}$$

It is clear that due to the mapping the internal structure of a domain gets lost. Therefore the mapping can in general not be exact.

3.3 Model definition

We now define our class of models in detail. We consider a one-dimensional ring with L sites. Each site i can be either vacant (0) or occupied by a positive (+) or a negative (−) particle (or charge). Positive particles are driven to the right while negative particles are driven to the left. In addition

to the hard-core repulsion, particles are subject to short-range interactions. These interactions are "ferromagnetic", in the sense that particles of the same kind attract each other. The dynamics conserves the number of particles of each species, N_+ and N_-. The total density of particles in the system is $\rho = (N_+ + N_-)/L$. The model is defined by a random-sequential local dynamics, whereby a pair of nearest-neighbor sites is selected at random, and the particles are exchanged with the following rates:

$$\begin{array}{lcll} +- & \rightarrow & -+ & \text{with rate} \quad 1-\Delta H \\ +0 & \rightarrow & 0+ & \text{with rate} \quad \alpha \\ 0- & \rightarrow & -0 & \text{with rate} \quad \alpha\ . \end{array} \tag{3.11}$$

Here ΔH is the difference in the ferromagnetic interactions between the final and the initial configurations. We begin by considering a model with only nearest neighbor interactions,

$$H = -\epsilon/4 \sum_i s_i s_{i+1}\ . \tag{3.12}$$

Here $s_i = +1$ (-1) if site i is occupied by a $+$ $(-)$ particle, and $s_i = 0$ if site i is vacant. The interaction parameter ϵ satisfies $0 \leq \epsilon < 1$ to ensure positive transition rates. The model is a generalization of the Katz-Lebowitz-Spohn (KLS) model, introduced in subsection 2.1.2 and studied in detail in [19,20], in which the lattice is fully occupied by charges and no vacancies exist. In this section we consider the case where the number of positive and negative particles is equal, $N_+ = N_-$.

We will demonstrate that for a certain range of the parameters defining the dynamics, namely for $\epsilon > 0.8$ and sufficiently large α (to be discussed below), a phase separation transition occurs as the density ρ is increased above a critical density ρ_c. In the phase separated state a macroscopic domain, composed of positive and negative particles, coexists with a fluid phase, which consists of small domains of particles (of both charges) separated by vacancies. Typical configurations obtained during the time evolution of the model starting from a random initial configuration are given in fig. 3.2. This figure suggests that a coarsening process takes place, leading to a phase separated state as described above. However, this by itself cannot be interpreted as a demonstration of phase separation in these models. The reason is that this behavior may very well be a result of a very large but finite correlation length, as is the case in the AHR [24–26,53] and the two-lane [28,56] models discussed above [58].

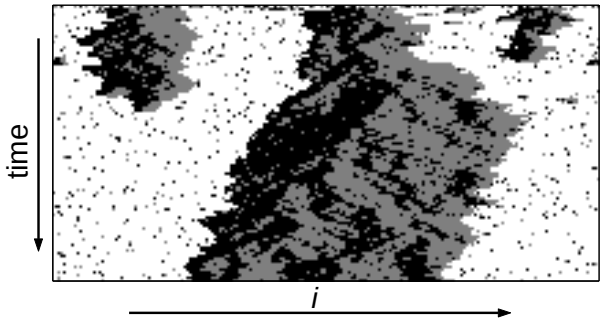

Figure 3.2: Evolution of a random initial configuration of model (3.11) with nearest-neighbor interactions, on a ring of 200 sites. Here $\epsilon = 0.9$, $\alpha = 2$, and the particle density is $\rho = 0.5$. Positive particles are colored black, and negative particles are colored grey. One hundred snapshots of the system are shown every 100 Monte-Carlo sweeps.

3.4 Application of the criterion

In order to decide on the possibility of phase separation in the present model we apply the criterion stated above (see eqs. (2.7) and (2.8)) [27]. To this end we note that a domain may be defined as an uninterrupted sequence of positive and negative particles bounded by vacancies from both ends. The current J_n corresponding to such a domain of length n may thus be determined by studying an open chain, fully occupied by positive and negative particles, with entrance and exit rates α. This is just the one-dimensional KLS model on an open chain. Phase separation is expected to take place only for sufficiently large α. We consider α such that the system is in its maximal current state, whereby J_∞ assumes its maximum possible value, and is independent of α.

To evaluate J_n we first consider the KLS model on a ring of n sites with no vacancies. We then extend these results to study the behavior of an open chain. Since we are interested in the maximal current phase we consider equal numbers of positive and negative particles $n_+ = n_- = n/2$. It can be shown, as was done for the noisy Burger's equation [59–61], that under quite general conditions, to be discussed below, the current J_n takes the following form for large n,

$$J_n = J_\infty \left(1 - \frac{\lambda \, \kappa}{2 J_\infty} \frac{1}{n} \right) . \tag{3.13}$$

Here $\lambda = \partial^2 J_\infty / \partial \rho_+^2$ is the second derivative of the current with respect to the density of positive particles ρ_+ in the system. The compressibility analog κ is defined by $\kappa = \lim_{n\to\infty} n^{-1} \left(\langle n_+^2 \rangle - \langle n_+ \rangle^2 \right)$, as calculated within a

grand canonical ensemble, as explained below. This can be demonstrated by considering the current $J_n(n_+)$ for charge densities close to $n_+ = n_- = n/2$. Expanding $J_n(n_+)$ in powers of $\Delta n_+ = n_+ - n/2$ one has

$$J_n(n_+) = J_n(n/2) + J_n' \, \Delta n_+ + \frac{1}{2} J_n'' \, (\Delta n_+)^2 \tag{3.14}$$

where the derivatives J_n' and J_n'' are taken with respect to n_+ and evaluated at $n/2$. We average (3.14) over n_+ with the steady state weights of a grand canonical ensemble. This is done by introducing a chemical potential μ which ensures that the average density satisfies $\langle n_+ \rangle = n/2$. We find

$$\langle J_n(n_+) \rangle_\mu = J_n(n/2) + \frac{1}{2} J_n'' \, \langle (\Delta n_+)^2 \rangle_\mu \, . \tag{3.15}$$

Noting that $\langle J_n(n_+) \rangle_\mu$ is J_∞ in the $n \to \infty$ limit, and $J_n(n/2)$ is just J_n, eq. (3.13) is obtained. Here we made use of the fact that finite size corrections to $\langle J_n(n_+) \rangle_\mu$, resulting from the next to leading eigenvalue of the transfer-matrix of the steady-state distribution, are exponentially small in n and may thus be neglected. The result of eq. (3.13) is rather general, and is independent of the exact form of the steady-state particle distribution. This is provided that the weights of the microscopic configurations are local and thus the density and chemical potential ensembles are equivalent.

In fact, an alternative way to derive (3.13) is to consider the correspondence between the driven lattice-gas models and the noisy Burger's equation or the Kardar-Parisi-Zhang (KPZ) equation for interface growth in $1+1$ dimensions [62]. In these models J_n corresponds to the growth velocity of the interface. Eq. (3.13) has been derived in [59–61], where λ is the coefficient of the non-linear term in the KPZ equation. The equivalence of the two alternative approaches relies on the fact that both κ and λ are invariant under renormalization transformations.

The result (3.13) can be used to evaluate J_n for the KLS model. It has been shown [19, 20] that for a ring geometry the steady state weight of a configuration $\{\tau_i\}$ is

$$P(\{\tau_i\}) = e^{-\beta \mathcal{H}} \;\; ; \;\; \mathcal{H} = -\sum_{i=1}^{n} \tau_i \tau_{i+1} - \mu \sum_{i=1}^{n} \tau_i \, , \tag{3.16}$$

with $\tau_i = \pm 1$ for positive and negative charges respectively, $e^{4\beta} = (1-\epsilon)/(1+\epsilon)$, and μ serves as a chemical potential which controls the density of, say, the positive particles. The chemical potential μ vanishes for the case $n_+ = n_-$. Using (3.16) expressions for $\kappa(\epsilon)$ and $J_\infty(\epsilon)$ of this model have been obtained in [20].

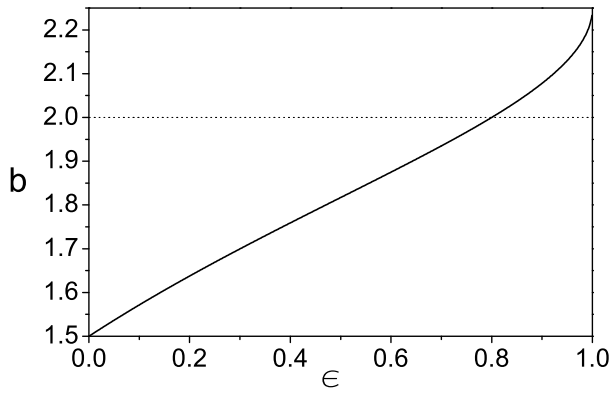

Figure 3.3: The coefficient $b(\epsilon)$, eq. (3.18).

We now consider the KLS model in an open chain, which is the relevant geometry in applying the phase-separation criterion. It has been argued [59, 60] that the finite size correction to the current of an open chain is given by the corresponding correction in a ring geometry, up to a universal multiplicative constant c which depends only on the boundary conditions. In the maximal current phase, c was found to be 3/2. Thus the current of an open system is given by $J_n \sim J_\infty(1 + b/n^\sigma)$ with $\sigma = 1$ and

$$b(\epsilon) = -c\frac{\lambda(\epsilon)\kappa(\epsilon)}{2J_\infty(\epsilon)} \ . \tag{3.17}$$

Using the values of J_∞ and κ obtained in [20] and $c = 3/2$ we find

$$b(\epsilon) = \frac{3}{2}\,\frac{(2+\epsilon)\upsilon + 2\epsilon}{2(\upsilon+\epsilon)} \ ; \ \upsilon = \sqrt{\frac{1+\epsilon}{1-\epsilon}} + 1 \ . \tag{3.18}$$

In figure 3.3 the coefficient $b(\epsilon)$ is plotted for $0 \leq \epsilon < 1$. This curve has been verified by direct numerical simulations of the KLS model on an open chain in the maximal current phase, demonstrating that the prefactor c indeed does not depend on ϵ . Using (3.18) it is readily seen that for $\epsilon > 0.8$ the value of b is larger than 2.

According to the criterion conjectured in [27] one expects phase separation to take place at high densities in model (3.11) for $\epsilon > 0.8$, as long as α is such that the KLS model is in the maximal current phase. This *condensed* phase separated state belongs to case B of the criterion. We have carried out extensive numerical simulations of the dynamics of the model for various values of ϵ. We find that for $\epsilon \lesssim 0.4$ no phase separation is observed. However, for $\epsilon > 0.4$ simulations of systems of sizes up to $L = 10^6$ show that the system evolves towards what seems to be a phase separated

state at sufficiently large densities. We argue that a genuine phase separation takes place only for $\epsilon > 0.8$. On the other hand, the seemingly phase separation found in simulations for $0.4 \lesssim \epsilon < 0.8$, is only a result of large but finite correlation lengths, as was found in the AHR and in the two-lane models. As pointed out in [58] such a behavior is related to corrections of order $1/n^2$ and higher in the current. These corrections were shown to lead to a crossover with a very sharp increase in the correlation length, which could be erroneously interpreted as a genuine phase transition in numerical studies of finite systems.

3.5 The nature of the phase transition

We now discuss the phase transition leading to the phase separated state. According to [27] the domain size distribution just below the transition takes the form

$$\mathcal{P}(n) \sim \frac{1}{n^b} e^{-n/\xi} \tag{3.19}$$

where ξ is the correlation length, which diverges at the transition. The particle density in the system is related to ξ by $\rho/(1-\rho) = \sum n\mathcal{P}(n)/\sum \mathcal{P}(n)$. The critical density ρ_c is given by this expression with $\xi \to \infty$. Note that with this form of the distribution function, ρ_c is 1 in the limit $b \searrow 2$, and is a decreasing function of b. It is straightforward to show [63] that the divergence of the correlation length at the critical density is given by

$$\xi \sim \begin{cases} |\rho - \rho_c|^{-\frac{1}{b-2}} & , \quad 2 < b < 3 \\ |\rho - \rho_c|^{-1} & , \quad b > 3 \, . \end{cases}$$

It is worthwhile noting that while $\partial \xi^{-1}/\partial \rho$ is continuous at the transition for $2 < b < 3$, it exhibits a discontinuity for $b > 3$. The transition may thus be considered continuous for $2 < b < 3$ and first-order for $b > 3$.

In the model defined above b is found to satisfy $3/2 \leq b < 9/4$. It is natural to ask whether larger values of b could be reached by increasing the range of the interactions. To answer this question we have extended model (3.12) to include next-nearest-neighbor interactions as well, and consider

$$H = -\epsilon/4 \sum_i s_i s_{i+1} - \delta/4 \sum_i s_i s_{i+2} \, . \tag{3.20}$$

We have calculated the value of b as a function of δ by Monte-Carlo simulations. This is done by measuring the current J_n in an open system of

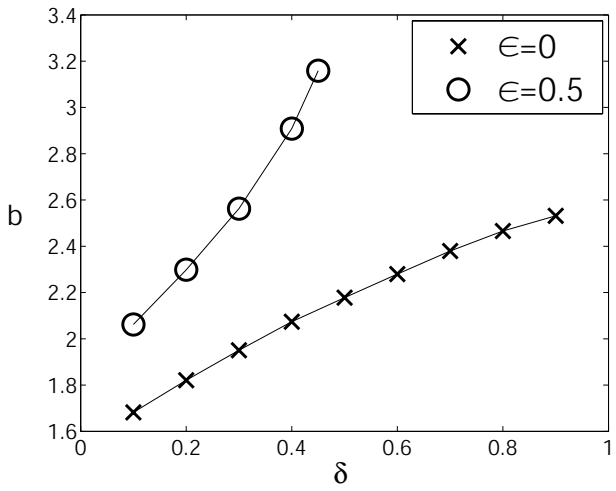

Figure 3.4: The coefficient $b(\delta)$, as calculated from Monte-Carlo simulations of domains of sizes up to 1024. Data are shown for $\epsilon = 0$ and $\epsilon = 0.5$.

size n, which is fully occupied by positive and negative particles. At the boundaries, the coupling to the rest of the system is modeled by injection of positive (negative) particles with rates α at the left (right). Simulating systems of size up to 1024 enables us to fit the measured values of J_n to the form $J_n \sim J_\infty(1 + b/n^\sigma)$ with $\sigma = 1$, and to extract b. In figure 3.4 we plot b as a function of δ, for $\epsilon = 0$ and for $\epsilon = 0.5$. We find that by extending the range of the interactions one can increase b to values even larger than 3, where the phase separation transition is expected to be first order.

3.6 Conclusion

In summary, a class of driven diffusive models in one dimension is introduced and analyzed using a recently conjectured criterion for phase separation [27]. These models are shown to exhibit a novel type of phase separation. In the phase separated state of these models the density is fluctuating in the bulk of the domains. Moreover, the models exhibit a homogeneous state at low densities, and a phase transition into the phase separated state occurs at a critical density. The nature of the phase transition in these models is also discussed.

While the validity of the criterion was proved for the AHR model, its general validity was conjectured based on some plausible assumptions on the behavior of the coarsening domains [27]. It would be of interest to analyze the class of models introduced in the present study by other analytical means,

in order to verify the validity of the criterion.

Chapter 4

Dynamics of spontaneous symmetry breaking

4.1 Introduction

While single-species driven diffusive systems in one dimension are largely understood, two-species models show a variety of phenomena that are a matter of current research, such as phase separation and spontaneous symmetry breaking (see [4] for a recent review). The first such model that was shown to exhibit spontaneous symmetry breaking was a model with open boundaries that became known as the 'bridge model' [30,31] (see subsection 2.2.2). In this model, two species of particles move in opposite directions. Although the dynamical rules are symmetric with respect to the two species, two phases with non-symmetrical steady states were found by Monte Carlo simulations and mean-field calculations. While the existence of one of the phases remains disputed [24,64], a proof for the existence of the other one was given for the case of a vanishing boundary rate [33]. Recently, a variant of the bridge model with non-conserving bulk dynamics was considered [9]. Although the phase diagram of this model is even richer than that of the original one, a proof for a symmetry broken state could again only be given in the case of a vanishing boundary rate.
All symmetry breaking models considered so far evolve by random sequential update. In this article, a variation of the bridge model with parallel sublattice update is studied. The update scheme ensures that the dynamics in the bulk is deterministic, while stochastic events occur at the boundaries. Thus the complexity of the problem is reduced, which allows to elucidate the mechanism by which spontaneous symmetry breaking occurs in this model as well as to give a proof for the existence of a symmetry broken phase. This proof is valid for the whole region in parameter space where symmetry breaking occurs and not just in some limiting case.
The model considered here is defined on a one-dimensional lattice of length L, where L is an even number. Sites are either empty or occupied by a single particle of either species, i.e. the particles are subject to an exclusion interaction. The dynamics is defined as a parallel sublattice update scheme in two half steps. In the first half-step the following processes take place: At site 1 it is simultaneously attempted to create a particle of species A with probability α if the site is empty, and to annihilate a particle of species B with probability β, provided the site is occupied by such a particle:

$$0 \xrightarrow{\alpha} A \quad B \xrightarrow{\beta} 0. \tag{4.1}$$

At site L, a particle of species B is created with probability α and a particle of species A is annihilated with probability β:

$$0 \xrightarrow{\alpha} B \quad A \xrightarrow{\beta} 0. \tag{4.2}$$

Note that at each boundary site, either annihilation or creation can take place in a given time step, but not both. In the bulk, the following hopping processes occur deterministically between sites $2i$ and $2i+1$ with $0 < i < L/2$:

$$A0 \xrightarrow{1} 0A \quad 0B \xrightarrow{1} B0 \quad AB \xrightarrow{1} BA. \tag{4.3}$$

In the second half-step, these deterministic bulk hopping processes take place between sites $2i-1$ and $2i$ with $0 < i \leq L/2$. Note that the dynamics is symmetric with respect to the two particles species.
In the next section, the phase diagram of the model is presented along with density profiles obtained from Monte Carlo simulations. In section 4.3 the mechanism leading to the symmetry broken phase is described. The behavior on the transition line is described in section 4.4 while section 4.5 treats the dynamics in the symmetric phase.

4.2 Phase diagram

The phase diagram of the model can be explored by Monte Carlo simulations. Two phases are found (see figure 4.1):

- If $\alpha < \beta$, the system exhibits a symmetric steady state. Here, the bulk densities are $\rho_A(i) = 0$, $\rho_B(i) = \alpha\beta/(\alpha+\beta)$ if i is odd, and $\rho_A(i) = \alpha\beta/(\alpha+\beta)$, $\rho_B = 0$ if i is even.

- If $\alpha > \beta$, the system resides in the symmetry broken phase. Assume the A particles to be in the majority. Then, the bulk densities in the steady state are $\rho_B(i) = 0$ for all i, $\rho_A(i) = 1$ for i even and $\rho_A(i) = 1-\beta$ for i odd. This means that the symmetry is broken and the minority species is completely expelled from the system. Thus, the dynamics of the majority species is as in the single species ASEP with parallel sublattice update. For this system, an analytical expression for the steady state density in a finite system is known [17]. The density profile of the majority species in the broken phase of the sublattice bridge model equals that of the high density phase in the sublattice ASEP at the given parameters α and β.

The behavior on the transition line is described in section 4.4.
If one of the boundary rates becomes 0 or 1, the steady state can be given exactly:

- If $\alpha = 0$, no injection takes place and the empty lattice is a stationary state.

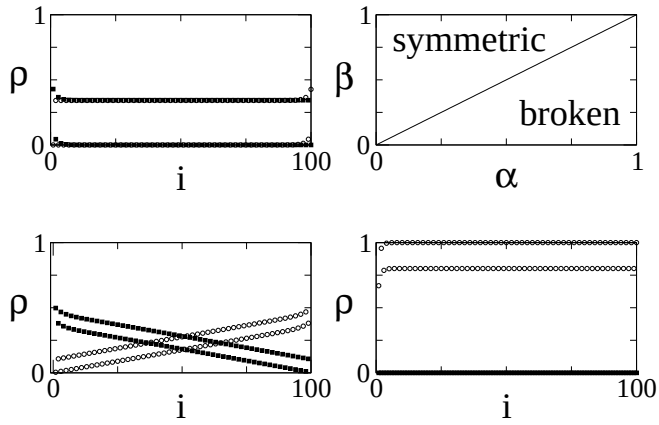

Figure 4.1: Upper right: Phase diagram of the sublattice bridge model. Density profiles as obtained from Monte Carlo simulations in the symmetric phase at $\alpha = 0.6$ and $\beta = 0.8$ (upper left), the broken phase at $\alpha = 0.6$ and $\beta = 0.2$ (lower right) and on the transition line at $\alpha = \beta = 0.2$ (lower left). Open (closed) symbols show A (B) densities.

- If $\beta = 0$, no ejection takes place. The dynamics of the model ceases as soon as the left (right) boundary site is blocked by an incoming B (A) particle.
- If $\alpha = 1$, two symmetry related stationary states exist. The product state where all even sites are occupied by A-particles with probability 1 and all odd sites are occupied by A-particles with probability $1 - \beta$ is stationary. Likewise the symmetry related product state with only B-particles is stationary as well.
- If $\beta = 1$, the symmetric product state with density $\alpha/(1+\alpha)$ for A (B) particles on even (odd) sites and density 0 of A (B) particles on odd (even) sites is stationary.

4.3 Symmetry breaking dynamics

In the following, the mechanism for symmetry breaking is elucidated and the respective time scales are determined. This mechanism shows that for

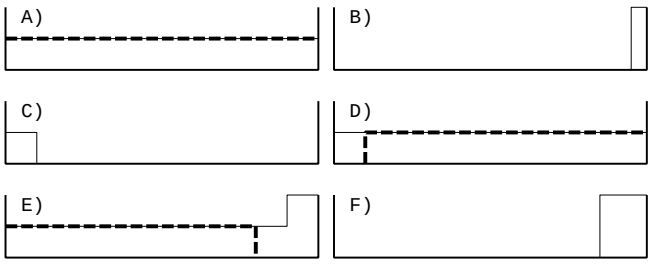

Figure 4.2: Illustration of the stages involved in the dynamics of spontaneous symmetry breaking. A-densities are depicted by thin, solid lines, B-densities by dashed, thick ones.

$\alpha > \beta$ the system needs a time T_1 which is algebraically increasing with L to reach a broken phase if it was started with symmetric initial conditions. Furthermore, assuming the system to be in a broken phase it is shown that it takes a time T_2 that is exponentially increasing with L until particles of the minority species can penetrate the system. Both facts together provide a proof for spontaneous symmetry breaking in this model for $\alpha > \beta$.

Dynamics of symmetry breaking: It is assumed that at $t = 0$ there are no particles in the system and that $\alpha > \beta$ (the case of other initial densities can be treated in a similar fashion). Starting from the empty lattice, A (B) particles are created at every time step with probability α at site 1 (L). Once injected, particles move deterministically with velocity 2 (-2). Therefore, at time $t = L/2$ the system is in a state where the density of A (B) particles is α (0) at all even sites and 0 (α) at all odd sites (see fig. 4.2 A)).
In this situation both creation and annihilation of particles are possible. However, it turns out that the effect of creation of particles is negligible [65]: Whenever the bulk density of A-particles is above $\beta/2$, the deterministic hopping transports on average more A-particles towards site L than can be annihilated there. This leads to the formation of an A-particle jam at the right boundary, blocking the injection of B-particles. The A density approaches 1 exponentially fast for $T \gg 1$. Therefore the effect of injection of B-particles is negligible in the large L limit. A similar argument holds for the reverse situation with A and B-particles interchanged.
Thus, due to jamming, in the limit of large L, the effect of creation of either species of particles becomes negligible. At both ends of the system, jams are formed, which block the entry of new particles into the system. In these jams, the only source of vacancies is annihilation at the boundaries with rate β. Therefore, in a jam, the density of A (B) particles at even (odd) sites is 1, while that at odd (even) sites is $1 - \beta$. In each time step, the number of

particles in each of the two jams reduces by one with probability β. By a fluctuation, one of the jams, say the B-jam at the left boundary, is dissolved first. Let the number of remaining A-particles at the time when the B-jam vanishes be ΔN_0 (see figures 4.2 B and 4.3).
Stage 1: All particles in the system are contained in the A-jam at the right boundary. The entry of B-particles is blocked, while the blockage at the left boundary is dissolved. Until the A-jam is dissolved after a time t_3, A particles are created with probability α and annihilated with probability β. The mean value of t_3 is $(\Delta N_0 + 1 - \beta)/\beta \approx \Delta N_0/\beta$. In this mean time, on average $\Delta N_0\alpha/\beta$ A-particles are created at the left boundary. The A-particles reside on even sites with density α, while odd sites are empty. The length of this cluster is $2t_3$ and thus on average $2\Delta N_0/\beta$ (see figs. 4.2 C and 4.3).
Stage 2: As now both jams are dissolved, both species of particles can be injected into the system with probability α. Until the cluster of A particles formed in the previous stage has reached the right boundary after time $L/2 - t_3$ (which is on average given by $L/2 - \Delta N_0/\beta$), no annihilation of particles takes place. On average, the difference in particle number of both species remains as at the end of stage 1, i.e. $\Delta N_0(\alpha/\beta)$ (see figs. 4.2 D and 4.3).
Stage 3: At the start of this stage, the density of A particles on all even sites in the system is α, while it is 0 on all odd sites. The density of B particles is α on the odd sites from $2t_3/\beta$ to L and 0 on all even sites. This especially implies that the situation at the right boundary is as before in stage 1, i.e. a jam is formed at the right boundary and the effect of injection of B particles can be neglected. At the left boundary, there is no such jam, as the B particles originating from the injection at the right boundary in stage 2 have not yet reached the left boundary. This only happens after a time of t_3 steps (which is $\Delta N_0/\beta$ on average). Till then, A-particles are injected with probability α and ejected with probability β, while B-particles are neither injected, nor ejected. On average, this increases the difference in particle numbers by $(\alpha - \beta)\Delta N_0/\beta$. Thus, the difference in particle numbers of each species at the end of this stage changes on average to $\Delta N_0(1 + 2(\alpha - \beta)/\beta)$ (see figs. 4.2 E and 4.3).
Stage 4: After the cluster of B particles created in stage 2 has reached the left boundary, it forms a jam and makes the effect of injection of A particles negligible. Thus, for both A and B particles, only ejection is possible and the situation is analogous to the one before stage 2, albeit with jams of particle numbers differing on average by $\Delta N_0(1 + 2(\alpha - \beta)/\beta)$. This will on average also be the particle number in the jam at the right end, once the B jam at the left boundary is dissolved (see figs. 4.2 F and 4.3).
The dynamics then proceeds as in stage 1. Therefore, stages 1 to 4 constitute an amplification mechanism for an initially created density difference. If the

initial density difference is ΔN_0, after cycling through stages 1 to 4 once, it is $\Delta N_1 = \Delta N_0(1 + 2(\alpha - \beta)/\beta)$ on average. In general, after i loops the difference is on average:

$$\Delta N_i = \Delta N_0 \left(1 + \frac{2(\alpha - \beta)}{\beta}\right)^i \tag{4.4}$$

If the cluster of A particles penetrating the system from the left boundary in stage 1 reaches the jam at the right boundary before it is dissolved, the amplification mechanism comes to an end and the system enters into the symmetry broken state. In this situation, the effect of injection of B-particles is negligible for large L due to jamming at the right boundary and the only relevant stochastic boundary processes are injection of A-particles at site 1 and annihilation of A at site L. As there is a constant supply of A-particles the system quickly fills with them and attains a state as for the single-species ASEP with sublattice update [17] at the given α, β.
As it takes the penetrating cluster of A-particles in stage 1 a time of $L/2$ to fill the whole system, this defines the minimum time that it must take to dissolve the jam at the right end. Therefore, the jam in stage 1 must on average have at least $\beta L/2$ particles. The particle number in the jam at the beginning of stage 1 is equal to the difference of particle numbers of A and B. Thus it is required that:

$$\Delta N_i = \Delta N_0 \left(1 + \frac{2(\alpha - \beta)}{\beta}\right)^i > \frac{\beta}{2} L. \tag{4.5}$$

In other words, the system enters the symmetry broken state if an initial particle number difference has been amplified by cycling through stages 1 to 4 $O(\ln(L))$ times, provided that in each stage the particle number difference is increased at least by the average value. Each such loop through stages 1 to 4 takes a time of less then $2L$ time steps. Although on average ΔN is enlarged, the stochastic processes at the boundaries might lead to a decrease of ΔN. At worst, ΔN could be reduced to zero, which means that the amplification procedure would have to begin again. Let the probability that in any stage during the necessary $O(\ln(L))$ amplification loops ΔN is increased at least by the average value be $\gamma > 0$. As $0 \leq \Delta N \leq L$ and on average ΔN is increasing, γ cannot be exponentially small in L. Thus, an upper limit for the time T_1 it takes for the system to leave the amplification loop for a symmetry broken state is given by

$$T_1 < 2L \left(\ln(L) + c\right)/\gamma, \tag{4.6}$$

where $c = \ln(\beta/2) - ln(\Delta N_0) - ln(1 + 2(\alpha - \beta)/\beta)$ (see eq. (4.5)).
Thus, by *amplification of fluctuations the system reaches a state of broken*

symmetry in a time algebraically increasing with L, provided that $\alpha > \beta$. The broken states that are attained are the steady states of the single species ASEP at the respective α, β. These states either contain only A- or B-particles, depending on initial fluctuations.
Residence time in the broken state: Assume the system to be residing in the broken state with particle species A in the majority, i.e. $\rho_A(i) = 1$ for even sites and $\rho_A(i) = 1 - \beta$ for odd sites, up to boundary effects at the left boundary. Particle species B is completely expelled from the system, i.e. $\rho_B(i) = 0$ for all i. In this state, injection of B particles is impossible, as site L is blocked. The only possible boundary processes are annihilation of A particles at site L with probability β and creation of A particles at site 1 with probability $\alpha > \beta$. Until the first B particle can be injected, the complete jam of A particles has to be dissolved. This jam consists of the order of L particles. To dissolve the jam, for a time $T \sim L$ the number of successful creation events X_+ must be less than the number of successful annihilation events X_-. The probability distribution of X_+ (X_-) is binomial with probability α (β), provided that site L is always occupied and site 1 always empty. The former assumption is always fulfilled, as the A-particles form a jam at the right boundary. To ensure the validity of the second assumption simply assume that the jam has already been partially dissolved, i.e. it occupies only a finite fraction of the lattice. Then all odd sites left of the jam are empty, including site 1. For large T the distributions for $X_+ - X_-$ can be treated as Gaussian with mean $(\alpha - \beta)T > 0$ and variance $\sigma \sim \sqrt{T}$. To leading order in L, the probability for $X_+ - X_-$ to be smaller than zero is for large $T \sim L$ given by $P_>(0) \sim \exp(-2(\alpha-\beta)^2 L)/(2\pi(\alpha-\beta)L)^{1/2}$, using an expansion for the error-function at large arguments. Thus the probability for an interval $T \sim L$ during which the jam of A particles is dissolved is exponentially small in L. Therefore, *the time* T_2 *until the minority species can penetrate a system started in the broken state is exponentially large in* L. This, together with the statement about T_1 above, proves spontaneous symmetry breaking.

For finite L, flips between the symmetry related steady states can be observed in Monte Carlo simulations (see fig. 4.4). Note that the flipping process itself is rapid compared to the residence time in the broken states.

4.4 Transition line

The line $\alpha = \beta$ is the transition line between the broken and the symmetric phase. The amplification mechanism outlined above does not apply here and no symmetry breaking takes place for $\alpha = \beta$. The density profile as seen in a Monte Carlo simulation is shown in fig. 4.1. In ref. [34] the phase transition

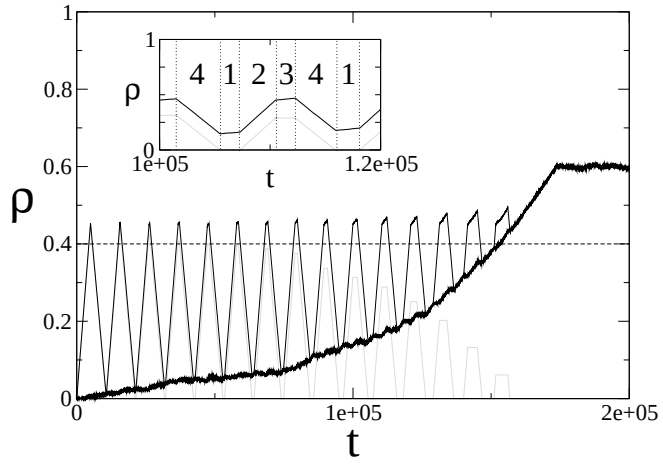

Figure 4.3: Symmetry breaking in the sublattice bridge model, starting from the empty lattice (MC simulation). Here, $\alpha = 0.9$, $\beta = 0.8$ and $L = 10000$. The density of A particles is drawn in black, that of B particles in grey and the difference as the thick black line. As soon as the difference exceeds $\beta/2$ (dashed line) at the start of stage 1, the system enters the symmetry broken state. The inset shows a close-up during the time evolution. Individual stages as described in the text are separated by dotted vertical lines.

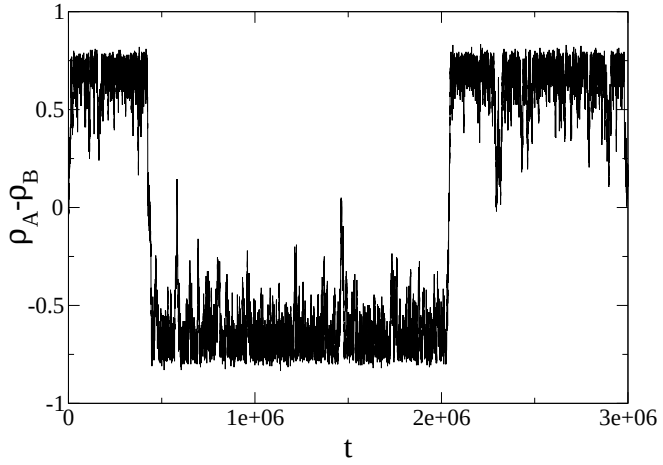

Figure 4.4: Time evolution of the density difference of A and B particles for $L = 200$, $\alpha = 0.5$ and $\beta = 0.49$.

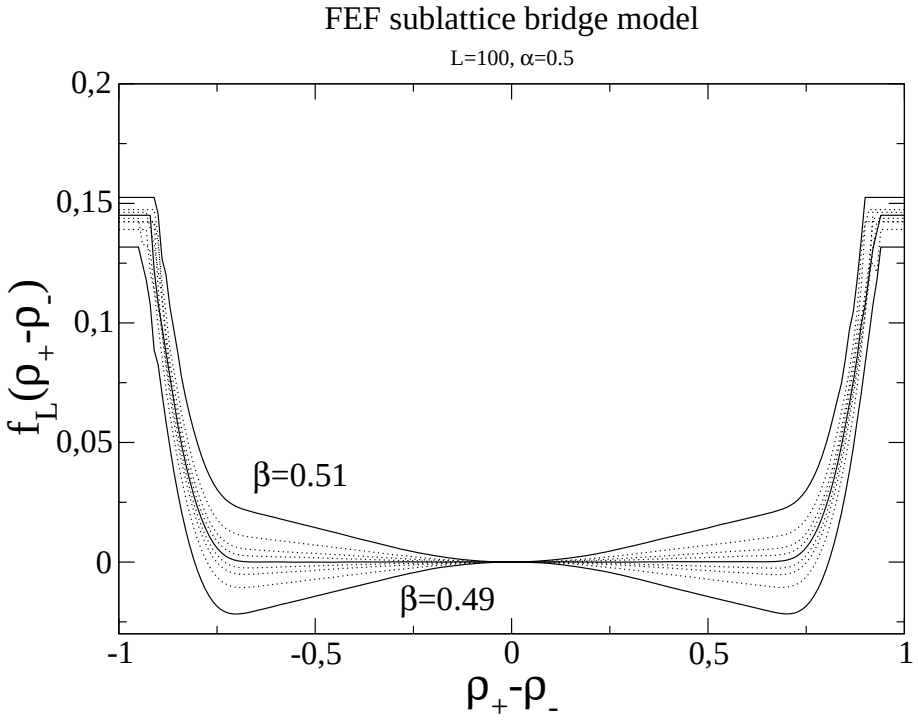

Figure 4.5: Free energy functional for the sublattice bridge model at $L = 100$, $\alpha = 0.5$ and various values of β above and below the transition. The solid line shows the functional at the transition, i.e. $\beta = 0.5$.

between the symmetry broken state and the symmetric state in the original bridge model was investigated using a 'free-energy functional' (FEF): The density difference $\rho_A - \rho_B$ is taken as an order parameter for the transition. The probability $P(L, \rho_A - \rho_B)$ for a system of size L to exhibit that order parameter is sampled in Monte Carlo simulations. Defining

$$f_L(\rho_A - \rho_B) = \frac{1}{L} \log P(L, \rho_A - \rho_B) \tag{4.7}$$

the FEF is given by

$$f(\rho_A - \rho_B) = \lim_{L\to\infty} f_L(\rho_A - \rho_B). \tag{4.8}$$

Using the free energy functional for the sublattice bridge model suggests that the transition is analogous to a first-order phase transition in equilibrium physics (see fig. 4.5).

It is very interesting to compare these findings to the results of a mean-field

treatment of the system. Performing a similar analysis as in ref. [31] yields the following results:

- For $\alpha > \beta$ the system is in a symmetry-broken state.The density of the majority species is 1 $(1-\beta)$ on even (odd) sites. The minority density is 0 throughout the system.
- For $\alpha < \beta$ the system is in a symmetric state. The density of A (B) particles in the bulk is $\alpha\beta/(\alpha+\beta)$ (0) on even sites and 0 $(\alpha\beta/(\alpha+\beta))$ on odd sites.
- Along the line $\alpha = \beta$ the system resides in a state where the density of A (B) particles in the bulk is α_1 (0) on even sites and 0 (α_2) on odd sites, with the constraint $\alpha_1 + \alpha_2 = \alpha$.

Note that mean-field theory and the results for the stochastic model coincide up to the transition line. Along this line mean-field theory predicts the existence of a second symmetry-broken phase. This phase corresponds to the disputed low-asymmetric phase of the original bridge model [24, 31, 64]. In the present model, in this phase only the sum of the A and B-densities is fixed. The specific densities attained by the system depend on the initial conditions. In the stochastic model, this phase does not exist, up to one special point: for $\alpha = \beta = 1$ all processes are deterministic. In this case the mean-field prediction is correct. For the remainder of the transition line, the mean-field ansatz leads to the prediction of a low-asymmetric phase, which does not exist in the stochastic model.

4.5 Symmetric phase

If $\alpha < \beta$, the system resides in the symmetric phase (see fig. 4.1). The approach to the steady state can be described in a similar manner as for the symmetry broken case:
Starting from the empty lattice at $t = 0$, the system starts to fill with A (B) particles injected at the left (right) boundary with rate α. These particles are transported deterministically with velocity 2 (-2) towards the right (left) boundary. Thus at $t = L/2$, all even (odd) sites are occupied by A (B) particles with probability α, leading to total densities of $\rho_A^{tot}(t = L/2) = \rho_B^{tot}(t = L/2) = \alpha/2$.
From $t = L/2$ on, both creation and annihilation of A- and B-particles are possible. For the next $L/2$ time steps, the particles created at times $t < L/2$ move deterministically towards the boundaries. The mean annihilation time

for A-particles, provided one of them occupies site L, is $\bar{t_\beta} = 1/\beta$. The mean time between the arrival of two subsequent A particles at site L is given by $\bar{t_\rho} = 1/(2\rho_A^{tot}) = 1/\alpha$. As $\bar{t_\beta} < \bar{t_\rho}$, no jam is formed. The annihilation process in this case is not limited by the rate β, but the supply of A-particles arriving at the right boundary. Therefore, the effective annihilation rate is given by $\beta_A^{eff} = 1/(2\rho_A^{tot})$. Analogously, $\beta_B^{eff} = 1/(2\rho_B^{tot})$. Similarly, an effective creation rate can be formulated: On average every $\bar{t_\rho}$ a new B-particles arrives at site 1 and stays there for a time $\bar{t_\beta}$ before annihilation. Thus the mean fraction of time that site 1 is not occupied is given by

$$\bar{t_1} = (\bar{t_\rho} - \bar{t_\beta})/\bar{t_\rho} = 1 - \frac{2\rho_B^{tot}(t = L/2)}{\beta}.$$

This leads to the following effective creation rate: $\alpha_A^{eff} = \alpha\bar{t_1}$. An analogous statement holds for the B-particles. Due to the effective creation rates, at time L all even sites are occupied with A particles with probability α_A^{eff}, while all odd sites are occupied by B particles with probability α_B^{eff}. This leads to total densities $\rho_A^{tot}(t = L) = \alpha_A^{eff}/2$ and $\rho_B^{tot}(t = L) = \alpha_B^{eff}/2$.
From $t = L$ on, the scenario described above is repeated, but this time with other densities. In general, every $L/2$ time steps, a new wave of particles reaches the boundary and changes the effective creation and annihilation rates. The effective rates for times $(i-1)L/2 < t < iL/2$ are given by:

$$\begin{aligned}
\beta_A^{eff} &= 2\rho_A^{tot}(t = (i-1)L/2) \\
\beta_B^{eff} &= 2\rho_B^{tot}(t = (i-1)L/2) \\
\alpha_A^{eff} &= \alpha\left(1 - \frac{2\rho_B^{tot}(t = (i-1)L/2)}{\beta}\right) \\
\alpha_B^{eff} &= \alpha\left(1 - \frac{2\rho_A^{tot}(t = (i-1)L/2)}{\beta}\right).
\end{aligned} \tag{4.9}$$

Note that the equations for $\alpha_{A/B}^{eff}$ connect the total densities at times $(i-1)L/2$ and $iL/2$. Thus, two recursion relations are obtained:

$$\begin{aligned}
\rho_A^{tot}(t = iL/2) &= \frac{\alpha}{2}\left(1 - \frac{2\rho_B^{tot}(t = (i-1)L/2)}{\beta}\right) \\
\rho_A^{tot}(t = iL/2) &= \frac{\alpha}{2}\left(1 - \frac{2\rho_A^{tot}(t = (i-1)L/2)}{\beta}\right).
\end{aligned} \tag{4.10}$$

The time dependent solutions of these equations are

$$\begin{aligned} \rho_A^{tot}(t = L/2) &= \alpha \left(1 - \frac{2\rho_B^{tot}(t=0)}{\beta}\right) \\ \rho_B^{tot}(t = L/2) &= \alpha \left(1 - \frac{2\rho_A^{tot}(t=0)}{\beta}\right) \\ \rho_{A/B}^{tot}(t = iL/2) &= \frac{\alpha\beta}{2(\alpha+\beta)} + c\left(\frac{\alpha^2}{\beta^2}\right)^{i-2} \end{aligned} \tag{4.11}$$

where the constants c are determined by the initial conditions.
The time independent solutions of the recursions are:

$$\rho_A^{tot} = \rho_B^{tot} = \frac{\alpha\beta}{2(\alpha+\beta)}. \tag{4.12}$$

Thus for $\alpha < \beta$ the system attains in the large L limit a steady state, where in the bulk all even (odd) sites are occupied by A (B) particles with probability $\alpha\beta/(\alpha+\beta)$ (see figure 4.1). The time evolution of the total density according to eqs. (4.10) is illustrated by a Monte Carlo simulation in figure 4.6. Note that due to eqs. (4.10) the densities are bounded by $0 \leq \rho_{A/B}^{tot} \leq \alpha/2 < \beta/2$. Thus it is ensured that the system can not develop a jam during its time evolution.

4.6 Conclusion

In this chapter, a two-species driven model with deterministic bulk behavior was investigated. The mechanism for spontaneous symmetry breaking in this model was described, leading to estimates for the relevant time scales in the broken phase and proving the existence of spontaneous symmetry-breaking without further assumptions on the rates. This puts the present model in contrast to the version with stochastic bulk dynamics, where symmetry breaking could only be proven for the case of a vanishing extraction rate at the boundaries. Along the transition line, the failure of a mean-field treatment, leading to the prediction of a second asymmetric phase, was explicitly demonstrated. This result sheds new light on the longstanding discussion on the existence of a second asymmetric phase. The time evolution of the total density was described for both the symmetric and the asymmetric phase.
It would be desirable to have an exact solution for this model.

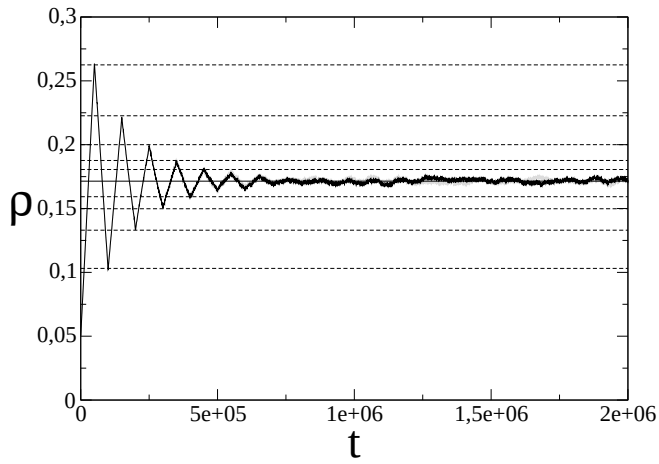

Figure 4.6: Monte Carlo time evolution of the total densities ρ_A^{tot} (black) and ρ_B^{tot} (grey) for $\alpha = 0.6$, $\beta = 0.8$, $L = 100000$. The system was started with a symmetric initial condition at densities of $\rho_{A/B}^{tot} = 0.05$. The dashed lines correspond to the densities at $t = iL/2$ according to equations (4.10).

Part II

Non-equilibrium models coupled to bulk reservoirs

Chapter 5

Introduction

In part II of this work, the effect of bulk reservoirs on non-equilibrium many-particle models is studied. The following two sections briefly discuss how bulk reservoirs can be coupled to each of the two groups of models considered in this work, namely driven-diffusive systems and model with absorbing phase transitions in the directed percolation universality class. In the following chapters the models treated in part I of this work are reconsidered with respect to the influence of the bulk reservoir.

5.1 Driven diffusive systems coupled to a bulk reservoir

The TASEP with open boundaries as introduced in subsection 2.1 can be viewed as modeling directed transport of particles from the left boundary reservoir to the right one. In the bulk, the number of particles is conserved, i.e. attachment and detachment of particles are not allowed. Recently, the consideration of two very different systems lead to studying the TASEP with bulk attachment and detachment:

- Consideration of the price dynamics in limit order markets lead to the model introduced in chapter 8 [8].
- The models of refs. [66, 67] were inspired by the motion of motor proteins along filaments.

Motor proteins are molecular machines that convert chemical energy into directed mechanical motion. In living cells there are three main families of motor proteins named myosins, dyneins and kinesins (see e.g. [68, 69]). Kinesins e.g. perform transport tasks in eucaryotic cells. These cells are too large for diffusion being an effective means of transport. Instead, directed motion is needed to transport cargo such as secretory vesicles or mitochondria across the cell. Kinesins move along microtubules, which are polymer strands acting as 'roads' inside the cell. This movement is performed in discrete steps, the step size being given by the repeat distance of the monomers in the microtubules (about 8 nm) which can be visualized in motility assays using x-ray diffraction techniques. Microtubules are polar molecules leading to kinesin performing a *directed* motion along the monomers. Microtubules have a typical length of 1000 steps. After being attached to the microtubules, the kinesins move a significant fraction of this length along the tubule before they become detached by a thermal fluctuation [70], i.e. the detachment probability is on the order of the inverse length of the microtubule (in units of steps).

Motor proteins mutually exclude each other, i.e. they can not simultaneously use the same binding site.
Attachment and detachment of motor proteins is an equilibrium process, while the directed motion of the proteins along the filament constitutes a net current and thus is intrinsically far from equilibrium.
The interplay of these equilibrium and non-equilibrium processes can be studied using lattice models such as the TASEP coupled to a *bulk reservoir*. In [67, 70, 71] models of this type are studied using a *single* reservoir with a concentration gradient which couples to both the ends of the TASEP as well as to the bulk.
In contrast to that, in this work the interplay of *two* types of reservoirs, namely *boundary* and *bulk reservoirs* (see figure 5.1), is studied.

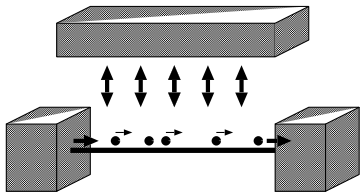

Figure 5.1: Illustration of the two types of reservoirs in non-conserving driven-diffusive systems with open boundaries: *Boundary reservoirs* causing a particle current in the steady state and the *bulk reservoir* which by itself would lead to an equilibrium steady state of the system.

The TASEP with Langmuir kinetics

The TASEP (see section 2.1) is one of the simplest driven models. Except for the boundary processes the particle number is a conserved quantity in the bulk of the lattice. The theory of boundary induced phase transitions explains the phase diagram quantitatively in terms of the dynamics of shocks [22]. In the stationary state these shocks exist as an upward density shock along the coexistence line between the high and low density phases, i.e., they connect a region with low density to the left of the shock position with a high density region to its right. On this first-order transition line of the TASEP, the shock is delocalized and performs random walk between the boundaries of the system.
In contrast to the TASEP, the independent single-site absorption and desorption kinetics of particles, termed 'Langmuir kinetics' (LK), is well understood within the framework of equilibrium statistical physics [72]:

If attachment and detachment rates are given by ω_a and ω_d, respectively, the equilibrium particle density attained by the system is given by

$$\rho_{\mathrm{LK}} = \frac{\omega_a}{\omega_a + \omega_d}. \tag{5.1}$$

The action of Langmuir kinetics on a lattice can be viewed as exchange of particles with a *bulk reservoir* of constant density ρ_{LK} with rate $\omega_a + \omega_d$ at all lattice sites independently.
In ref. [66] the interplay of these two simple models, the TASEP with 'Langmuir kinetics' (LK) was considered. Being an equilibrium process, LK is well understood, while the combined process of TASEP and LK shows the new feature of a localized shock in the density profile of the stationary state [66]. The model is defined by equipping the TASEP with the additional feature of local particle creation at empty sites with rate ω_a and annihilation with rate ω_d (see fig. 5.2) [8, 66]. In the thermodynamic limit $L \to \infty$ there are

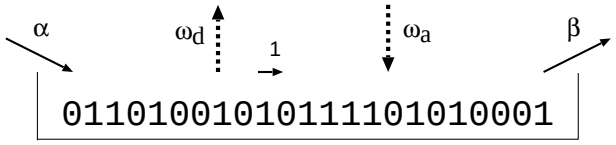

Figure 5.2: Possible processes and their rates in the model of the TASEP with Langmuir kinetics

three regimes to be distinguished:

- If ω_a and ω_d are of an order larger than $1/L$ the steady state of the system will be that of Langmuir kinetics, i.e., there will be a uniform density of $\rho_{\mathrm{LK}} = \omega_a/(\omega_a + \omega_d)$ in the system (up to boundary layers). In this regime, the driving reservoirs at the boundaries have no effect in the interior of a large system, as any particle that is injected at the left boundary will be annihilated before reaching the right boundary.

- In case of ω_a and ω_d being of smaller order than $1/L$, the local kinetics is negligible and the system will behave as the TASEP. Here, the action of the particle reservoir governing the Langmuir kinetics is negligible compared to the boundary reservoirs in large systems.

- The case of the local rates being of order $1/L$ is the most interesting one and will be investigated further on. In this case, the Langmuir reservoir and the boundary reservoirs have comparable strength. While the

former one couples with a rate of order $1/L$, but on L sites, the latter ones couples at one site each with rates of order 1.
As pointed out in [73], the interesting effects originating from the interplay of the reservoirs are also observed in the special case of the LK rates being of order $1/L^{1+a}$, where $0 \leq a < 1$ and $\rho_- = 1 - \rho_+$.

Phase diagram of the TASEP with LK

In [66,74] the phase diagram of the TASEP with Langmuir kinetics was investigated using Monte Carlo simulations and a mean field approach. Writing

$$\omega_a = \Omega_a/L, \quad \omega_d = \Omega_d/L \tag{5.2}$$

the phase diagram can be formulated in terms of Ω_a, Ω_d, ρ_- and ρ_+. Defining

$$K = \frac{\Omega_a}{\Omega_d}, \tag{5.3}$$

the cases $K \neq 1$ and $K = 1$ have to be distinguished. In case of $K \neq 1$, three phases are found [66]:

- A low density phase, where the left boundary density ρ_- determines the density profile in the bulk. In contrast to the TASEP, the profile is non linear, where the curvature depends on the strength of the Langmuir kinetics.
- In the high density phase, the right boundary density ρ_+ determines the density profile in the bulk. Also here, in contrast to the TASEP, the profile is not flat.
- The coexistence phase: Here, a *localized* shock separates a region of low density from a region of high density (see figure 5.3). This is in contrast to the first order transition line in the TASEP, where the shock position is diffusing in the system, leading to a linear steady state density profile. In the steady state of the TASEP with LK, the shock position fluctuates around a fixed position, leading to a localized shock with a width of order $1/\sqrt{L}$.

The equations for bulk dynamics of the TASEP with LK are

$$\frac{dn_i}{dt} = n_{i-1}(1 - n_i) - n_i(1 - n_{i+1}) + \omega_A(1 - n_i) - \omega_D n_i, \tag{5.4}$$

while the boundary equations read:

$$\begin{aligned} dn_1/dt &= \alpha(1 - n_1) - n_1(1 - n_2)\,, \\ dn_N/dt &= n_{N-1}(1 - n_N) - \beta n_N\,. \end{aligned} \tag{5.5}$$

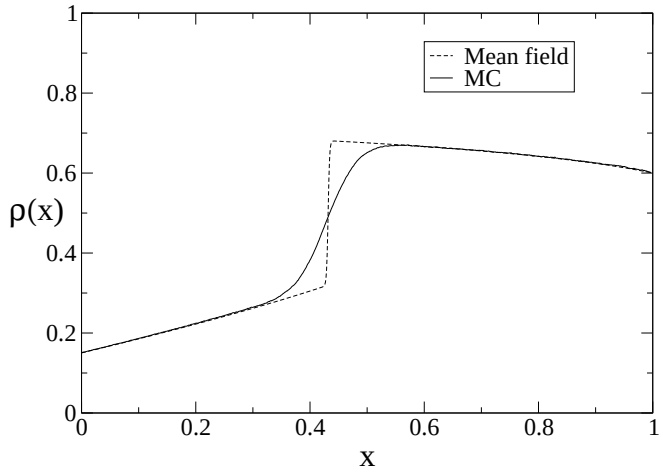

Figure 5.3: Plot of the average particle density ρ versus the rescaled coordinate x ($site\ number/L$) of a localized density shock in the ASEP with Langmuir kinetics. Parameters are $\rho_- = 0.15$, $\rho_+ = 0.6$, $\Omega_a = 0.3$ and $\Omega_d = 0.1$. We show the results of both Monte Carlo simulations for L=1000 and the mean field approach.

In [66], a mean field approach with subsequent coarse-graining of the lattice with lattice constant $1/L$ to a continuum was performed to obtain the following equation:

$$\frac{\varepsilon}{2}\partial_x^2\rho + (2\rho - 1)\partial_x\rho + \Omega_A(1-\rho) - \Omega_D\rho = 0\,. \tag{5.6}$$

In the limits $L \to \infty$ and $\epsilon \to 0$, mean-field density profiles as well as the mean-field phase diagram are obtained from this equation. Comparison with Monte Carlo simulations reveals that the mean-field approach indeed captures the features of the stochastic model. The reason for this agreement will be explained in the next chapter.
An example for a comparison between Monte Carlo and mean-field density profiles in the coexistence phase is displayed in fig. 5.3.
The mean field phase diagram for $K \neq 1$ is shown in fig. 5.4.

In case that $\Omega_a = \Omega_d$, i.e $K = 1$, the phase diagram exhibits seven phases [74]. Here, the density profiles are composed out of parts with constant slope and flat parts. The phase diagram and density profiles can be easily constructed using eq. (5.6).

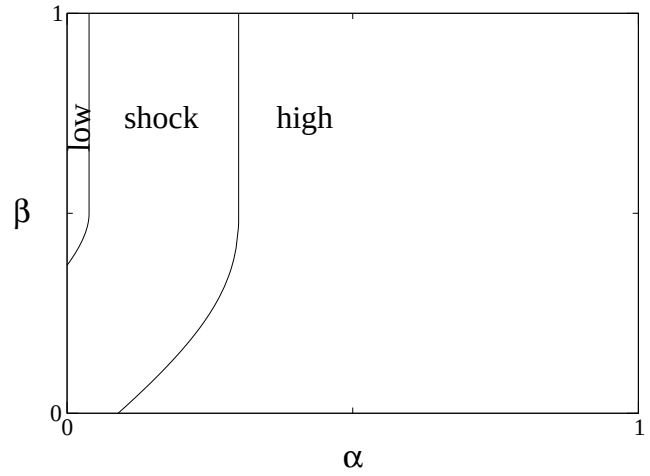

Figure 5.4: Phase diagram for the TASEP with LK at $\Omega_a = 0.3$ and $\Omega_d = 0.1$.

Compared to the TASEP, it is remarkable that adding an additional source of noise, i.e. the Langmuir kinetics, leads to the *localization* of the shock. The movement of the shock position can indeed be described as a single particle random walk in a spatially dependent potential [74, 75]. In ref. [75] it was demonstrated that this random walk picture can be used to recover the phase diagram.
In the following chapter, we argue why the mean-field approach for the TASEP with Langmuir kinetics is successful and demonstrate its failure for related models. We propose a general hydrodynamic equation that allows to treat the class of models of which the TASEP with LK is the simplest.
Chapter 7 covers driven models with periodic boundary conditions and non-conserving reaction kinetics.
In chapter 8 a toy model for a limit order market using the TASEP with LK is introduced.
Spontaneous symmetry breaking in driven-diffusive models which was already treated in chapter 4 is considered again under the influence of Langmuir kinetics in chapter 9.

5.2 Directed percolation in an external field

Directed percolation (DP) as introduced in subsection 2.3 is a non-equilibrium critical phenomenon. In contrast to driven-diffusive systems there are usually

no boundary reservoirs considered and the bulk dynamics is not conserving. Instead, in models belonging to the DP universality class, there are competing processes of proliferation and annihilation of active particles. The rate of both types of processes is controlled by a single parameter p which can be used to drive the system from the active to the absorbing phase. Especially, no active particles can be created from the lattice devoid of active particles, being the absorbing state.
This spontaneous creation of active particles can be accomplished by coupling the system to a bulk reservoir of constant density *unidirectionally* (see fig. 5.5). Let the transition rate for particles from the reservoir with unit density

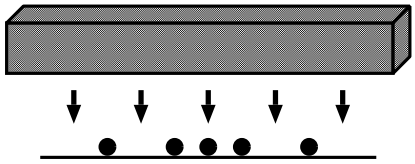

Figure 5.5: Sketch of a bulk reservoir coupling *unidirectionally* to each lattice site in a model with a DP transition.

to each lattice site be given by h. This unidirectionally coupled bulk reservoir implements an external field creating particles spontaneously at empty sites with rate h. Clearly, the action of this field will remove the phase transition to the absorbing state.
A coupling of the bulk reservoir in the reverse direction (or a bidirectional coupling) is not considered due to the following reason: A hopping process of an active particle into the reservoir is equivalent to an annihilation process. As the latter is anyway implemented in any process showing an absorbing phase transition, the presence of the reservoir would just increase the annihilation rate and yield a shift of the critical point of the transition.
The effect of the external field is analogous to that of an external magnetic field in a ferromagnet. Especially, the scaling behavior of the system around the critical point as a function of p and h can be studied, which is the topic of chapter 10. In section 10.1 the universal scaling behavior of site directed percolation is studied in various dimensions. Furthermore, the scaling behavior of the pair-contact process in an external field is considered in comparison to that of directed percolation in section 10.2.

Chapter 6

Localization of shocks in driven diffusive systems without particle number conservation

6.1 Introduction

As described in subsection 5.1, in ref. [66] the interplay of the TASEP with non-conserving dynamics, termed Langmuir kinetics, was investigated. Parmeggiani et.al. presented not only Monte Carlo simulations but derived also a mean field equation for the density profile which was shown to coincide with the simulation profiles. We argue here that the mean field approximation can not be used in general. The coincidence with the Monte Carlo results in [66] is due to lack of correlations in the true steady state of the TASEP. We claim that the stationary density profile can be derived in general using a hydrodynamic equation taking correlations into account (in case of the TASEP this equation is equal to that obtained within a mean field approach). For the Katz-Lebowitz-Spohn (KLS) model, which is a generic model of interacting driven diffusive systems [19,21] (see subsection 2.1.2) we show that this hydrodynamic equation correctly describes the density profiles on a quantitative level, while a mean field approach would fail to reproduce even basic qualitative features of the system, e.g., phase separation into three distinct density regimes.
The results presented in this chapter were obtained in collaboration with V. Popkov, A. Rakos and A. Kolomeisky and published in ref. [7].

6.2 Hydrodynamic equation

In the following we are interested in the $L \to \infty$ limit which we perform by tuning the lattice spacing $a = 1/L \to 0$ and rescaling of time $t = t_{\text{lattice}}/L$ (Eulerian scaling) to get the continuous (hydrodynamic) limit of the model. In this framework $\Omega_{a,d}$ are the attachment/detachment rates per unit length. We claim that the hydrodynamic equation describing the time dependence of the local density $\rho(x)$ for a general driven diffusive system with Langmuir kinetics takes the form

$$\frac{\partial}{\partial t}\rho + \frac{\partial}{\partial x}j(\rho) = \mathcal{L}(\rho), \tag{6.1}$$

where $j(\rho)$ is the *exact* current in a driven diffusive system with homogeneous density ρ without LK and $\mathcal{L}(\rho)$ the source term describing the Langmuir kinetics. Here, we consider only that choice of $\mathcal{L}(\rho)$ which corresponds to the process depicted on fig. 5.2:

$$\mathcal{L}(\rho) = \Omega_a(1 - \rho(x,t)) - \Omega_d\rho(x,t) \tag{6.2}$$

Other choices of $\mathcal{L}(\rho)$, which correspond to non-conserving dynamics comprising several sites are discussed e.g. in ref. [75].

As is usually done in the rigorous derivation of the hydrodynamic limit of conservative systems [76], our nonconservative eq. (6.1) implicitly assumes that the system is locally stationary because the exact form of the stationary flux is used. We argue that this assumption is justified since the nonconservative part of the dynamics of the system at macroscopic scale is so slow that locally the system reaches stationarity with respect to the conservative part of the dynamics. Any finite perturbation caused by the nonconservative dynamics would travel a macroscopic distance and hence dissipate before interacting with another perturbation. Hence the hydrodynamic description (after time rescaling $t \to \epsilon t$) is adequate for describing the full dynamics. For physical insight in the formation of shocks one needs other tools which are discussed below.

Rewriting equation (6.1) by using that $\partial_t \rho(x,t) = 0$ in the stationary state and $\partial_x j = \partial j/\partial\rho \cdot \partial\rho/\partial x$ yields for the stationary density profile $\rho(x)$:

$$v_c(\rho)\frac{\partial \rho(x)}{\partial x} = \mathcal{L}(\rho). \tag{6.3}$$

Here, $v_c = \partial j/\partial\rho$ is the collective velocity, i.e., the drift velocity of a center of mass of a local density perturbation on a homogeneous stationary background with the density ρ (for a system with the Langmuir kinetics switched off) [3, 22]. The stationary density profile has to satisfy (6.3) as well as the boundary conditions $\rho(0) = \rho_-$ and $\rho(1) = \rho_+$. As equation (6.3) is of first order there will be in general no smooth solution fitting both boundary conditions. In the original lattice model this discrepancy is resolved by the appearance of shocks and/or boundary layers. To regularize the problem, one can add to (6.1) and correspondingly to (6.3) a vanishing viscosity term

$$v_c(\rho)\frac{\partial \rho(x)}{\partial x} = \mathcal{L}(\rho) + \nu\frac{\partial^2 \rho(x)}{\partial x^2}, \tag{6.4}$$

where $\nu > 0$ is of order of $1/L$. This term makes the hydrodynamic equation second order and ensures a smooth solution fitting both boundary conditions. The shock has then a width of order $1/L$ (see [66]), i.e., in the thermodynamic limit the rescaled solution becomes discontinuous. We claim that equation (6.4) gives the same result in the $L \to \infty$ limit as Monte Carlo simulations, therefore it can be used as a tool to compute the stationary density profile. The main difference between (6.4) and MC is that the former does not take fluctuations into account which leads to a shock width of order $1/L$ while in a MC simulation after averaging it is of the order of $1/\sqrt{L}$ due to the fluctuation of the shock position.

The stationary density profile for a given $j(\rho)$ and parameters Ω_a, Ω_d, ρ_- and ρ_+ can be derived from the flow-field of the differential equation (6.3) by using the rules formulated and explained below:

(A) In the interior of the lattice the stationary density profile either follows a line of the flow field of the differential equation (6.3) or makes a jump. Jumps can only occur between densities yielding the same current, i.e., *the current is continuous in the interior of the lattice.*

(B) Let $\rho'_\pm$ be defined as limiting left and right densities with the boundary layers cut away:

$$\rho'_- = \lim_{x\to+0}\rho(x), \quad \rho'_+ = \lim_{x\to1-0}\rho(x),$$

where $\rho(x)$ is the stationary profile in the hydrodynamic limit. The boundary layer at $x = 0$ (i.e., if $\rho_- \neq \rho'_-$) has to satisfy the following condition:

$$\text{if } \rho_- < \rho'_- \text{ then } j(\rho) > j(\rho'_-) \text{ for any } \rho \in (\rho_-, \rho'_-) \tag{6.5}$$
$$\text{if } \rho_- > \rho'_- \text{ then } j(\rho) < j(\rho'_-) \text{ for any } \rho \in (\rho'_-, \rho_-) \tag{6.6}$$

The condition for the stability of the boundary layer at $x = 1$ (if there is) is similar:

$$\text{if } \rho'_+ < \rho_+ \text{ then } j(\rho'_+) < j(\rho) \text{ for any } \rho \in (\rho'_+, \rho_+) \tag{6.7}$$
$$\text{if } \rho'_+ > \rho_+ \text{ then } j(\rho'_+) > j(\rho) \text{ for any } \rho \in (\rho_+, \rho'_+) \tag{6.8}$$

(C) Shocks between a density ρ_l to the left of the shock and ρ_r to the right of the shock are stable only if they are stable in the absence of Langmuir kinetics [3, 20].

Remarks:

- Although LK does not conserve locally the number of particles, eq. (6.1) with the vanishing viscosity added (6.4) can be rewritten formally in the form

$$\frac{\partial\rho(x,t)}{\partial t} + \frac{\partial}{\partial x}\tilde{j}(x,t) = 0, \quad \tilde{j}(x,t) = j(\rho) - \int_A^x \mathcal{L}(\rho)dx - \nu\frac{\partial\rho}{\partial x} - \mathcal{F}(t) \tag{6.9}$$

where $\mathcal{F}(t)$ is some time-dependent function. Suppose that there is a shock at the position X_0 connecting the densities ρ_l and ρ_r. The mass transfer across the shock is

$$\frac{\partial}{\partial t}\int_{X_0-0}^{X_0+0}\rho(x,t)dx = \tilde{j}(X_0+0,t) - \tilde{j}(X_0-0,t) = j(\rho_r) - j(\rho_l), \tag{6.10}$$

since the Langmuir term and the viscosity term change only infinitesimally across the shock. In the stationary state, the RHS of (6.10) vanishes which explains the rule (A).

- The rule (B) is due to the fact that in the boundary layer of the vanishing length $\delta l \to 0$, the LK term in (6.9) can be neglected. Consequently, for the stationary current at the boundaries we have $\tilde{j}(x) = j(\rho(x)) - \nu\frac{\partial\rho}{\partial x} = J$, which yields the known maximization/minimization principle [3,23], and is equivalent to rule (B). Indeed at the left boundary $J = j(\rho'_-)$ (see (6.5) for notations), and if e.g., $\rho_- < \rho'_-$, then $\frac{\partial\rho}{\partial x} > 0$. Consequently, we obtain $j(\rho_-) = J + \nu\frac{\partial\rho}{\partial x} > J$, which is exactly (6.5). Analogously one obtains (6.6)-(6.8).

- The rule (C) is explained by the marginal role the Langmuir kinetics plays locally in space and in time. Firstly, LK is very slow locally for large L (see (5.2)), and secondly, it acts "orthogonally" on the particle distribution, not affecting directly the particle motion. Hence, the local perturbations will still spread with the velocity corresponding to the local density level ρ, thus rendering the same stability conditions for a shock as for the diffusive system without LK.

  Condition (C) is easy to check geometrically through the current-density relation: an upward (downward) shock is stable if the straight line connecting the points $(\rho_l, j(\rho_l))$ and $(\rho_r, j(\rho_r))$ stays below (above) the $j(\rho)$ curve [20,23]. Because of criterion (A) these lines are always horizontal in this case which gives zero mean velocity (but not localization) for the shock in absence of Langmuir kinetics.

- In the cases we have considered (ASEP, KLS model), the rules (A)-(C) define an unique stable solution (see an Appendix) and we believe that this is true also in general case, i.e., for arbitrary $j(\rho)$ dependence and the given choice (6.2) of Langmuir kinetics.

In the following we apply the general theory to specific models.

6.3 Revisiting the ASEP with Langmuir kinetics

Using the differential equation (6.3) and the rules given above we reconsider the ASEP with Langmuir kinetics [8,66]. Here, the current-density relation is given by $j(\rho) = \rho(1-\rho)$, which yields $v_c(\rho) = 1 - 2\rho$. Thus equation (6.3) becomes

$$\big(1 - 2\rho(x)\big)\partial_x\rho(x) = \Omega_a - (\Omega_a + \Omega_d)\rho(x), \tag{6.11}$$

which is identical to the mean field equation (5.6) [66] in the thermodynamic limit. We would like to stress that this coincidence is caused by the fact

that the mean field current-density relation for the TASEP is exact. As is demonstrated below, equation (6.3) also holds when this is not the case, as e.g. for the one-dimensional KLS model.

Due to rule (A) as stated above (continuity of the current in the interior of the lattice) shocks in the interior can only occur in the case that $\rho_l = 1 - \rho_r$, as $j(\rho)$ is symmetric to $\rho = 1/2$. Rule (C) (stability of the shock) furthermore requires that $\rho_r > \rho_l$. These observations coincide with the findings of [66].

We also applied our rules to k-hop exclusion models [77] (with LK added), which are a generalization of the TASEP with stationary product measures and asymmetric current-density relations. Due to this fact shocks appear, which are non-symmetric with respect to $\rho = 1/2$. MC simulations are in full accord with our predictions [78].

6.4 KLS model with Langmuir kinetics

A much studied one-dimensional driven diffusive system with interactions between the particles is the following variant of the KLS model [6, 20, 23]: The bulk hopping rates as defined in eq. (2.1) depend on two parameters δ and ϵ. At site 1 particles can enter the lattice provided the target site is empty. The rate depends on the state of site 2. Similarly, particles can leave the system at site L with a rate depending on the state of site $L-1$. The boundaries mimic the action of reservoirs with densities ρ_- and ρ_+. For $\rho_- = \rho_+$ the stationary state is that of a one-dimensional Ising model with boundary fields. The current-density relation can be calculated exactly using transfer matrix techniques [20]. It turns out that for strong enough repulsion between the particles ($\epsilon \gtrsim 0.9$) a current-density relation with two maxima arises (see fig. 6.1). The parameter δ determines the skewness of $j(\rho)$ with respect to the vertical line $\rho = 1/2$. For $\delta = 0$, the system has particle-hole symmetry resulting in $j(\rho)$ being symmetric with respect to $1/2$. For simplicity we consider this case in the rest of the chapter.

The phase diagram of this family of models with strong particle repulsion is known to exhibit 7 different phases, among them two maximal-current and one minimal-current phase. The phase diagram is determined by the interplay of diffusion, branching and coalescence of shocks [23].

When equipping these models with Langmuir kinetics one expects that a very rich phase diagram with many more than the original 7 phases will appear. We will not attempt to give this full phase diagram here, but instead present two new features, which cannot be observed in systems without a concave region in the current-density relation: localized downward shocks and double shocks.

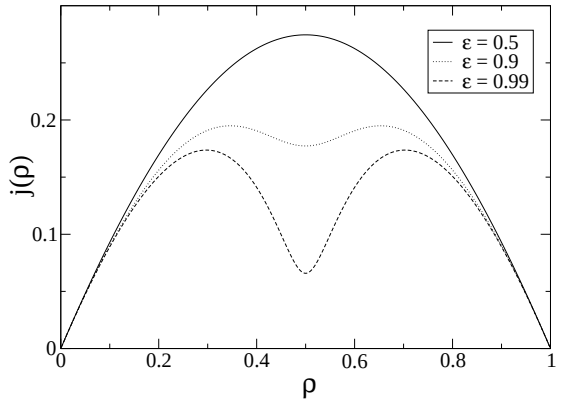

Figure 6.1: Current-density relation for the one-dimensional KLS model for various ϵ.

6.5 Localized downward shocks

In the regime where the current-density relation of the KLS model exhibits two maxima at densities ρ_1^* and ρ_2^*, where $\rho_1^* < \rho_2^*$ and a minimum at $\rho = 1/2$ (at $\delta = 0$) there is a region where downward shocks are stable according to [20, 23] (and rule (C)). These are characterized by $\rho_l \in (0.5, \rho_2^*)$ and $\rho_r \in (\rho_1^*, 0.5)$. This suggests that localized downwards shocks may appear when introducing the kinetic rates. Indeed, in the KLS model with Langmuir kinetics for certain values of the boundary densities ρ_- and ρ_+ ,which strongly depend on the kinetic rates Ω_a and Ω_b, one gets a stable downward shock according to rules (A,B,C). We give an example for this case on fig. 6.2.

One can see that employing the general theory described above yields a stationary profile with a localized downward shock, which coincides with the MC results up to finite size effects, while a simple mean field approach would fail as it would not be able to capture the difference between the KLS model with $\epsilon > 0$ and the TASEP (KLS with $\epsilon = 0$).

6.6 Localized double shocks

Let $\rho'_{1,2}$ be defined as the inflection points of the current-density relation ($\rho'_1 < \rho'_2$). As is known from the studies of the KLS model [20, 23], if we start an infinite system from a step-like initial density profile with $\rho_- \in (\tilde{\rho}_1, \rho'_1)$

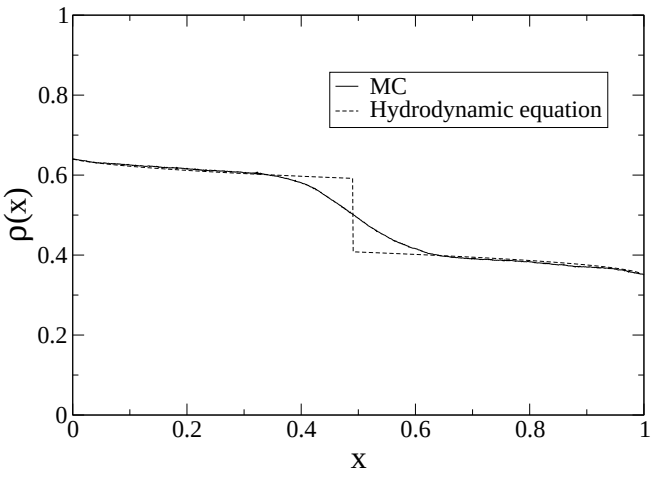

Figure 6.2: Density of particles ρ versus rescaled coordinate x ($site\ number/L$) in a localized downward shock in the KLS model with Langmuir kinetics. Parameters are $\rho_- = 0.64$, $\rho_+ = 0.35$, $\Omega_a = \Omega_d = 0.05$. We show the results of both hydrodynamic equation and Monte Carlo simulation for $L = 1000$. The smoothness of the MC result is due to the fluctuation of the shock position [75].

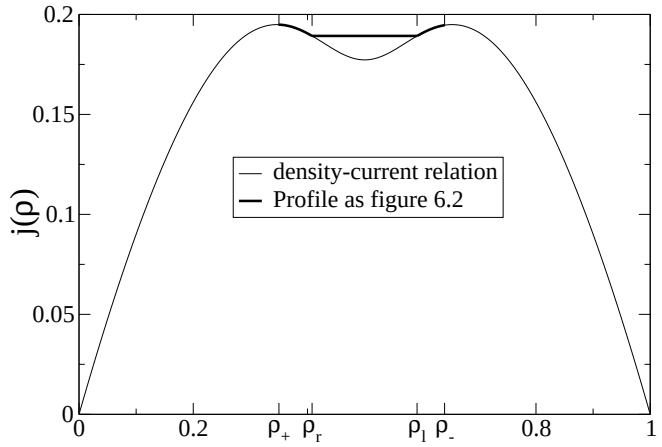

Figure 6.3: Path in the current-density relation for the profile shown in figure 6.2.

on the left and $\rho_+ \in (\rho_2', \tilde{\rho}_2)$ on the right, we get a time-dependent solution having two shocks: One of these has negative mean velocity, while the other has positive and in the middle there is an expanding region with $\rho = 1/2$ (for $\delta = 0$) which corresponds to the minimal current phase in a system with open boundaries [20, 23].

This leads us to the conjecture that introducing the kinetic rates for certain values of $\rho_-, \rho_+, \Omega_a, \Omega_d$ one may achieve a stable double shock structure. In fig. 6.4 we present an example for such a case. Application of rules (A,B,C), which is presented in detail in section 6.8, yields the same double shock structure as the MC up to finite size effects. Note, that a simple mean field approach could not predict a double shock.

6.7 Conclusions

In this chapter we presented a hydrodynamic equation which, together with some rules treating the discontinuities, correctly describes the stationary states of one-dimensional driven diffusive systems with Langmuir kinetics and open boundaries. It captures both systems without correlations in a steady state (as e.g. the TASEP and the k-hop exclusion models) and systems with correlations as the KLS model. For the latter the two new phenomena of a stationary localized downward shock and a localized double shock (corresponding to phase separation to three distinct regions) were presented which a mean field approach would not reproduce. The exact current of driven diffu-

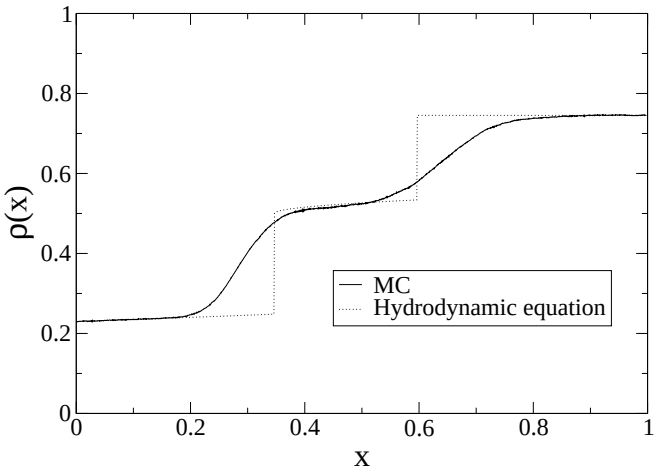

Figure 6.4: Density of particles ρ versus rescaled coordinate x ($site\ number/L$) in a localized double shock in the KLS model with Langmuir kinetics. Parameters are $\rho_- = 0.23$, $\rho_+ = 0.745$, $\Omega_a = 0.03$ and $\Omega_d = 0.01$. We show the results of both hydrodynamic equation and Monte Carlo simulation for $L = 1000$. The smoothness of the MC result is due to the fluctuation of the shock position [75].

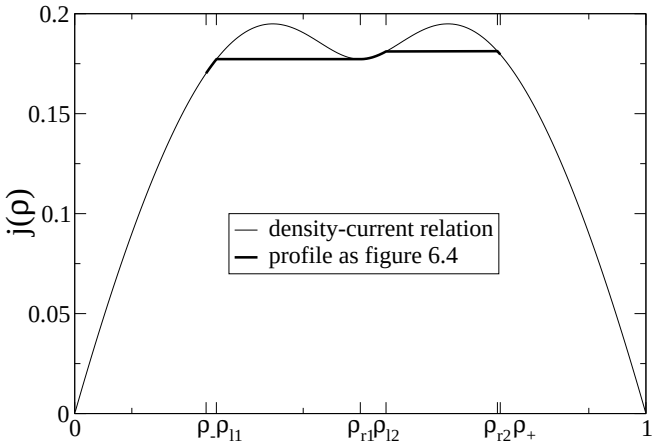

Figure 6.5: Path in the current-density relation for the profile shown in figure 6.4.

sive systems without LK enters the hydrodynamic description since the bulk has sufficient time to relax between subsequent annihilation/creation events. An interesting, paradoxical feature of these phenomena is that fluctuating shocks get localized due to extra noise (LK), which is highly unexpected.

6.8 Appendix: Double shock density profile

Here we demonstrate how one determines the stationary density profile using the rules (A), (B) and (C) from subsection 6.2. As an example we take the parameters which yield a double (localized) shock structure in the KLS model ($\rho_- = 0.23$, $\rho_+ = 0.745$, $\Omega_a = 0.03$ and $\Omega_d = 0.01$). The KLS-model parameters are: $\delta = 0, \epsilon = 0.9$ (see subsection 6.4).

First suppose that there is a boundary layer at $x = 0$. According to rule (B) it is stable only if $\rho'_- > 1 - \rho_- = 0.77$. If this is the case then in the bulk there is no allowed jump since these trajectories of the flow-field (see fig. 6.6) stay always above $\rho = 0.75$ (rules (A) and (C)) which yields $\rho'_+ > 0.75$. But then the boundary layer at $x = 1$ does not satisfy rule (B). This contradiction shows that there is no boundary layer at $x = 0$. One can use the same argument to show that there is no boundary layer at $x = 1$ either.

Now one can see that the stationary density profile close to the left boundary follows the line of the flow-field for which $\rho(x = 0) = \rho_- = 0.23$. Since there is no boundary layer at the right end it is clear that somewhere in the bulk it has to make a jump.

Note that this trajectory crosses the line $\rho = \tilde{\rho}_1$ at $x = x_1$. Suppose that the jump takes place before at $x < x_1$. In this case, according to rule (A) it would jump over $\tilde{\rho}_2 = 1 - \tilde{\rho}_1$ which would result in a boundary layer at $x = 1$ which is not allowed. If the jump takes place at $x > x_1$ then $\rho_1^* < \rho_r < 0.5$ and since from this region there is no allowed jump it would end up at $\rho_1^* < \rho'_+ < 0.5$ resulting again in an unstable boundary layer on the right side. This shows that the jump is located at $x = x_1$ and from here the density profile follows the trajectory which starts at $x = x_1$ with the value $\rho = 0.5 + 0$.

One can easily see that we need another jump to connect this trajectory with the one which ends at $x = 1$ with $\rho = \rho_+$. Applying rule (A) (continuity of the current) we can get the point x_2 where the second jump is located.

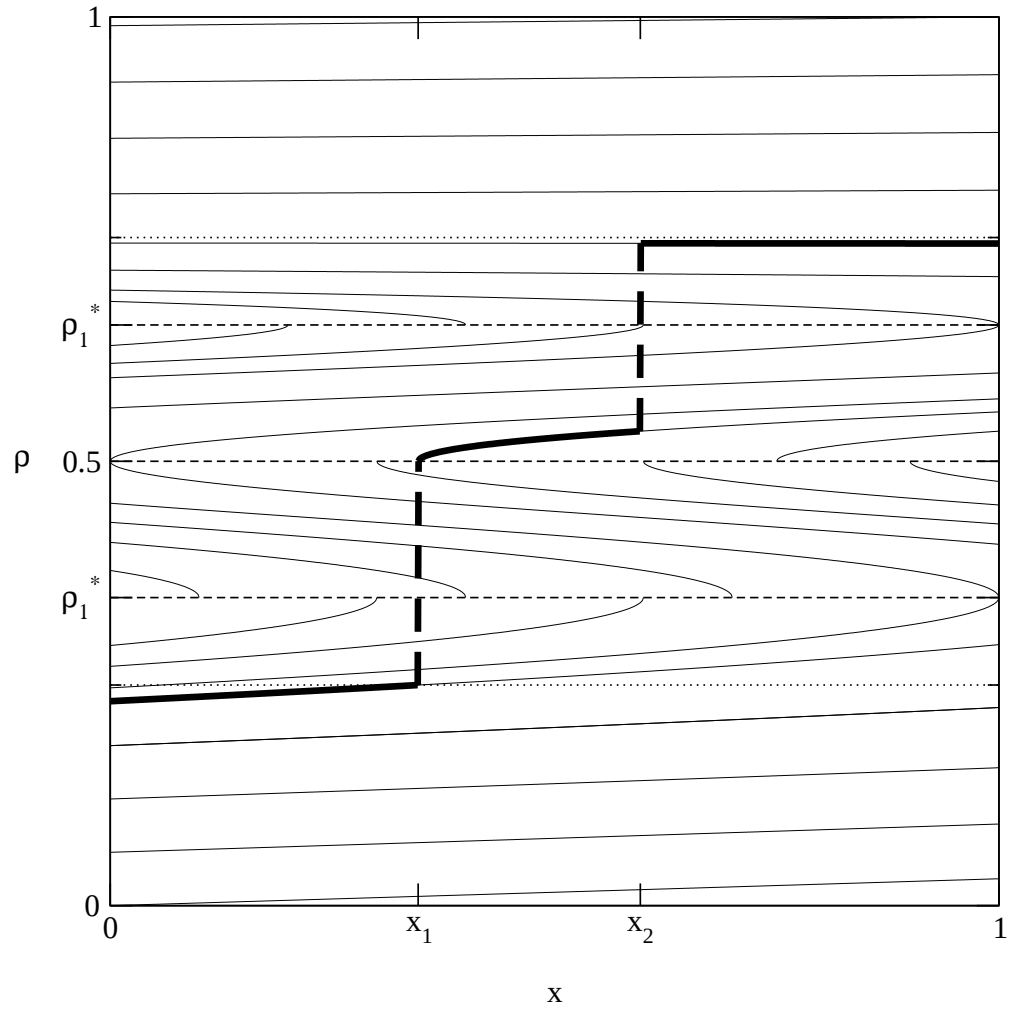

Figure 6.6: The flow field of the hydrodynamic equation in the KLS model with Langmuir kinetics. Parameters are $\delta = 0, \epsilon = 0.9, \Omega_a = 0.03, \Omega_d = 0.01$. The thick lines show the stationary density profile for $\rho_- = 0.23, \rho_+ = 0.745$ given by the rules (A,B,C). The dotted lines are $\rho = \tilde{\rho}_1 \approx 0.24821$, $\rho = \tilde{\rho}_2 \approx 0.75178$ (see subsection 6.6 for notations). The axes: x is a rescaled coordinate (*site number*$/L$), $\rho(x)$ is an average density of particles at point x.

Chapter 7

Phase transitions in non-conserving driven models with periodic boundaries.

7.1 Introduction

In ref. [66] a driven diffusive system with open boundary conditions and reaction kinetics having rates scaling with the inverse system size was investigated (see subsection 5.1). In the previous chapter it was concluded that for large L due to the $1/L$ scaling, successive events of the kinetics are sufficiently rare, so that locally the conservative driven dynamics can relax to its steady state between reaction events [7]. In this case, the competition between the boundary effects and those of the reaction dynamics lead to new phenomena, most prominently to localized shocks. In the thermodynamic limit any dynamics scaling with $1/L^{1+a}$ with $a > 0$ is irrelevant in this case, except for $a < 1$ on a special line in parameter space [73].
In contrast to the system with open boundary conditions, the total density in a *periodic* driven system with reaction kinetics is always governed by this kinetics. If successive events of the reaction kinetics occur on average on a time scale shorter than the relaxation time of the driven dynamics, the presence of the kinetics will locally affect the correlations and thus the current-density relation in the system. In contrast, if the kinetics is slow enough to allow the driven dynamics to locally relax to its steady state between successive events, the correlations in the system will be as in absence of the kinetics.
The relevant relaxation time scale of the systems considered here scales with the system size as L^z, where z is the dynamical exponent of the KPZ universality class [3]. Therefore, reaction kinetics with rates scaling like $L^{-3/2}$ or slower lead to correlations as given by the driven dynamics on a ring. If the driven dynamics is such that no correlations arise, as e.g. for the ASEP, the treatment is similar to the infinite diffusion case considered in [79]. The system can thus be described by the total particle number N:

$$\frac{\partial}{\partial t}\langle N\rangle = \frac{\partial}{\partial t}\sum_{i=1}^{L}\langle n_i\rangle = \sum_{i=1}^{L}\langle S_i\rangle. \tag{7.1}$$

Here, S_i corresponds to the reaction kinetics, evaluated at site i. For large systems and uniform steady states, the system can be described by its density ρ. Equation (7.1) then simply becomes

$$\frac{\partial \rho}{\partial t} = S(\rho). \tag{7.2}$$

Thus any uniform steady state density corresponds to a node of the source term $S(\rho)$. The possibility of non-uniform steady states is discussed in subsection 7.5.
Assuming a uniform steady state solution with $\rho = c$ and $S(c) = 0$, its

stability can be investigated by linear stability analysis. Let $\delta\rho$ be a small perturbation, so that $\rho = c + \delta\rho$. Inserting into equation (7.2) and keeping only terms up to first order in $\delta\rho$ yields:

$$\frac{\partial(\delta\rho)}{\partial t} = S'(c)\delta\rho \tag{7.3}$$

This implies two things:

- Stable uniform steady states with density $\rho = c$ have to fulfill $S(c) = 0$ and $S'(c) < 0$. The latter condition ensures that perturbations diminish in time.
- The form of the density-current relation $j(\rho)$ or that of the collective velocity v_c are irrelevant for stability. All that matters are the correlations created by the driven dynamics, as this affects the source term $S(\rho)$. Models with identical correlations but different density-current relations (such as k-step exclusion processes) have the same stable uniform steady states.

In the following several kinds of reaction kinetics for both the TASEP and the KLS model are investigated.

7.2 The periodic TASEP with reaction kinetics

The occurrence of phase transitions depends on the type of reaction kinetics, i.e. single-site, two-site or higher order interactions. As the periodic TASEP does not exhibit correlations in the steady state, contributions of multiple point interactions to the source term can be obtained trivially. As the density in the TASEP is restricted to the interval $[0, 1]$, the following requirements for $S(\rho)$ hold: $S(0) \geq 0$ and $S(1) \leq 0$.

7.2.1 Single-site interaction

The most general source term in this case is given by:

$$S(\rho) = A(1 - \rho) - B\rho. \tag{7.4}$$

Thus, there is only one stationary density $\rho_{\mathrm{LK}} = A/(A + B)$ which is stable for all A, B. This density is the equilibrium density of Langmuir kinetics as mentioned in section 5.1. No phase transitions are possible in this case.

This single-site dynamics corresponds to coupling a periodic system to a *bulk reservoir* of density ρ_{LK} exchanging particles with the system at unit rate at each site independently.
Although multiple-point interactions can *not* be formulated as the action of a bulk reservoir, they shall be considered in the following as they lead to a variety of interesting phase transitions.

7.2.2 Two-site interaction

All possible processes for the kinetics and their contribution to the source term are listed in table 7.1. In a quantum Hamiltonian formulation the operators for two site interactions are four-by-four matrices, having 16 entries. The four diagonal entries are fixed by the normalization in each column, leaving 12 independent processes (see e.g. [80]). These processes are listed in table 7.1. Other processes can be expressed as combined actions of these processes, e.g. particle creation at a single site by the processes with rates D and G. For a large system, the source term can generally be written as

$$S(\rho) = \delta p \rho - \Lambda \rho^2 + \kappa h. \tag{7.5}$$

Table 7.1: The configuration of adjacent lattice sites before ($\mathcal{C}$) and after ($\mathcal{C}'$) an event. Empty sites are marked by $\circ$, and occupied sites by $\bullet$. $p(\mathcal{C} \to \mathcal{C}')$ denotes the contribution to the source term $S(\rho)$. Here, $c > z = 3/2$.

$\mathcal{C}$	$\mathcal{C}'$	$p(\mathcal{C} \to \mathcal{C}')$
$\circ\circ$	$\circ\bullet$	$L^{-c}A(1-\rho)^2$
$\circ\circ$	$\bullet\circ$	$L^{-c}B(1-\rho)^2$
$\circ\circ$	$\bullet\bullet$	$L^{-c}2C(1-\rho)^2$
$\circ\bullet$	$\circ\circ$	$-L^{-c}D\rho(1-\rho)$
$\circ\bullet$	$\bullet\circ$	0
$\circ\bullet$	$\bullet\bullet$	$L^{-c}F\rho(1-\rho)$
$\bullet\circ$	$\circ\circ$	$-L^{-c}G\rho(1-\rho)$
$\bullet\circ$	$\circ\bullet$	0
$\bullet\circ$	$\bullet\bullet$	$L^{-c}H\rho(1-\rho)$
$\bullet\bullet$	$\circ\circ$	$-L^{-c}2I\rho^2$
$\bullet\bullet$	$\circ\bullet$	$-L^{-c}J\rho^2$
$\bullet\bullet$	$\bullet\circ$	$-L^{-c}K\rho^2$

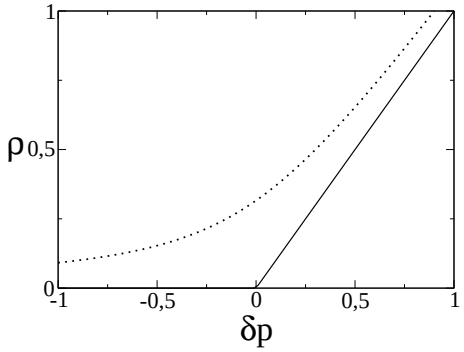

Figure 7.1: The equation of state for directed percolation describing transitions for the TASEP with two-point kinetics. Dotted line: $\kappa h = 0.1$, full line: $\kappa h = 0$.

Here, κ, δp and λ are functions of the parameters A to K. As mentioned above, $S(0) \geq 0$ and $S(1) \leq 0$. A second order source term can thus have at most one non-trivial node $S(c) = 0$, which is always stable. Additionally, there may be unstable trivial stationary densities. If the dynamics is such that these states (where either $\rho = 0$ or $\rho = 1$) are absorbing, phase transitions are possible. Especially, if $\Lambda \neq 0$, such an absorbing phase transition is possible. In this case, equation 7.5 is the mean-field equation of state of directed percolation with an external field h . The solutions of this equation, expressing the stable uniform steady-state density are given by:

$$\rho = \frac{c_1 \delta p}{2} \pm \sqrt{c_2^2 h + \left(\frac{c_1 \delta p}{2}\right)^2}. \tag{7.6}$$

The negative square root solution has to be discarded as ρ must not be negative. $c_1 = 1/\Lambda$ and $c_2 = \kappa/\Lambda$ are non-universal metric factors. For $h = 0$, $\rho = c_1 \delta p$, implying $\beta = 1$. On the other hand, for $\delta p = 0$, $\rho = c_2\sqrt{h}$, thus $\sigma = 2$. These are the exponents for mean-field directed percolation (see subsection 2.3). The equation of state is sketched in figure 7.1. The fact that the transitions are of DP type is to be expected from the Janssen and Grassberger universality hypothesis [39,40]: The order parameter is a scalar, the transition is continuous and there are no additional symmetries (like e. g. particle-hole symmetry) in the model, therefore the model is in the DP universality class.
The periodic TASEP with two-site interactions is thus linking the two classes of non-equilibrium models introduced in chapter 2: The correlations in the system are determined by the driven dynamics while the actual phase tran-

sition is of the directed percolation universality class.

7.2.3 Three and more site interaction

In the case of three site interactions, the source term becomes a third order polynomial. In this case, *two* non trivial nodes c_1 and c_2 with $S(c_1) = S(c_2) = 0$ and $S'(c_1) < 0$, $S'(c_2) < 0$ are possible. For interactions comprising more than three sites, the polynomial S might even have more non-trivial nodes.

Mean field Ising class

To construct a dynamics that shows the features of the mean field Ising model, all that has to be done is to pay attention to the symmetry of the Ising model, i.e. particle-hole symmetry. Furthermore, the dynamics $S(\rho)$ must be capable of showing three nodes, one at $\rho = 1/2$ and the other two symmetric to that. If this is fulfilled, then by universality the mean field Ising model exponents are found, as is demonstrated below. Take the dynamics as follows:

$$0 \quad \to 1 \qquad \text{with rate} \qquad \frac{1 - A + h}{2L^c} \tag{7.7}$$

$$101 \quad \to 111 \qquad \text{with rate} \qquad \frac{1 + A}{2L^c} \tag{7.8}$$

$$1 \quad \to 0 \qquad \text{with rate} \qquad \frac{1 - A}{2L^c} \tag{7.9}$$

$$010 \quad \to 000 \qquad \text{with rate} \qquad \frac{1 + A}{2L^c}. \tag{7.10}$$

Here, $c > z = 3/2$. $A \in [-1, 1]$ will play the role of the control parameter. The term with rate h is introduced to break the symmetry. It acts like an external magnetic field in the Ising model. Figure 7.2 shows how the source term $S(\rho)$ looks like in the high and low temperature phase, respectively. As the rates of the kinetics in the source term are scaling with L^{-c} and $c > z$, the system is always in a product state as for the unperturbed ASEP. In the thermodynamic limit the source term reads:

$$\begin{aligned} S(\rho) = \; & \tfrac{1}{2L^c}\left((1 - A + h)(1 - \rho) + (1 + A)(1 - \rho)\rho^2\right) \\ & - \tfrac{1}{2L^c}\left((1 - A)\rho + (1 + A)\rho(1 - \rho)^2\right) \end{aligned} \tag{7.11}$$

Note that for a finite system the expressions for the densities in the source term have to be expressed as ratios of particle number N and lattice size L. The contribution $\rho^2(1 - \rho)$ e.g. then becomes $N(N - 1)(L - N)/[L(L - 1)(L - 2)]$.

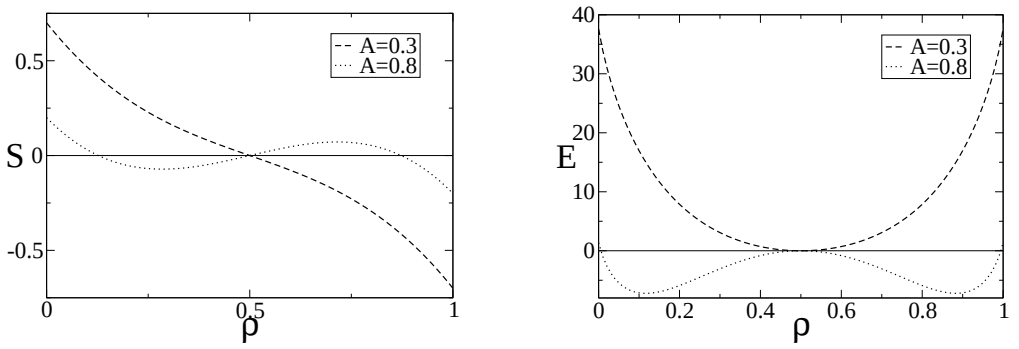

Figure 7.2: Left: Shapes for the source term $S(\rho)$ when varying the control parameter A. The dashed curve shows S in the high temperature phase for $h = 0$ and $A = 0.3$, the dotted one in the low temperature phase at $h = 0$ and $A = 0.8$. Right: Energy landscapes constructed from the detailed balance condition, corresponding to the source terms.

The dynamics of the density ρ can be understood as that of a random walker with site dependent hopping rates. The rate for hopping from a state with N particles to one with $N + 1$ is given by the positive terms in S at density $\rho = N/L$. Conversely the rate for hopping to a state with $N - 1$ particles is given by the negative terms in S. Knowing the hopping rates and setting $E(N = L/2) = 0$, the energy landscape (or by $P \propto e^{-\beta E}$ the occupation probability) of the random walker can be computed by using the detailed balance condition. The results of this construction in the high- and low-temperature phase are shown in figure 7.2. A comparison of the computed occupation probability with a Monte Carlo simulation is shown in figure 7.3. Equation (7.11) can be solved for its stationary densities, i.e. the nodes of the source term. At $h = 0$ the three solutions are $\rho = 1/2$, and $\rho = 1/2\,\frac{1+A\pm\sqrt{-3+2\,A+5\,A^2}}{1+A}$. Using the mapping from the lattice gas to an Ising spin model, i.e. $s_i = 2n_i - 1$, the first solution for the density translates to $m = 0$ in the language of the Ising model. The other solutions correspond to positive and negative magnetization, respectively. Equating these magnetizations to zero yields the critical value for the control parameter A, i.e. $A_c = 0.6$. In presence of the field h, the solutions are less handy and shall not be given here. For a graph see figure 7.4. Knowing the density (or equivalently the magnetization) as a function of the control parameter A and the external field h, the critical exponents can be worked out. Here the 'reduced temperature' $\tau = (A - 0.6)/0.6$ is used.

- For $h = 0$ near $\tau = 0$, a series expansion of the density yields $\rho =$

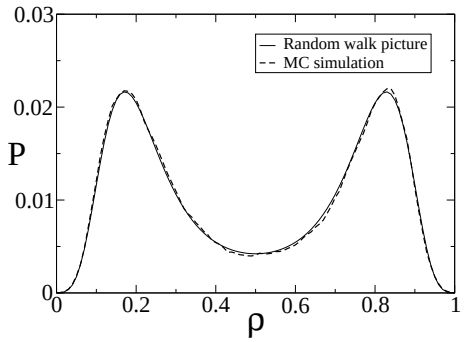

Figure 7.3: Comparison of Monte Carlo and analytical results for the probability distribution $P(\rho)$ of a particle-hole symmetric dynamics with two stationary stable states. Here, the dynamics is: $000 \to 010$ with rate $0.08L^{-2}$, $101 \to 111$ with rate L^{-2}, $100 \to 110$ with rate $0.58L^{-2}$ and the particle-hole symmetric processes.

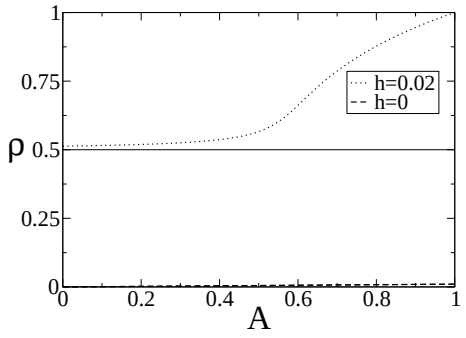

Figure 7.4: The magnetization $m = 2\rho - 1$ as a function of the control parameter A with and without the external field h. At $h = 0$, the magnetization vanishes at $A = 0.6$. The curve without transition is taken at $h = 0.02$.

$0.5 + \text{const}\ \tau^{1/2} + O(\tau^{2/3})$. Therefore $\beta = 1/2$.

- At the critical A, i.e. $\tau = 0$, a series expansion of the density for small h yields: $\rho = 0.5 + \text{const}\ h^{1/3} + O(h^{2/3})$. Thus $\delta = 3$.
- For small τ and small h, to leading order $m \propto h/\tau$. Therefore, $\chi = \partial m/\partial\tau \propto 1/\tau$, which means that $\gamma = 1$.
- Computing the specific heat above and below $\tau = 0$ shows $\alpha = 0$.

All critical exponents are as for the mean-field Ising model.

Hysteresis

In case the kinetics is not symmetric with respect to exchange of particles and vacancies, the model does not correspond to the mean field Ising model. Still, in both cases the phenomenon of hysteresis can be observed. Consider as an example the following reaction kinetics:

$$\begin{aligned} 0 &\to 1 && \text{with rate } 0.01L^{-c} \\ 1000 &\to 1100 && \text{with rate } L^{-c} \\ 1011 &\to 1111 && \text{with rate } L^{-c} \\ 1 &\to 0 && \text{with rate } xL^{-c} \\ 01 &\to 00. && \text{with rate } 10xL^{-c} \end{aligned} \tag{7.12}$$

(7.13)

Here, $c > z = 3/2$. Depending on the rate x there may either be one or two stable stationary states. When varying the rate x, $S(\rho)$ takes shapes as exemplified in figure 7.5. Especially, the transition from the high-density to the low-density phase exhibits hysteresis. The shape of the loop for an infinite system can be computed from the nodes of $S(\rho)$. When comparing it to Monte Carlo simulations the usual velocity dependence of the area the hysteresis loop covers becomes apparent (figure 7.5).

7.3 The periodic KLS model with reaction kinetics

While the previous subsection focused on the TASEP, which exhibits no correlations, this subsection covers a periodic system with KLS dynamics (see subsection 2.1.2), which in one dimension is known to have a steady state distribution as an Ising model [19]. The source term now contains

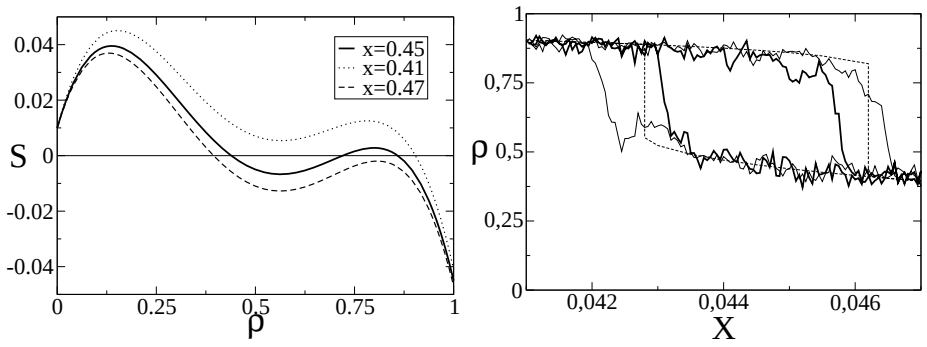

Figure 7.5: Left: Shapes for the source term $S(\rho)$ when varying the parameters x of the reaction kinetics. The full curve shows S in the coexistence region ($x = 0.45$), the dotted one in the high-density phase ($x = 0.41$) and the dashed one in the low-density phase ($x = 0.47$). Right: Hysteresis loop in a Monte Carlo simulations at two different speeds for changing x (solid lines, bold one at slower speed) compared to the result from the hydrodynamical equation (dashed line).

correlators which have to be computed using transfer matrices (see e.g. [20]). The rates for the kinetic processes are again scaling with L^{-c}, where $c > z$. Clearly, for single-site interactions, which might be described as the action of a bulk reservoir, nothing changes compared to the case of the TASEP discussed above.
In case of two-site interactions, new phenomena arise. Note again that in this case the non-conserving dynamics can not be formulated in terms of a bulk reservoir.
Consider the following process, which is the dynamics of the contact process with an external field:

$$01 \overset{pL^{-c}}{\to} 11 \qquad\qquad 1 \overset{L^{-c}}{\to} 0 \qquad\qquad 0 \overset{hL^{-c}}{\to} 1. \tag{7.14}$$

The corresponding source term reads as

$$S(\rho) = \frac{1}{L^c} \left(p\langle 01 \rangle - \langle 1 \rangle + h\langle 0 \rangle \right), \tag{7.15}$$

where $\langle 01 \rangle$ is the expectation value of having a vacant site adjacent to an occupied one and $\langle 1 \rangle = 1 - \langle 0 \rangle$ denotes the particle density. When computing the correlator, the transfer matrix T as well as its eigenvalues $\lambda_{0,1}$ and associated eigenvectors $u_{0,1}$ are needed:

$$T = \begin{pmatrix} e^{-\beta-h} & e^{\beta} \\ e^{\beta} & e^{-\beta+h} \end{pmatrix} \tag{7.16}$$

$$\lambda_{0,1} = e^{-\beta}\cosh(h) \pm \sqrt{e^{-2\beta}\sinh(h)^2 + e^{2\beta}} \tag{7.17}$$

$$\langle u_0| = (\alpha_+, \alpha_-) \quad \langle u_1| = (\alpha_-, -\alpha_+) \tag{7.18}$$

$$\alpha_\pm^2 = \frac{1}{2}\left(1 \mp \frac{e^{-\beta}\sinh(h)}{\sqrt{e^{-2\beta}\sinh(h)^2 + e^{2\beta}}}\right). \tag{7.19}$$

Using the matrices

$$v = \begin{pmatrix} 1 & 0 \\ 0 & 0 \end{pmatrix} \quad n = \begin{pmatrix} 0 & 0 \\ 0 & 1 \end{pmatrix} \tag{7.20}$$

the correlator $\langle 01 \rangle$ is given as

$$\langle 01 \rangle = \langle 0 \rangle\langle 1 \rangle + \frac{\lambda_1}{\lambda_0}\langle u_0|v|u_1\rangle\langle u_1|n|u_0\rangle \tag{7.21}$$

$$= \rho(1-\rho) - \frac{\lambda_1}{\lambda_0}\rho(1-\rho). \tag{7.22}$$

Solving for the nodes of $S(\rho)$ shows that two cases have to be distinguished:

- For $\epsilon \neq 1$ the stationary density at $h = 0$ shows a continuous transition from $\rho > 0$ at $p > 1$ to $\rho = 0$ at $p < 1$. Note that the empty lattice is an absorbing state at $h = 0$. The transition vanishes in presence of an external field, as which in this case the particle creation with rate h acts (see figure 7.6). Computing the critical exponents $\beta = 1$ and $\delta = 2$, as well as the equation of state yields the same results as for mean-field DP.

- For $\epsilon = 1$ the stationary density shows at $h = 0$ a first order phase transition from $\rho > 1/2$ at $p > 1$, to $\rho = 0$ below. Again, the empty lattice is an absorbing state at $h = 0$. This discontinuity also shows in presence of the external field ($h > 0$). In this case, the derivative of ρ with respect to p has a discontinuity at $p = 1 - h$ (figure 7.6).

7.4 SSB in two coupled TASEP with exchange kinetics

In this section, the possibility of spontaneous symmetry breaking in a system of two coupled periodic TASEP is demonstrated.
Consider two TASEP with periodic boundary conditions. Let an exchange kinetics, i.e. processes which detach particles from site i on the one ring and

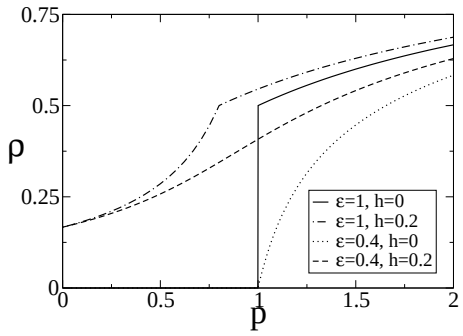

Figure 7.6: Stationary density for the periodic KLS model with reaction kinetics. For $\epsilon = 0$ a first order absorbing phase transition occurs at $h = 0$. At $h \neq 0$ the phase transition vanishes, but the derivative of $\rho(p)$ is discontinuous. For $\epsilon \neq 1$ a continuous transition occurs.

attach them on site i on the other ring, have rates scaling with L^{-c}, where $c > z = 3/2$:

$$\cdot\ \circ\ \cdot \quad \overset{aL^{-c}}{\longrightarrow} \quad \cdot\ \bullet\ \cdot \qquad (7.23)$$
$$\bullet\ \bullet\ \bullet \qquad\qquad \bullet\ \circ\ \bullet$$

$$\bullet\ \circ\ \bullet \quad \overset{L^{-c}}{\longrightarrow} \quad \bullet\ \bullet\ \bullet \qquad (7.24)$$
$$\cdot\ \bullet\ \cdot \qquad\qquad \cdot\ \circ\ \cdot$$

Here, filled circles denote occupied sites, open circles empty sites and dots any of the two states. In this geometry, one TASEP acts as a particle reservoir of the other. The situation is fundamentally different to the *bulk reservoirs* considered before, which have a constant density. Here, the number of particles in the system is fixed.
As in the previous subsections, the relaxation of the two TASEP on the rings is fast compared to the time scale of successive events of the reaction kinetics. Thus, the correlations on the rings are as in the TASEP, i.e. the correlators vanish. Denoting the densities on the two rings as ρ and ν, respectively, the source terms for the two densities read for a large system as follows:

$$S_\rho = \frac{1}{L^c}\left(a\nu^3(1-\rho) + \nu\rho^2(1-\rho) - a\rho^3(1-\rho) - \rho\nu^2(1-\nu)\right) \quad (7.25)$$
$$S_\nu = \frac{1}{L^c}\left(a\rho^3(1-\rho) + \rho\nu^2(1-\nu) - a\nu^3(1-\rho) - \nu\rho^2(1-\rho)\right) \quad (7.26)$$

In the stationary state, both source terms have to be zero. The locus of stationary densities is shown in figure 7.7 for $a = 0.1$. As the coupled system

is conserving, the total density $\rho+\nu$ is an external parameter. As can be seen from figure 7.7, $\rho = \nu$ is a solution for all possible total densities. But there are also total densities for which three solutions are possible: The symmetric solution with $\rho = \nu$ and two symmetry broken solutions with $\rho \neq \nu$. The stability of the solutions in this region has to be probed with linear stability analysis. Let $(\rho_0, \nu_0)^T$ be a stationary solution. Then a perturbed state

$$\begin{pmatrix} \rho \\ \nu \end{pmatrix} = \begin{pmatrix} \rho_0 \\ \nu_0 \end{pmatrix} + \begin{pmatrix} \delta\rho \\ \delta\nu \end{pmatrix} \tag{7.27}$$

will develop to linear order as

$$\frac{\partial}{\partial t}\begin{pmatrix} \delta\rho \\ \delta\nu \end{pmatrix} = \begin{pmatrix} \frac{\partial S_\rho}{\partial \rho} & \frac{\partial S_\rho}{\partial \nu} \\ \frac{\partial S_\nu}{\partial \rho} & \frac{\partial S_\nu}{\partial \nu} \end{pmatrix}\begin{pmatrix} \delta\rho \\ \delta\nu \end{pmatrix}. \tag{7.28}$$

When evaluated at $(\rho_0, \nu_0)^T = (c, c)$, i.e. a symmetric solution, there is a positive eigenvalue of the matrix in the region with three solutions, implying that the symmetric solution is unstable. When evaluated for the non-symmetric solutions, the matrix turns out to have an eigenvalue of $\lambda_1 = 0$ and one eigenvalue $\lambda_2 < 0$. It turns out that the eigenvector corresponding to λ_2 is of the form $(\rho_2, -\rho_2)$, i.e. a perturbation with this eigenvector does not change the total density, in contrast to the eigenvector of $\lambda_1 = 0$. As the system considered is conservative, only perturbations corresponding to $\lambda_2 < 0$ are relevant. These decay to zero in time, which means that in the region where the total density permits three solutions, the symmetry broken ones are stable. Note that the two symmetry broken solutions are equivalent and one of them is spontaneously chosen as the steady state.

The study of this system is motivated by a model for pattern formation of *myxobacteria* [81]. These simple rod-like bacteria can move in either direction of their long axis. By contact interactions, collective behavior is induced and patterns out of a spatially homogeneous population are formed. Note that these bacteria have an internal degree of freedom, given by the direction of their motion and are thus different from the particles in the ASEP.

7.5 On the possibility of non-uniform steady states

The kind of reaction kinetics considered in this chapter has rates scaling as L^{-c} where $c \geq 3/2$. If there are non-uniform stationary states, then on the Euler scale they obey the following equation:

$$\frac{\partial \rho(x)}{\partial t} + v_c \frac{\partial \rho(x)}{\partial x} = \tilde{S}(\rho(x)). \tag{7.29}$$

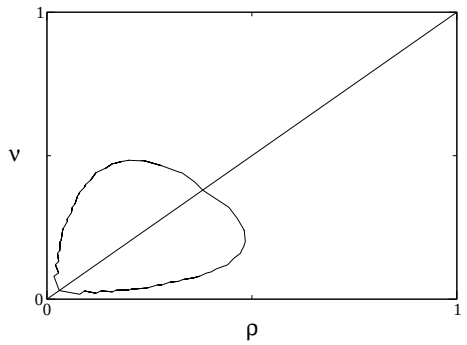

Figure 7.7: The possible stationary solutions for the densities ρ and ν (y-axis) for the two coupled TASEP with $a = 0.1$. In the region where the total density allows for three solutions, the symmetric one becomes unstable.

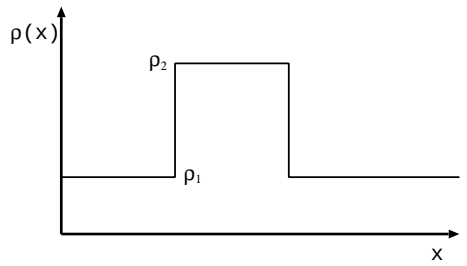

Figure 7.8: Example of a non-constant profile due to two shocks from density ρ_1 to ρ_2 and back.

Here, $\tilde{S}(\rho(x)) = L\,S(\rho(x))$, i.e. $\tilde{S}$ scales like L^{-c+1}. Therefore, the density profiles resulting from equation (7.29) will have zero slope on the Euler scale, i.e. they are flat up to density shocks. Any non-uniform steady state would thus involve shocks as depicted in figure 7.8, i.e. show coexistence of at least two phases of constant density. From the stability criterion for the shocks (see eq. (2.5) in subsection 2.1.3) it is clear that one of them, either the upward or downward shock, is unstable. Therefore, the systems considered in this section, i.e. those where the reaction kinetics occurs on a time scale that is long compared to the relevant time scale of the driven dynamics, are not capable of showing non-uniform steady states on a ring.
On the other hand, if the reaction kinetics occurs on the same time scale or faster than the relevant time scale of the driven dynamics, the density-current relation of that dynamics will *not* be identical to the one in absence of the kinetics. In general, this relation is not analytically known for these

cases, so that no general statements can be made.
These arguments also hold for the two-species systems considered in [82]. There, generically double shocks appear. Still, the density profiles must also be flat on Euler scale for the given dynamics, apart from shocks. Also in this case, either the upward or downward shocks must be unstable, enabling only uniform steady states on a ring.

7.6 Conclusion

The relevant time scale for the dissipation of perturbations in a periodic system is L^z, where $z = 3/2$ is the dynamic exponent of the KPZ universality class. Single species periodic driven diffusive systems with reaction kinetics occurring on a slower time scale than this are only capable of showing uniform steady states. This especially means that no phase separation can occur in these models.
The TASEP with two-point reaction kinetics shows absorbing phase transitions in the mean-field DP universality class. The KLS model with two-point kinetics is capable of showing a first-order absorbing phase transition.
For three-point interactions, phase transitions between non-trivial steady states are possible. Thus phenomena like hysteresis are observed.
A system of two coupled TASEP with exchange kinetics shows spontaneous symmetry breaking.

Chapter 8

Exact Hurst exponent and crossover behavior in a limit order market model

8.1 Introduction

Financial markets have in recent years been at the focus of physicists attempts to apply existing knowledge from statistical mechanics to economic problems [83–86]. These markets, though largely varying in details of trading rules and traded goods, are characterized by some generic features of their financial time series, called 'stylized facts' [83,84,86]. Agent based models of financial markets are successful to reproduce some stylized facts [87–92], such as volatility clustering, fat-tailed probability distribution of price increments and over-diffusive price behavior at short time scales and diffusive behavior at later times. But all of them need an explicit price formation rule that links excess demand to price changes [87, 93–95], that can be itself problematic. Another approach consists in modeling the price formation, for instance in limit order markets [96–100]. So far, all these models of limit order markets have under-diffusive prices at short times, with a crossover to diffusive prices at longer times for some of them. Under-diffusive behavior at short times is realistic in limit order markets, but all these models lack the over-diffusive price behavior observed in real markets at medium time scales.
In this chapter we introduce a crude non-equilibrium model with over-diffusive price that is able to reproduce the crossover from a Hurst exponent $H = 2/3$ to $H = 1/2$ at larger times, when correlations in the price dynamics are washed out by cancellations of existing orders and independent placements of new orders. The Hurst exponent is defined via the mean square displacement of the price x as a function of time:

$$\sqrt{\langle x^2(t)\rangle} \sim t^H. \tag{8.1}$$

In the early time regime our model belongs to the $1d$-KPZ universality class [101], hence, its mechanism for over-diffusive price spreading is robust and analytically tractable.
In section 8.2 we define our model in terms of the limit order market dynamics. Our simulation results are presented in section 8.3. In section 8.4 the equivalence of the early-time regime of our model to the totally asymmetric exclusion process (TASEP) [3] with a second class particle is established and its relation to the KPZ [102] and noisy Burgers [62] equation as well as the TASEP with Langmuir kinetics (see subsection 5.1) are discussed.
The results in this chapter were obtained in collaboration with D. Challet and published in ref. [8].

8.2 Model definition

We consider two types of orders: *limit orders* that are wishes to buy or sell a given quantity of stock at a given price, and *market orders* that are orders to immediately sell or buy an asset at the best instantaneous price. Limit orders are stored in an order book until they are either canceled,[1] or fulfilled, provided that the current market price has moved towards their prices. The model is constructed as a one-dimensional lattice model, in a similar spirit as in [96, 103]. Let the lattice of length L represent the price axis, with the lowest price on the left end at site 1 and the highest one on the right at site L. Limit orders of the two different kinds, i.e., asks (A) and bids (B) are placed on the lattice according to the price that the order is based on. As bids name lower prices than asks, they will be found on the left side of the lattice. The current market price (x) separates the two regions. Sites representing prices at which currently no order is placed are indicated as 0.

In the model we made the following simplifying assumptions:

- Only one kind of asset is traded and its price dynamics is not directly influenced by outside sources but just by the state of its limit order book.
- Each site can only carry one order (exclusion model).
- Limit orders of either kind come in a unit size.
- Only a finite price interval of width L is considered.

The last assumption is justified as trade only takes place in a narrow interval around the market price. In our model L can be chosen arbitrarily. For a discussion on differences between models and real limit order markets see e.g. [104].

The dynamics of the lattice is as follows (see figure 8.1):

- At site 1 bids enter the system at rate α: $0 \to B$.
- At site L asks enter the system at rate γ. $0 \to A$.
- Asks and bids can diffuse one site towards the market price at rate p provided no other order is already placed at the target site: $B0 \to 0B$, $0A \to A0$.

[1] For instance because they had a predefined maximal lifetime.

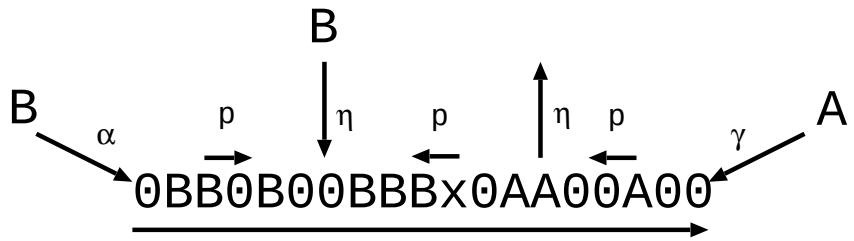

Figure 8.1: Example of a configuration and possible moves with their assigned rates.

- Bids can be placed at unoccupied sites left of the market price at rate η. The same holds for asks being placed right of the market price: $0 \to A,\ \ 0 \to B$.
- Bids and asks can be evaporated at rate η: $A \to 0,\ \ B \to 0$. This reflects both orders being canceled as well as being timed out. We have made the simplifying assumption of a constant removal rate at each site instead of considering the lifetimes of individual orders.
- An ask can be fulfilled at rate p by an incoming market order, provided it is adjacent to the current market price. Thus the order is removed: $xA \to 0x$.
- A bid can be fulfilled at the same condition and rate, leading to a decrease of the market price and removal of the order: $Bx \to x0$.

The role of order injection and diffusion is to ensure a fluctuating order density on both sides of the price. On the other hand, the dynamics of the special particle which represents the price, is such that the sign of price increments is constant as long as the bid-ask spread is not minimal, i.e., as long as the price is not surrounded by two orders. This is a crude but efficient way of implementing trends in limit order market models. Notice that this dynamics implies that the price is always between the best bid and best ask orders, which is true 95% of the time in ISLAND ECN (www.island.com). Even if it is likely that orders do not diffuse [98], we use this ingredient as a way of obtaining exact results for the Hurst exponent.

8.3 Simulation results

Throughout our simulations we chose initial configurations where each site of the lattice is randomly occupied by an order with probability 1/2. Further-

more we chose $\alpha = \gamma = 1/4$, $p = 1/2$. The lattice size L was chosen such that the market price M could not fluctuate out of the represented price interval during the simulation time. The choice of rates guarantees that the price has no drift but on average remains on its initial position, i.e., $L/2$. Averaging over initial conditions is implied in all our simulations.

In the case $\eta = 0$ we remain with a model where price dynamics is solely caused by diffusion of limit orders. We are mainly interested in the Hurst exponent H defined by the relationship $\langle(\delta x)^2\rangle^{1/2} \propto \Delta t^H$.

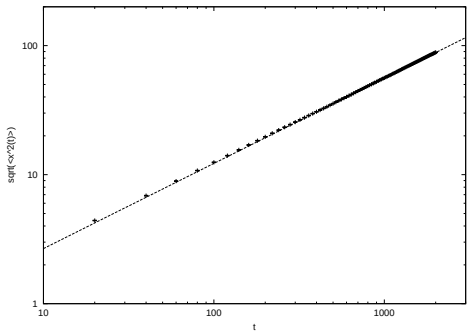

Figure 8.2: Fluctuations of the price signal $\sqrt{\langle x^2(t)\rangle} \propto t^H$ at $\eta = 0$ and fit with $H = 2/3$.

In fig. 8.2 we show the fluctuation of the price position x relative to the initial price versus time, in a double-logarithmic plot. As can be seen the Hurst exponent of the model is $H = 2/3$ for all times without a crossover. This behavior is in contrast to the corresponding result from the basic Bak, Paczuski, Shubik (BPS) model [96, 103]. In the BPS models offers to buy and sell diffuse on a lattice representing prices just as in our model. The difference is that upon meeting offers to sell and buy mutually annihilate in the BPS model, thus carrying the model to the universality class of the $A + B \to 0$ reaction diffusion model. For that model it is known analytically that $H = 1/4$ at long times plus logarithmic corrections at shorter times [105]. In our model no mutual annihilation (of ask and bid), takes place, but just one type of order vanishes (ask or bid, fulfilled together with a market order), thus causing a price change. This carries our model into the realm of the KPZ universality class as we will illustrate in the next subsection and yields $H = 2/3$.

Price increments $\delta x(t) = x(t' + t) - x(t')$ show algebraically decaying correlations (figure 8.3), with $\langle \delta x(t')\ \delta x(t' + t)\rangle \propto t^{-1/2}$ whereas these correlations should be essentially zero; this is due to the absence of evaporation

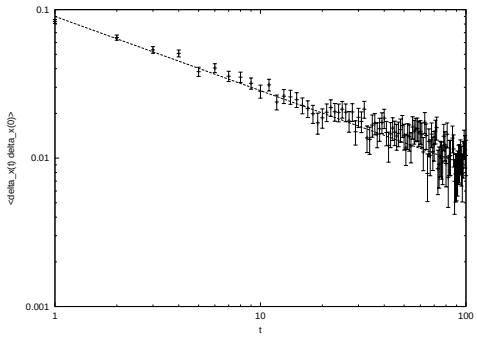

Figure 8.3: Correlations of the increments $\langle \delta x(t') \; \delta x(0) \rangle$ versus t at $\eta = 0$ and fit by the eye with a function decaying algebraically as $t^{-1/2}$.

(see below); the correlation of absolute increments has algebraically decreasing autocorrelation with an exponent of approximately 1. These long ranged correlations cause the over-diffusive behavior.

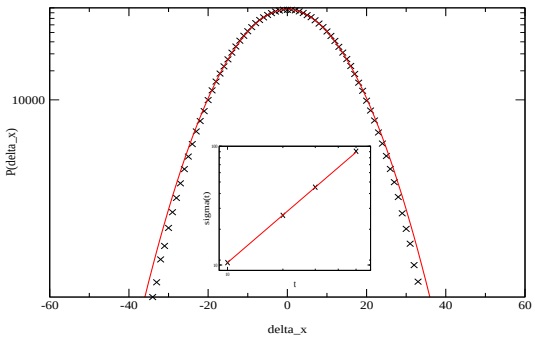

Figure 8.4: Distribution of the increments (logarithmic scale) for $t = 50$ at $\eta = 0$ and Gaussian fit. The inset shows the variance of the distribution as a function of time and a fit proportional to $t^{4/3}$.

Due to the price process itself ($|\delta x(1)| \in 0, 1$), the histogram of $\delta x(t)$ is almost Gaussian in shape, the tails appear even less pronounced than a Gaussian pdf (figure 8.4). The variance of the distribution of increments $\delta x(t)$ increases as $\sigma \propto t^{4/3}$ (see inset of figure 8.4). The dynamical exponent of the price process extracted from this property is $z = 3/2$. Clearly the stochastic process causing the price movements is not Gaussian, not even a rescaled Gaussian.

In what follows we consider the case $\eta \neq 0$. Clearly this is more realistic than $\eta = 0$ as it is possible to place orders of either kind at any unoccupied

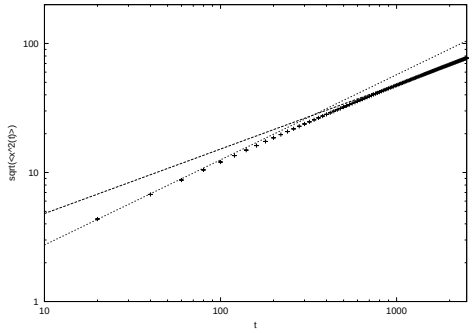

Figure 8.5: Fluctuations of the price signal $\sqrt{\langle x^2(t)\rangle} \propto t^H$ at $\eta = 1/512$ and fit with $H = 2/3$ in the early time regime and $H = 1/2$ at late times.

site on the price axis without having to perform diffusion steps all the way from the boundaries. Also the withdrawal of orders due to cancellation and timeout becomes thus possible. As seen in figure 8.5 the fluctuations of the price signal show a crossover from super-diffusive behavior at short times, characterized by the Hurst exponent $H = 2/3$ to diffusive behavior at later times, implying $H = 1/2$.

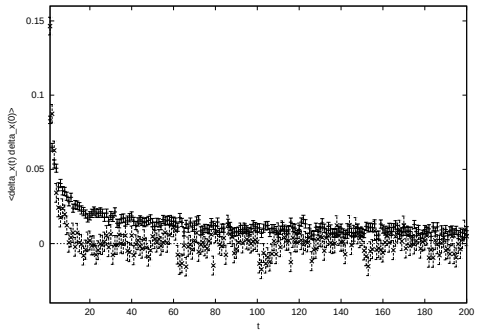

Figure 8.6: Decay of the correlations of the increments for $\eta = 0$ (upper curve) and $\eta = 1/8$ (lower curve).

The local random events controlled by the parameter η destroy the long ranged time correlations of the price increments. This can be seen in figure 8.6, showing the correlation of increments $\langle \delta x(t)\ \ \delta x(0)\rangle$ as a function of t for $\eta = 0$ and $\eta = 1/8$. At $t = 200$ the correlation function for the $\eta = 0$ case is still different from zero, while a decay to zero for the other case occurred long since. Note that the autocorrelation of price increments should be negative

for short time whereas it is positive in our model; this is due to the fact that we do not allow the coexistence of the two types of markets orders (see [106]).

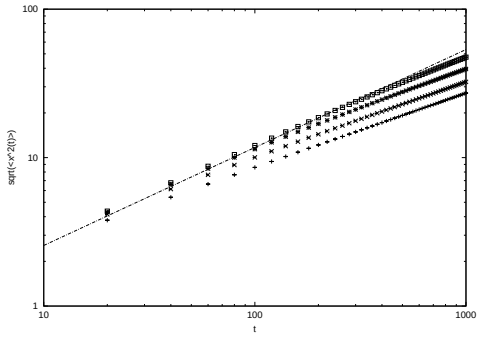

Figure 8.7: Fluctuations $\sqrt{\langle x^2(t)\rangle}$ for $\eta = 1/8$, $\eta = 1/32$, $\eta = 1/128$ and $\eta = 1/512$ (from below). The parameter η controls the range over which $H = 2/3$ (dashed line).

Adjusting the rate η serves as a parameter to control the crossover point. Figure 8.7 shows the price fluctuations for values of η between $1/8$ and $1/512$. The larger the rate η for local events, the shorter is the time span for over-diffusive fluctuations. In fact, in our simulations over-diffusive behavior over a longer time interval appears only to be possible at seemingly meaningless low rates η, namely $\eta \approx 1/L$, compared to $\alpha = \gamma = 1/4$ and $p = 1/2$. From the study of empirical data of the Island ECN limit order market conducted in [98] it is known that about 80 per cent of limit orders in the respective market vanished due to timeouts. Only 20 per cent of the offers were (at least partially) fulfilled. We measured these quantities as a function of η in our simulations, where fulfillment of an order means either the process $Bx \to x0$ or $xA \to 0x$ and timeouts are reflected by the rate η. It turns out that for a lattice of $L = 1000$ at $\eta = 1/512$ about 8 per cent of orders were fulfilled and at $\eta = 1/1024$ about 16 per cent. Thus the choice of small η matching the observed fulfillment rate is realistic and could in fact be used as a means to gauge the simulation time by comparing the known empirical crossover time and the simulation crossover.

In the spirit of dynamical scaling it is tempting to assume that the price fluctuations with sufficiently low η can be described in terms of a scaling function F with

$$< x^2(t) >= \eta^{-\mu_1} F(\eta^{\mu_2} t).$$

Since η is a rate with inverse dimension of time one expects $\mu_2 = 1$ for covariance of $< x^2(t) >$ under rescaling of time. For small times, i.e., small

arguments of the scaling function, this ansatz should reproduce the behavior $< x^2(t) > \propto t^{4/3}$ which implies $F(y) \propto y^{4/3}$ for $y \to 0$. Independence of η thus yields the scaling relation

$$4/3\mu_2 = \mu_1. \tag{8.2}$$

Hence one expects $\mu_1 = 4/3$. For large times crossover to diffusion implies $F(y) \propto y$ for $y \to \infty$. For large η (of order 1 and larger) we obtain ordinary random walk behavior even at early times and the scaling relations are not expected to be valid.

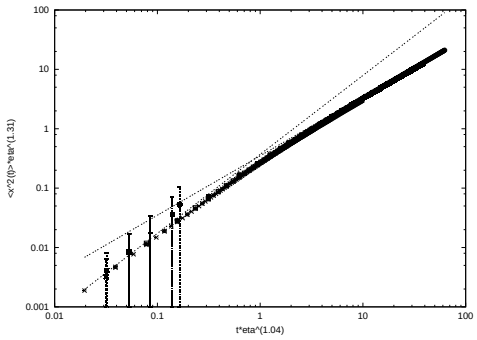

Figure 8.8: Data collapse for the data for $\eta = 1/32$, to $\eta = 1/1024$ using the scaling function given in the text and lines to guide the eye corresponding to $H = 2/3$ and $H = 1/2$.

These arguments are well born out by Monte Carlo simulations. The best fit for the data could be achieved for the choice $\mu_1 = 1.31$ and $\mu_2 = 1.04$. These exponents are used in the plot (fig. 8.8). The scaling property suggests that the relevant time scale of the model is $\tau = 1/\eta$, which is the average time between successive placements or evaporations of an order at a given site.

The increments of the price signal $\delta x(t)$ for $\eta \neq 0$ (fig. 8.9) differ from $\eta = 0$ in two important respects. Firstly, the tails of the distribution are closer to a Gaussian. A second and more pronounced difference is the behavior of the variance σ of the distribution as a function of time, which shows a crossover from $\sigma \propto t^{4/3}$ to $\sigma \propto t$ just as the price signal itself. This means that the price performs an ordinary random walk at long times. A snapshot of the price movement is shown in figure 8.10.

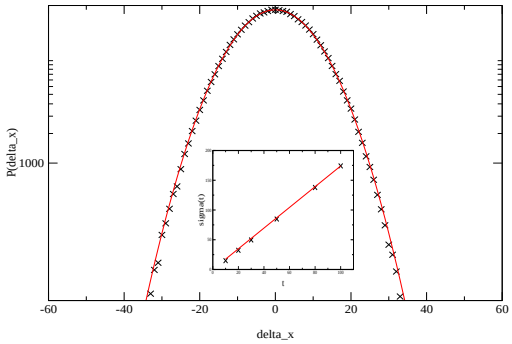

Figure 8.9: Distribution of the increments for t=50 at $\eta = 1/8$ and Gaussian fit. The inset shows the variance of the distribution as a function of time and the linear asymptote.

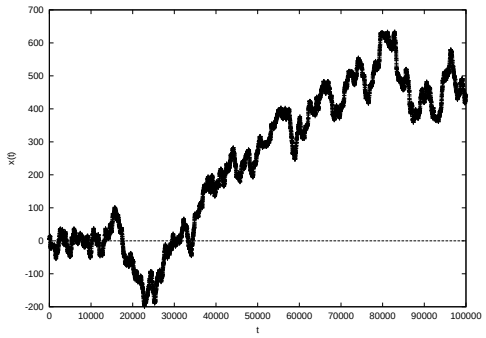

Figure 8.10: Snapshot of price movement at $\eta = 1/8$.

8.4 Connection to the TASEP

The virtue of our model is the equivalence at $\eta = 0$ to the totally asymmetric exclusion process (TASEP) for which a wealth of exact results exists [3]. At $\eta \neq 0$ it is equivalent to the TASEP with Langmuir kinetics (see subsection 5.1).
In the TASEP excluding particles enter a lattice at rate α from the left and hop with rate p to the right, provided the target site is empty. At the right end they can leave the system with rate β. In connection with the TASEP a 'second class' particle [107] has been defined to have the following dynamics: A first class particle meeting upon a second class particle to its right will exchange places. A second class particle with a vacant right neighboring site hops to that site. The second class particles motion is designed such that

it does not interfere with the motion of the first class particles. In fact, the motion of a single second class particle in the system is on average that of a density fluctuation in the system.

Upon coarse graining the dynamics of the TASEP can be described by the noisy Burgers equation, which is closely related to the KPZ equation known to have a universal dynamical exponent $z = 3/2$ [101]. This implies a Hurst exponent $H = 2/3$ as discussed above. For the noisy Burgers equation the over-diffusive spreading of a density fluctuation (i.e., the spreading of the second class particle, representing the price signal in our model) with $H = 2/3$ has been shown analytically [62] in the case of statistically averaging over initial positions as well as realizations, which is always implied in our simulations.

The mapping between our model and the TASEP at $\eta = 0$ is as follows: The market price x represents the second class particle. Left of its position, bids are first class particles in the sense of the TASEP and vacancies remain what they are. To the right of the market price vacancies take the role of first class particles in the TASEP sense and asks that of vacancies. The price dynamics in our model is precisely that of a second class particle or density fluctuation in the TASEP.

The TASEP may be seen as a discretized version of the noisy Burgers equation. It is an exactly solvable model for which $z = 3/2$ has been obtained through the Bethe ansatz [108]. More recently, also the distribution of the second class particle for averaged random initial conditions has been calculated exactly through a correspondence with statistical properties of random matrices [109]. This confirms the results of our simulations for a finite lattice with open boundaries, but system large enough to be equivalent to an infinite system. We have also performed simulations for a *fixed* random initial state. We found that the super-diffusive spreading of the second class particle prevails, but the amplitude $< x^2 > /t^{4/3}$ depends on the initial condition. This is in accordance with expectations [110].

At $\eta \neq 0$, bids and asks can be placed and evaporated at arbitrary positions. The placement (evaporation) of bids is equivalent to the attachment (detachment) of TASEP-particles on the lattice left of the second class particle. The placement (evaporation) of asks is equivalent to the detachment (attachment) of TASEP-particles right of the second class particle. Thus for $\eta \neq 0$ the system is equivalent to a TASEP with Langmuir kinetics where in the language of subsection 5.1 $\omega_a = \omega_d = \eta$. As mentioned in subsection 8.3, in the limit order market model, over-diffusive behavior of the price could only be observed for longer times if $\eta \sim 1/L$. Thus in this model the realistic parameter range is $\omega_a = \omega_d = \eta \sim 1/L$, which is precisely the type of scaling considered in ref. [66] for the TASEP with Langmuir kinetics.

8.5 Conclusions

In this chapter we have presented a model exhibiting the empirically observed crossover of the Hurst exponent from $H > 1/2$ to $H = 1/2$. By a mapping to the totally asymmetric exclusion process we obtain the exact value $H = 2/3$ which is close to what is often observed in real markets. The existence of an exact analytic solution puts our model in contrast to the model by Bak [96] exhibiting over-diffusive spreading by volatility feedback into the system and a copying strategy of the traders, but for which no analytical solution is known. The over-diffusive behavior results from time correlations build up in the biased internal motion of asks and bids respectively which together with market orders drive the price process. We identify the average time between evaporation events of orders (due to time-out or cancellation respectively) at a given site as the relevant time scale of the model before crossover to diffusive Gaussian behavior. Placement and evaporation events for orders play the role of Langmuir kinetics in the mapping of the model to an exclusion process.

Chapter 9

Spontaneous symmetry breaking in a non-conserving model

9.1 Introduction

In this chapter we study a variant of the bridge model (see section 2.2.2 and chapter 4), in which non-conserving dynamics is introduced in the bulk of the system. All dynamical rates, both conserving and non-conserving, respect the CP-symmetry between the two species of particles. By its nature, this dynamics acts to balance the densities of the two species. If the non-conserving transitions occur at finite rates, spontaneous symmetry breaking does not occur. However, we find that when these rates are inversely proportional to the system size, spontaneous symmetry breaking appears. This model is related to the single-species non-conserving asymmetric exclusion process which was introduced and studied recently [7, 66, 74] (see subsection 5.1). As in that model, the two-species model exhibits new phases with localized shocks. Transitions in the phase diagram can be understood by considering the position of the localized shocks. Furthermore, the phenomenon of induced localized shocks is observed, as predicted in [82].

The chapter is organized as follows. The next section contains the definition of the model. In section 9.3 we calculate the phase diagram within mean field approximation for some cases where the bulk dynamics of the two species are decoupled. Different limits of the model are discussed, and in particular the phase diagram of the bridge model is recovered as the non-conserving rates are reduced to zero. Next, we present in section 9.7 results of Monte Carlo simulations, and compare them with the predictions of mean field analysis. The phenomenon of induced shocks is addressed in section 9.9. In section 9.10 we present an exact solution for the case where fluctuations in the number of particles in the system are taken to zero. A physical picture is introduced and analyzed in section 9.11. We conclude and summarize in section 9.12.

The results of this chapter were obtained in collaboration with E. Levine and published in ref. [9].

9.2 Model Definition

The model considered in this section is defined on a one-dimensional lattice of size N. Each lattice site can either be occupied by a positive (+) particle, occupied by a negative (−) particle, or vacant (0). The system evolves through three types of stochastic rates: In the bulk of the system particles move on the lattice according to the rates

$$+0 \xrightarrow{1} 0+ \qquad\qquad +- \xrightarrow{q} -+ \qquad\qquad 0- \xrightarrow{1} -0\ . \tag{9.1}$$

In addition, each site in the bulk of the system, $1 < i < N$, can change its state with rates

$$+ \underset{\omega_X}{\overset{\omega_X}{\rightleftharpoons}} - \qquad + \underset{\omega_A}{\overset{\omega_D}{\rightleftharpoons}} 0 \qquad - \underset{\omega_A}{\overset{\omega_D}{\rightleftharpoons}} 0 \ , \tag{9.2}$$

corresponding to charge exchange, desorption of a particle from the lattice, and adsorption of a particle at an empty site. At the boundaries particles may be introduced and removed. At the left boundary, site $i = 1$, positive particles are introduced and negative particles are removed with rates

$$0 \overset{\alpha}{\rightarrow} + \qquad - \overset{\beta}{\rightarrow} 0 \qquad (i = 1) \ , \tag{9.3}$$

while at the right boundary, $i = N$, negative particles are introduced and positive particles are removed with rates

$$0 \overset{\alpha}{\rightarrow} - \qquad + \overset{\beta}{\rightarrow} 0 \qquad (i = N) \ . \tag{9.4}$$

Note that all dynamical rules, conserving and non-conserving, are CP symmetric, namely symmetric under the exchange of positive-negative charges and left-right directions. Generalizations of this model to the case were both types of particles can move in both directions, and when the dynamical rules break the CP symmetry, will be considered elsewhere.

Considering the bulk non-conserving rates, one distinguishes three possible scenarios [7]. If the rates are finite, in the thermodynamic limit the bulk densities are dominated by the non conserving kinetics. Otherwise, if the rates decay to zero faster than $1/N$, the bulk non-conservation should have no effect, and the properties of the system in the thermodynamic limit are identical to those with bulk conservation. The third case, which we consider here, is the one in which the non-conserving rates scale down linearly with the system size. It is useful to introduce the notation $\omega_A = \Omega/N$, $\omega_X = \Omega u_X/N$, $\omega_D = \Omega u_D/N$.

Without the non-conserving dynamics in the bulk of the system, eq. (9.2), the model is identical to the bridge model introduced in [30, 31] and further studied in [33, 34, 64].

The model considered here can be thought of as two interacting single-species totally asymmetric exclusion processes coupled to bulk reservoirs. The TASEP with Langmuir kinetics (LK) is an extension of the well-known totally asymmetric exclusion process (TASEP) [17,18,111] with bulk absorption and desorption dynamics (see subsection 5.1). Using mean field calculations [74], which were argued to be exact [7], the phase diagram of this model was obtained. In addition to the three phases of the TASEP, namely the maximal-current phase, the high-density phase and the low-density phase, it

was found that the TASEP with LK may also exhibit four additional phases. The most interesting one is a shock phase which consists of a localized shock in the bulk of the system, separating a low-density region to its left from a high-density region to its right. In the bulk-conserving TASEP shocks appear only on the boundary line between the high-density and low-density phases. On that line a delocalized shock appears in the system. As the position of the shock is equally probable at any site in the system, the average profile on the transition line is linear. In contrast, the TASEP with LK exhibits a distinct phase in which a localized shock, whose position is selected by the dynamics, is present. The existence of this phase plays a main role in our analysis of the two-species model.

The maximal-current phase of the TASEP appears in the TASEP with LK only when the two non-conserving rates, namely particle absorption and desorption, are equal. In this case there exist three more phases. These include a low-max phase, in which the density increases linearly from a boundary density $< \frac{1}{2}$ towards density $\frac{1}{2}$, where it remains constant for the rest of the system ; a max-high phase, in which the density rises linearly from a constant profile of density $\frac{1}{2}$ to a boundary density $> \frac{1}{2}$; and a low-max-high phase, in which the density rises linearly from a left-boundary density $< \frac{1}{2}$ towards $\frac{1}{2}$, where it remains constant up to a point where it climbs linearly again towards a right-boundary density $> \frac{1}{2}$.

9.3 Mean Field Theory

In this section we study the mean field equations of our model in the thermodynamic limit $N \to \infty$. We introduce the occupation variables τ_i and θ_i, such that $\tau_i = 1$ ($\theta_i = 1$) if site i is occupied by a positive (negative) particle, and 0 otherwise. The densities of the positive and negative particles are then defined by

$$p_i = \langle \tau_i \rangle \qquad\qquad m_i = \langle \theta_i \rangle \ , \tag{9.5}$$

where angular brackets denote averaging over realizations.

The time evolution of the particle densities is governed by

$$\begin{aligned} \frac{dp_i}{dt} &= j^+_{i-1} - j^+_i + S^+_i \\ \frac{dm_i}{dt} &= j^-_{i+1} - j^-_i + S^-_i \ , \end{aligned} \tag{9.6}$$

where the currents are given by

$$\begin{aligned} j^+_i &= \langle \tau_i(1 - \tau_{i+1} - (1-q)\theta_{i+1}) \rangle \\ j^-_i &= \langle \theta_i(1 - \theta_{i-1} - (1-q)\tau_{i-1}) \rangle \ , \end{aligned} \tag{9.7}$$

and the source terms are

$$\begin{aligned} S_i^+ &= \omega_A (1 - p_i - m_i) - \omega_D p_i + \omega_X (m_i - p_i) \\ S_i^- &= \omega_A (1 - m_i - p_i) - \omega_D m_i + \omega_X (p_i - m_i) \ . \end{aligned} \tag{9.8}$$

At the boundaries the source terms vanish, and the currents are given by

$$\begin{aligned} j_0^+ &= \alpha (1 - p_1 - m_1) \\ j_N^+ &= \beta p_N \\ j_1^- &= \beta m_1 \\ j_{N+1}^- &= \alpha (1 - p_N - m_N) \ . \end{aligned} \tag{9.9}$$

The mean field theory for this model is defined by replacing two-point correlation functions with products of one-point averages. Within this approximation, the currents become

$$\begin{aligned} j_i^+ &= p_i (1 - p_{i+1} - (1 - q) m_{i+1}) \\ j_i^- &= m_i (1 - m_{i-1} - (1 - q) p_{i-1}) \ . \end{aligned} \tag{9.10}$$

In the steady-state all time derivatives vanish, and one has

$$j_i^+ = j_{i-1}^+ + S_i^+ \qquad\qquad j_i^- = j_{i+1}^+ + S_i^+ \ . \tag{9.11}$$

Defining $\mathcal{J}_i^+ = j_i^+ - \sum_{k=0}^{i} S_k^+, \mathcal{J}_i^- = j_i^- - \sum_{k=i}^{N} S_k^-$, one notices that in fact $\mathcal{J}_i^+ \equiv \mathcal{J}^+$ and $\mathcal{J}_i^- \equiv \mathcal{J}^-$ are conserved throughout the lattice, and $\mathcal{J}^+ = j_0^+, \mathcal{J}^- = j_{N+1}^-$.

9.4 Solution of the mean field equations in the bulk-decoupled case

The case $q = 1, u_X = 1$ is special, as in this case the bulk equations (9.6) with the mean field currents (9.10) are decoupled. The currents and source terms in this case are just

$$\begin{aligned} j_i^+ &= p_i (1 - p_{i+1}) \qquad & S_i^+ &= \tfrac{\Omega}{N} [1 - (2 + u_D) p_i] \\ j_i^- &= m_i (1 - m_{i-1}) & S_i^- &= \tfrac{\Omega}{N} [1 - (2 + u_D) m_i] \ . \end{aligned}$$

In the bulk of the system, the hopping rates for say a positive particle do not distinguish between a negative particle and a vacancy. Also, the fact that attachment of a positive particle is limited by the presence of negative ones, is exactly compensated by the charge exchange rate. The coupling between the

two species is limited in this case only to the boundaries. Following [30, 31], one readily notices that upon the definition

$$\begin{aligned} \alpha^+ &= \frac{\alpha(1-p_1-m_1)}{1-p_1} = \frac{\mathcal{J}^+}{\frac{\mathcal{J}^+}{\alpha}+\frac{\mathcal{J}^-+\mathcal{S}^-}{\beta}} = \frac{j_0^+}{\frac{j_0^+}{\alpha}+\frac{j_0^-}{\beta}} \\ \alpha^- &= \frac{\alpha(1-p_N-m_N)}{1-m_N} = \frac{\mathcal{J}^-}{\frac{\mathcal{J}^-}{\alpha}+\frac{\mathcal{J}^++\mathcal{S}^+}{\beta}} = \frac{j_0^-}{\frac{j_N^-}{\alpha}+\frac{j_N^+}{\beta}} , \end{aligned} \tag{9.12}$$

with $S^\pm = \sum_{i=1}^N S_i^\pm$, the problem is reduced to two single-species TASEP with LK. One process corresponds to the positive particles with injection rate α^+ at the left boundary and ejection rate β at the right, and the other to the negative particles with injection rate α^- at the right boundary and ejection rate β at the left. The two processes may or may not share the same phase. The latter case corresponds to a phase of the two-species system, where the symmetry between the two species is broken. In the other case, it may be that the average densities of the two species are not equal, although the two lie in the same phase of the corresponding TASEP with LK. A trivial restriction on the possible phases in the model is $p_i + m_i \leq 1$ at all sites. This immediately excludes several possibilities, such as ones which mix the high-density phase of one species with anything but the low-density of the other.

In this section we explore the possible phases in the bulk decoupled case. Symmetric phases are presented first, followed by asymmetric phases. In the symmetric phases, $\alpha^+ = \alpha^-$, so for these phases only α^+ is quoted in the following. For the asymmetric phases it is always assumed, with no loss of generality, that the positive particles are in the majority. When describing density profiles we always take a language in which the lattice is rescaled to the segment $[0, 1]$. The emerging phase diagram is discussed in the following paragraph.

Maximal-current symmetric phase

In this phase the bulk density of both species is $\frac{1}{2}$, and the boundary currents are given by

$$j_0^+ = j_0^- = \frac{1}{4} . \tag{9.13}$$

The conditions for this phase to exist are

$$\alpha^+ > \frac{1}{2} \qquad\qquad \beta > \frac{1}{2} . \tag{9.14}$$

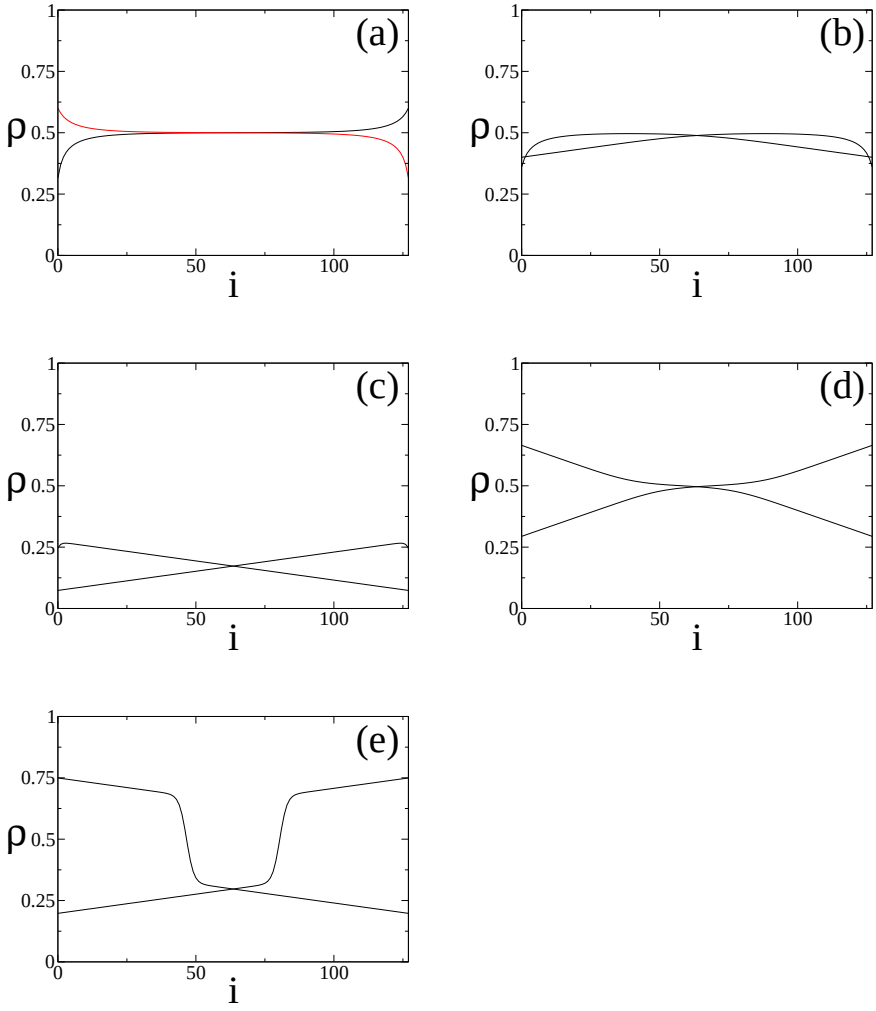

Figure 9.1: Density profiles of the symmetric phases, as obtained by integrating the mean field equations for a system of size $N = 128$. (a) max phase, $\alpha = 3.0$, $\beta = 0.8$, $\Omega = 0.2$, $q = 1$. (b) low-max phase, $\alpha = 1.0$, $\beta = 0.7$, $\Omega = 0.2$, $q = 1$. (c) low phase, $\alpha = 0.1$, $\beta = 0.8$, $\Omega = 0.2$, $q = 1$. (d) low-max-high phase, $\alpha = 5.0$, $\beta = 1/3$, $\Omega = 0.5$, $q = 1$. (e) shock phase, $\alpha = 3.0$, $\beta = 0.25$, $\Omega = 0.2$, $q = 1$.

Typical density profiles of the two species in this phase, as obtained from integrating the mean field equations, are shown in figure 9.1 (a).

Low - max symmetric phase

The density profile in this phase is composed of a low density part where the density increases linearly with slope Ω on the rescaled lattice, as well as a part with constant density $\frac{1}{2}$. The boundary currents are

$$j_0^+ = \alpha^+(1-\alpha^+) \qquad\qquad j_0^- = \frac{1}{4}\,. \tag{9.15}$$

The conditions for the existence of this phase are

$$\alpha^+ < \frac{1}{2} \qquad\qquad \alpha^+ > \frac{1}{2} - \Omega \qquad\qquad \beta < \frac{1}{2}\,. \tag{9.16}$$

The density profiles shown in figure 9.1 (b) for a finite system furthermore exhibits a boundary layer, which does not scale with the system size.

Low density symmetric phase

In this phase both densities remain below $\frac{1}{2}$, increasing throughout the system with constant slope Ω (figure 9.1(c)). The boundary currents are given by

$$j_0^+ = \alpha^+(1-\alpha^+) \qquad\qquad j_0^- = (\alpha^+ + \Omega)(1-\alpha^+-\Omega)\,. \tag{9.17}$$

Necessary conditions for the existence of this phase are

$$\begin{aligned} \alpha^+ &< \beta - \Omega \quad \text{for} \quad \beta < \frac{1}{2} \\ \alpha^+ &< \frac{1}{2} - \Omega \quad \text{for} \quad \beta \geq \frac{1}{2}\,. \end{aligned} \tag{9.18}$$

Inserting the boundary currents (9.17) into (9.12) yields a quadratic equation for α^+. Using (9.18) one readily identifies the relevant solution.

Low - max - high symmetric phase

The density profiles in this phase are a mixture of three different pieces - a linear profile of low densities and constant slope Ω, followed by a flat density profile at density $\frac{1}{2}$, and a linear profile of high-densities of the same slope (figure 9.1(d)). The boundary currents are now

$$j_0^+ = \alpha^+(1-\alpha^+) \qquad\qquad j_0^- = \beta(1-\beta)\,. \tag{9.19}$$

This phase region is defined by the conditions

$$\alpha^+ > \frac{1}{2} - \Omega \qquad\qquad \beta < \frac{1}{2}\,. \tag{9.20}$$

Again, one solves the equation for α^+ given by (9.12) and (9.19), and uses (9.20) to identify the relevant solution. For a finite system (as seen in figure 9.1(d)) the transition between the three parts is not sharp. It only becomes so on the rescaled lattice as $N \to \infty$.

Shock symmetric phase

This phase is characterized by a localized shock, separating a low-density region from a high-density one, both of linear profile with slope Ω. The boundary currents are given by

$$j_0^+ = \alpha^+(1-\alpha^+) \qquad\qquad j_0^- = \beta(1-\beta)\ . \tag{9.21}$$

Notice that α^+ in this phase is identical to the one of the low-max-high phase. The shock symmetric phase is defined by the conditions

$$\beta - \Omega < \alpha^+ < \frac{1}{2} - \Omega\ . \tag{9.22}$$

The position of the shock x_s is given by

$$x_s = \frac{\beta-\alpha^+}{2\Omega} + \frac{1}{2} = \frac{2\beta - (1+\alpha) + \sqrt{(1+\alpha)^2 - 4\alpha\beta}}{4\Omega} + \frac{1}{2}\ . \tag{9.23}$$

In contrast to the thermodynamical limit, the shocks in a finite system such as in figure 9.1 (e) are not sharp.

Shock - low asymmetric phase

In this phase the majority species exhibits a localized shock, while the minority species is in the low phase throughout the system (figure 9.2 (a)). The boundary currents for the two species are

$$\begin{aligned} j_0^+ &= \alpha^+(1-\alpha^+) & j_0^- &= (\alpha^- + \Omega)(1-\alpha^- - \Omega) \\ j_N^+ &= \beta(1-\beta) & j_N^- &= \alpha^-(1-\alpha^-)\ . \end{aligned} \tag{9.24}$$

The conditions for the existence of this phase are given by

$$\alpha^+ > \beta - \Omega \qquad\qquad \alpha^+ < \beta + \Omega \qquad\qquad \beta < \frac{1}{2}\ . \tag{9.25}$$

The equation for α^- does not involve α^+, and can be solved as in previous phases. Plugging this solution into the equation for α^+ one can solve the equation, and identify the only solution which obeys (9.25).

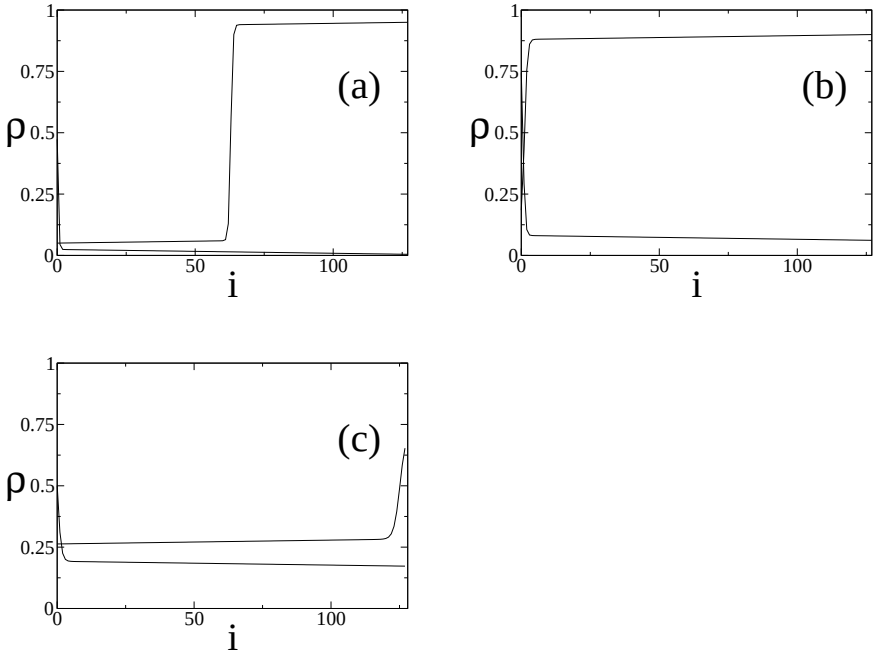

Figure 9.2: Density profiles of the asymmetric phases, as obtained by integrating the mean field equations for a system of size $N = 128$. (a) shock-low asymmetric phase, $\alpha = 0.1$, $\beta = 0.05$, $\Omega = 0.02$, $q = 1$. (b) high-low asymmetric phase, $\alpha = 1.5$, $\beta = 0.1$, $\Omega = 0.02$, $q = 1$. (c) low asymmetric phase, $\alpha = 0.82$, $\beta = 0.31$, $\Omega = 0.02$, $q = 1$.

High - low asymmetric phase

This phase is analogous to the strong asymmetric phase of the Bridge model. In this phase the majority sustains a high density in the bulk of the system, while the minority density is low. Here, however, the density profiles are not constant, but rather of opposite slopes $\pm\Omega$ (figure 9.2 (b)). The boundary currents for the two species are

$$\begin{aligned} j_0^+ &= (\beta+\Omega)(1-\beta-\Omega) & j_0^- &= (\alpha^-+\Omega)(1-\alpha^--\Omega) \\ j_N^+ &= \beta(1-\beta) & j_N^- &= \alpha^-(1-\alpha^-)\,. \end{aligned} \tag{9.26}$$

The conditions for the existence of this phase are

$$\alpha^+ > \beta+\Omega \qquad\qquad \beta+\Omega < \frac{1}{2}\,. \tag{9.27}$$

Expressions for $\alpha^\pm$ are obtained from (9.26), (9.27) just as in the shock-low phase.

Low asymmetric phase

In this phase both particle species maintain a low density profile with constant slope Ω. Still, the phase is asymmetric as the boundary densities of the two phases are different. An analogous phase is also observed on the mean field level in the bridge model. The boundary currents are given by

$$\begin{aligned} j_0^+ &= \alpha^+(1-\alpha^+) & j_0^- &= (\alpha^- + \Omega)(1-\alpha^- - \Omega)\,, \\ j_0^+ &= \alpha^-(1-\alpha^-) & j_0^+ &= (\alpha^+ + \Omega)(1-\alpha^+ - \Omega)\,. \end{aligned} \tag{9.28}$$

Plugging the currents (9.28) into (9.12) gives

$$\begin{aligned} \alpha^+ &= 1 - \frac{\alpha^+(1-\alpha^+)}{\alpha} - \frac{(\alpha^- + \Omega)(1-\alpha^- - \Omega)}{\beta} \\ \alpha^- &= 1 - \frac{\alpha^-(1-\alpha^-)}{\alpha} - \frac{(\alpha^+ + \Omega)(1-\alpha^+ - \Omega)}{\beta}. \end{aligned} \tag{9.29}$$

Let $D = \alpha^+ - \alpha^-$ and $S = \alpha^+ + \alpha^-$. Subtracting the equations in (9.29) yields

$$D = D\left((1-S)\frac{\alpha-\beta}{\alpha\beta} - \frac{2\Omega}{\beta}\right). \tag{9.30}$$

In the asymmetric phase, $D \neq 0$, thus an expression for S is obtained. Summing the equations in (9.29) and using this result yields D as a function of α and β. The effective boundary rates are obtained as $\alpha^+ = \frac{1}{2}(S+D)$ and $\alpha^- = \frac{1}{2}(S-D)$. Necessary conditions for the existence of this phase are

$$\begin{aligned} \alpha^+ < \beta - \Omega \quad &\text{and} \quad \beta < \frac{1}{2} \\ \alpha^+ < \frac{1}{2} - \Omega \quad &\text{and} \quad \beta \geq \frac{1}{2} \\ D > 0\,. & \end{aligned} \tag{9.31}$$

A typical profile for this phase is shown in figure 9.2 (c).

9.5 Phase Diagram

In the previous section we have listed all phases which are found to exist in this model, and derived the phase boundaries in which they reside in parameter space. We now turn to describe the emerging phase diagram. First note that the full parameter space is covered by the four symmetric phases. In fact, all asymmetric phases reside in regions of phase space where the low-density symmetric state is also stationary. Which of the solutions

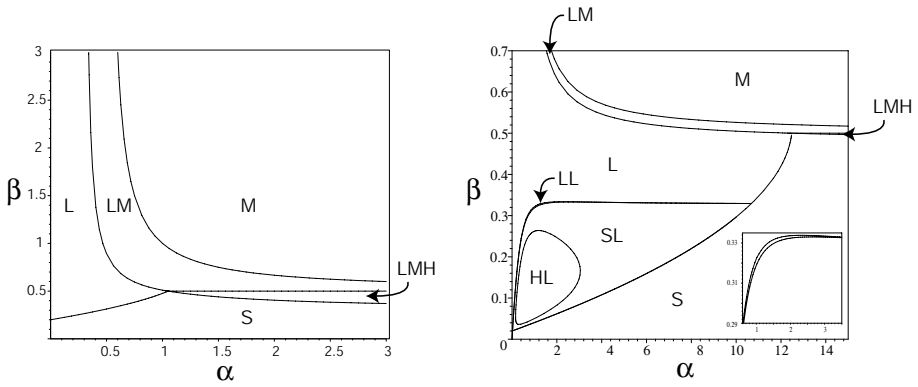

Figure 9.3: Mean field phase diagram for the bulk decoupled case with $\omega_D = 0$ and $\Omega = 0.2$ (left), $\Omega = 0.02$ (right). The inset focuses on the regime where the low-asymmetric phase is most pronounced. Abbreviations used for the phases: M - maximal-current symmetric phase; LM - low-max symmetric phase; LMH - low-max-high symmetric phase; S - shock symmetric phase; L - low symmetric phase; SL - shock-low asymmetric phase; HL - high-low asymmetric phase; LL - low asymmetric phase.

is realized is a matter of stability, as will be discussed shortly. Except for the boundary of the maximal-current phase, the phase boundaries of the symmetric phases share a common point Q in the (α, β) plane, given by

$$Q = \left(\frac{1 - 4\Omega^2}{4\Omega} \, , \, \frac{1}{2} \right) . \tag{9.32}$$

The intersection point of the phase boundary between the low and the shock symmetric phases meets the β axis at the point

$$R = (0 \, , \, \Omega) \ . \tag{9.33}$$

In figure 9.3 we plot the phase diagram for the cases $\Omega = 0.2, 0.02$. Note that at the higher value of Ω no asymmetric phases exist, while at the smaller value all phases described in the previous section exist. This fact will be addressed below. Taking Ω to zero the original phase diagram of the bridge model is retrieved, as discussed below.

Stability

As mentioned above, all asymmetric phases reside in regions of phase space in which the symmetric low density is also a stationary solution of the mean

field equations. On the mean field level, the realization of one stationary solution rather than the other is a matter of initial conditions. In all cases both the symmetric and asymmetric solutions are linearly stable. However, any initial condition for which the density of at least one of the two species is higher than $\frac{1}{2}$ in some region evolves into the state of broken symmetry. Thus a disordered initial condition, in which the density of particles at any site is an independent uniformly distributed random variable, resides in the basin of attraction of the asymmetric solution.

Considering the model beyond mean field approximation, where the dynamics is noisy, one expects a random perturbation to take the system away from the symmetric solution. In physical terms this can be understood by the fact that nucleation of a high density domain leads to its flow towards the boundary, where it reduces the inflow of particles of the other species due to the exclusion interaction. Once the symmetry is broken, the high density phase expands and takes its steady state position. This picture is substantiated in a quantitative manner for the limit $\beta \to 0$ in section 9.10. Note that this line of argument cannot be followed for the asymmetric low phase.

Extinction of the asymmetric phases at high Ω

So far we have considered the case $\omega_D = 0$, where detachment of particles from the bulk is suppressed. In this case the non-conserving rates allow for attachment of particles of either species with rate ω_A and for charge exchange with rate ω_X. While the former process affects the densities of both species in the same way, the charge exchange process tends to diminish the density difference between species. Thus it is clear that for large $\omega_X \sim \Omega$, when this process becomes dominant, the asymmetric phases will vanish. This effect can only increase in the presence of detachment, which acts stronger on the majority species. In the case $\omega_D = 0$ we find that the high-low phase ceases to exist beyond $\Omega \simeq 0.035$. The shock-low phase vanishes at $\Omega \simeq 0.138$, and with it the low asymmetric phase. The vanishing of the asymmetric phases can be understood in a more quantitative manner from the blockage picture described in section 9.11.

The limit $\Omega \to 0$

In the limit of $\Omega \to 0$ the non-conserving model considered here must coincide with the bridge model. In this limit, the point R defined above is shifted towards the origin. The point Q is pushed to infinity, which means that the low-max-high symmetric phase cannot exist. The boundary line between the

low symmetric and the shock symmetric phase is given generally by

$$\beta_{\rm LS} = \Omega + \frac{1}{2} - \frac{1}{2}\sqrt{1-4\alpha\Omega} \;\text{ for }\; \alpha \leq \frac{1-4\Omega^2}{4\Omega}. \tag{9.34}$$

Thus $\beta_{\rm LS} \to 0$ for all α as $\Omega \to 0$, and the shock symmetric phase cannot exist. Furthermore the low-max symmetric phase vanishes in this limit. The boundary between this phase and the maximal-current phase,

$$\beta = \frac{\alpha}{2\alpha - 1} \;\text{ for }\; \alpha > \frac{1}{2}\,, \tag{9.35}$$

coincides in the limit $\Omega \to 0$ with its boundary with the low phase,

$$\beta = \frac{\alpha}{2\alpha - 1 + 4\Omega(\alpha+\Omega)} \;\text{ for }\; \frac{1}{2} < \alpha < \frac{1-4\Omega^2}{4\Omega}\,. \tag{9.36}$$

Thus, of the symmetric phases only the maximal-current phase and the low phase remain in the $\Omega \to 0$ limit, as expected from the bridge model.

As for the asymmetric phases, one notices in the same way that as Ω decreases, the high-low phase region grows on the expense of the shock-low phase. As $\Omega \to 0$, the boundary lines of both phases coincide, and the shock-low phase ceases to exist. Exact expressions for these phase boundaries are rather lengthy, and are omitted here. Finally, the low density asymmetric phase takes in the $\Omega \to 0$ limit its form as in the bridge model.

9.6 Detachment from the bulk: the case $\omega_D \neq 0$

We now turn to consider a more general case, still within the bulk-decoupled regime ($q = 1, \omega_D = \omega_X$), where the non-conserving dynamics includes detachment of particles. This case corresponds to the TASEP with LK and non-equal attachment and detachment rates. The phase diagram of that model includes only three phases: high density, low density and localized shock. All phases where a part of the profile is constant at $\frac{1}{2}$ do not exist. This comes from the fact that the equilibrium density of the kinetics is given by the Langmuir density rather than $\frac{1}{2}$.

The phase diagram of our model in the case $\omega_D \neq 0$ exhibits only two symmetric phases - the symmetric low-density phase and the shock symmetric one. All asymmetric phases which were obtained for the case $\omega_D = 0$ are also present here. As in the TASEP with LK, the density profiles in this case are not linear, but rather curved. This makes the analysis of the phase diagram

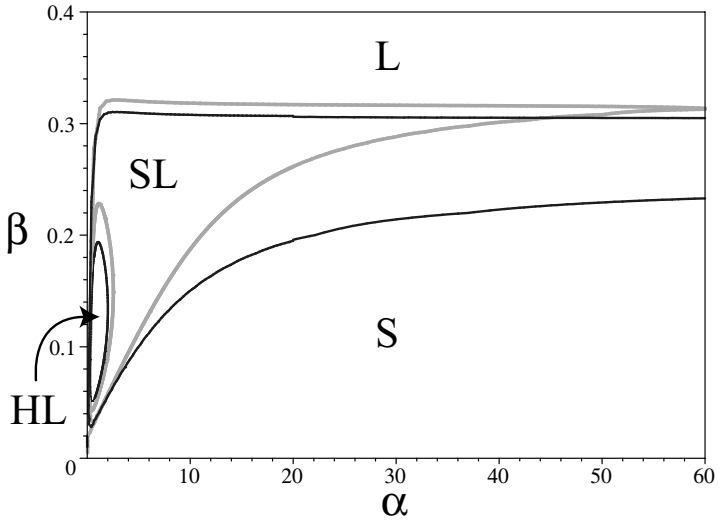

Figure 9.4: Mean field phase diagram for the bulk-decoupled case, with $\Omega = 0.02$ and $u_D = 1$ (gray lines), $u_D = 2$ (dark lines) . The boundary line between the asymmetric low-density phase and the symmetric low phase is omitted. Abbreviations for the different phases are the same as in figure 9.3.

somewhat more cumbersome, although not different in principle from the one presented in section 9.4. Details of this calculation are given in the appendix.

In figure 9.4 we plot the mean field phase diagram for the cases $u_D = 1$ and $u_D = 2$, where u_D is defined as before by $u_D = \omega_D/\omega_A$. The boundary line between the asymmetric low-density phase and the symmetric low phase is not presented. We could not obtain the boundary densities in this phase in a closed form. For several values of u_D we have found numerically that this line lies just above the transition line between the shock-low phase and the asymmetric low phase. Certainly, the region of phase space covered by this phase does not increase compared with the case $\omega_D = 0$. It is readily noticed that the part of phase space spanned by the high-low asymmetric phase decreases as ω_D is increased. This is expected from the fact that the detachment process acts stronger on the majority phase, thus reducing its density. For any given Ω the detachment process can be increased to a level in which the high-low asymmetric phase does not occur.

The detachment process can be considered as cooperating with the boundary ejection rate β, and competing with the boundary injection rate α. It is no surprise then that the asymmetric shock-low phase grows in the α direction of phase space and shrinks in the β direction as ω_D is increased. In the regions of phase space which compose the three phases identified only

for the case $\omega_D = 0$, the density profiles approach continuously, as ω_D is decreased towards zero, to the ones described in the corresponding phases of the $\omega_D = 0$ case.

9.7 Monte Carlo simulations

As was already noticed in earlier works about the bridge model [30, 31, 34], the mean field phase diagram captures the correct topology of the phase boundary lines. The exact location of the boundary lines, however, is shifted in the noisy model with regard to those of the mean field solution. For our model we did not try to obtain the exact location of the phase boundary lines from Monte Carlo (MC) simulations. Still we note, based on our simulations, that these lines cannot lie too far from those of the mean field phase diagram obtained in the previous section. Here we concentrate on giving evidence for each of the phases by finding representative points in parameter space. In figure 9.5 we present the density profiles of the two species in the different phases as obtained from MC simulations. The profiles in each phase were taken at the same parameters as the respective mean field profiles shown in figures 9.1 and 9.2. For all phases shown here the mean field profiles capture the features of the noisy model. While MC simulations were done for a system of size $N = 2000$, the mean field results are obtained for $N = 128$. A quantitative comparison between the profiles becomes meaningful in the limit $N \to \infty$ using rescaled coordinates $x = i/N$. In this limit the localized shocks in the shock-low and symmetric shock phase become sharp [66]. In figure 9.5 the density profile for the low asymmetric phase is omitted. This phase is addressed in the following paragraph.

9.8 The low asymmetric phase

The existence of the low asymmetric phase is an issue of longstanding discussion [34, 64] (see also chapter 4). It was noted already in the mean field solution of the bridge model [30, 31] that the region in phase space covered by this phase is very small compared to the others. Furthermore MC simulations indicate that the particle densities in this region of phase space fluctuate strongly [64]. These facts also hold true in the model considered here. Therefore we refrain from presenting a MC density profile as was done for the other phases. In [64] the existence of the low-asymmetric phase in the bridge model is deduced from sampling the probability distribution $P(\bar{p}, \bar{m})$, where $\bar{p}$ and $\bar{m}$ are the average densities of positive and negative particles

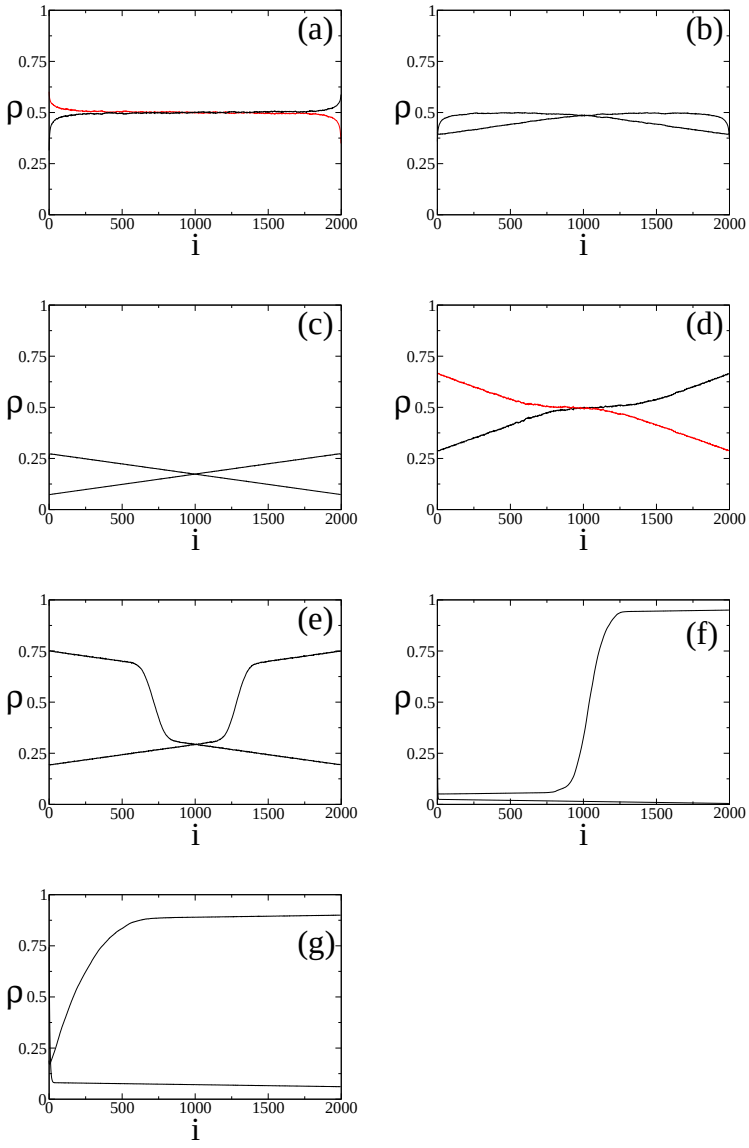

Figure 9.5: Density profiles as obtained from a Monte Carlo simulation of a system of size $N = 2000$. (a) max phase, $\alpha = 3.0$, $\beta = 0.8$, $\Omega = 0.2$, $q = 1$. (b) low-max phase, $\alpha = 1.0$, $\beta = 0.7$, $\Omega = 0.2$, $q = 1$. (c) low phase, $\alpha = 0.1$, $\beta = 0.8$, $\Omega = 0.2$, $q = 1$. (d) low-max-high phase, $\alpha = 5.0$, $\beta = 1/3$, $\Omega = 0.5$, $q = 1$. (e) shock phase, $\alpha = 3.0$, $\beta = 0.25$, $\Omega = 0.2$, $q = 1$. (f) shock-low asymmetric phase, $\alpha = 0.1$, $\beta = 0.05$, $\Omega = 0.02$, $q = 1$. (g) high-low asymmetric phase, $\alpha = 1.5$, $\beta = 0.1$, $\Omega = 0.02$, $q = 1$.

in the system respectively. In our model, this line of argument fails. On the level of average densities, the low-low and shock-low phases cannot be distinguished. This is because both phases can exhibit distributions $P(\bar{p}, \bar{m})$ with two peaks at $\bar{p}$ and $\bar{m}$ smaller than $\frac{1}{2}$.

The blockage picture outlined in section 9.11 yields no arguments in favor of the low asymmetric phase. At the upper boundary of the shock-low phase the localized shock position retracts to $x_s = 0$. This allows particles of both species to enter the system. A symmetry broken low phase beyond this point would require some kind of blockage being formed at the exit of the majority species. The nature of such a blockage is not clear. It remains to be clarified, whether the existence of this phase, which is evident in the mean field treatment, can be demonstrated in the noisy model.

9.9 Induced shocks

In the case $q \neq 1$ the bulk dynamics of the two particle species are not decoupled. Thus, one cannot solve the mean field equations in the way it was done in section 9.3. Still, the phase structure can be explored by integrating the mean field equations numerically, or by MC simulations. It shall not be attempted here to give the full phase diagram of the model. We do note, however, that phases with broken symmetry exist also in the general case.

In the shock symmetric phase and the shock-low phase the coupling of the dynamics of the two species gives rise to an *induced shock* phenomenon. Here the existence of a localized shock in the density profile of one species induces a shock in the density profile of the other species. For example, in the shock symmetric phase one notices that the density profile of each one of the species exhibits actually *two* shocks in the steady state (figure 9.6). One is a *primary shock*, created by the same localization mechanism which was already identified in the bulk-decoupled case. The existence of this shock, albeit not its detailed properties, relies only on the properties of the density profile of the very same species. The second shock is *induced* by the primary shock in the density of the other species, and it shares its location. Across both shocks the current is continuous. This phenomenon also occurs in the shock-low phase (figure 9.6). Here, the localized shock in the majority phase induces a shock in the low phase. In fact, it was shown in [82] that for general two species systems with coupled density-current relation a shock in one particle species induces a shock in the other one.

For general q the current-density relation of, say, the positive particle species, $j_i^+(p_i, m_i)$, depends on the local density of both species. In general this current-density relation is not known, except for two cases: the case

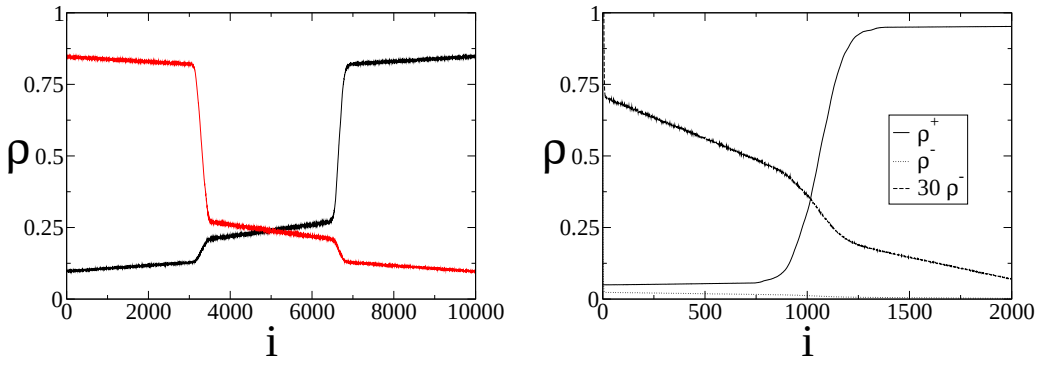

Figure 9.6: *Induced shocks.* (Left) Density profiles in the symmetric shock phase, as obtained in Monte Carlo simulations. A primary shock in one of the species is accompanied by an induced shock in the other species. Here $q = 2$ and $\alpha = 3.0$, $\beta = 0.25$, $\Omega = 0.02$. (Right) Density profiles in the shock-low phase, as obtained in Monte Carlo simulations. The localized shock in the majority species is accompanied by an induced shock in the minority species. The profile of the minority species is additionally shown when multiplied by a factor of 30, in order to demonstrate the induced shock phenomenon. Here $q = 2$ and $\alpha = 0.1$, $\beta = 0.05$, $\Omega = 0.02$.

$q = 1$ (the decoupled case), where $j^+ = p(1-p)$, and the case $q = 2$, where $j^+ = p(1-p+m)$ [30, 31].

As discussed in [7] the current across a localized shock is continuous. This requirement implies when $q = 1$ that shocks are symmetric with respect to $p = 1/2$, irrespective of the local density m of particles of the opposite species. In general, however, this is not the case. The properties of both the primary and induced shock in the density profile of each species rely on the local densities of both.

The continuity of the current across the shocks can in principle be used to determine the properties of the primary and induced shocks, if one can develop the density characteristics from the boundaries of the system. For the case $q = 1$ the equations for the two density profiles are decoupled, and one uses this method to determine the position of the shock. Of course, no induced shocks are present in this case. For general q, however, the equations for the density profiles are coupled, and an analytical solution is not available.

9.10 Exact solution for the limit $\beta, \Omega \to 0$

In [33] a *toy model* was presented to allow for the exact solution of the limit $\beta \to 0$ of the bridge model. In this section a generalization of the toy model is presented. The solution of this model gives an exact description of the $\beta \to 0,\ \Omega \to 0$ limit of the model, and proves that to lowest order in β mean field theory recovers the exact phase diagram.

In the limit $\beta \to 0, \Omega \to 0$ the only relevant configurations are those composed of three blocks, containing (from left to right) negative particles, vacancies, and positive particles. A configuration of this type is long-lived, as all exit rates from it scale to zero. In this limit, all other configurations rearrange themselves into one of these three-block configurations. A configuration of this type is identified by two variables, y and x, defined as the size of the left (negative particle) block and the right (positive particle) one, respectively. Thus, for example,

$$\overbrace{- - - -}^{N_-}\ \overbrace{0\,0\,0\,0\,0}^{N-N_--N_+}\ \overbrace{+ + + + +}^{N_+} \quad \longleftrightarrow \quad (x = N_+, y = N_-)\ .$$

Let us assume that the system is in a three-block configuration (x, y), and consider the ways it can leave it. First, a particle can leave the system through a boundary with rate β, leaving a vacancy behind it. This vacancy can travel into the system with rate $(1+\alpha)^{-1}$, in which case the system is again in a three-block configuration. Otherwise, the particle which had left the system can be replaced by a particle of the opposite species with rate $\alpha(1+\alpha)^{-1}$. On a short time scale this particle travels through the system until it joins the block on the other side, thus returning the system into a three-block state.

Another possible way out of a three-block configuration is through the non-conserving processes in the bulk. First, a particle can be attached to the system in the vacancy domain with rate $\omega_A(N-x-y)$. This particle joins on a short time scale to the block of its own species. Second, a positive (negative) particle can be detached from the system with rate $\omega_D x$ ($\omega_D y$), thus creating a vacancy within a particle block. On a short time scale this vacancy travels into the system and joins the vacancy block. Finally, a positive (negative) particle can change its species with rate $\omega_X x$ ($\omega_X y$), and move from one particle block to the other.

When the last particle of its species leaves the system, the other type of particles can rush into the system through the boundary. The system fills rapidly with particles of this type. Thus, the only possible configurations with $x = 0$ or $y = 0$ are $(0, N)$ and $(N, 0)$.

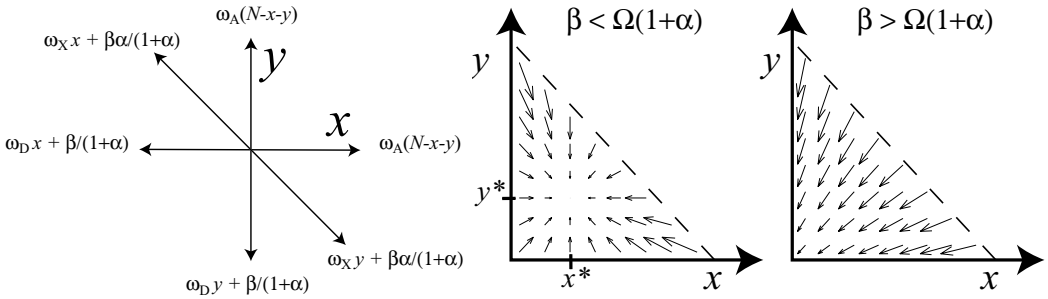

Figure 9.7: *Toy model* for the limit $\beta, \Omega \to 0$. (Left) The rates defining the corresponding random-walk model (9.37). (Right) Flow fields of the model.

To summarize, consider a two-dimensional random walker, whose position (x, y) corresponds to the block-configuration of the two-species system. The transition rates for this walker are (see also figure 9.7)

$$\begin{aligned}
(x,y) \to (x+1,y) \quad & \text{with rate} \quad \omega_A(N-x-y) \\
(x,y) \to (x,y+1) \quad & \text{with rate} \quad \omega_A(N-x-y) \\
(x,y) \to (x-1,y) \quad & \text{with rate} \quad \beta\frac{1}{1+\alpha} + \omega_D x \\
(x,y) \to (x,y-1) \quad & \text{with rate} \quad \beta\frac{1}{1+\alpha} + \omega_D y \\
(x,y) \to (x-1,y+1) \quad & \text{with rate} \quad \beta\frac{\alpha}{1+\alpha} + \omega_D x \\
(x,y) \to (x+1,y-1) \quad & \text{with rate} \quad \beta\frac{\alpha}{1+\alpha} + \omega_D y \\
(1,y) \to (0,N) \quad & \text{with rate} \quad \beta \\
(x,1) \to (N,0) \quad & \text{with rate} \quad \beta\ .
\end{aligned} \tag{9.37}$$

It can be shown that this toy model is mapped exactly to the two-species model in the limit $\beta, \Omega \to 0$, in the sense formulated in appendix A of [33].

Let us first consider the case where the dynamics defined in (9.37) leads to a fixed point solution. This is the case where the net flows on both the x and y directions vanish at some point (x^*, y^*). The fixed points must satisfy the equations

$$\begin{aligned}
(\omega_X - \omega_A)x^* - (\omega_X + \omega_A + \omega_D)y^* &= -\omega_A N + \frac{\beta}{1-\alpha} \\
-(\omega_X + \omega_A + \omega_D)x^* + (\omega_X - \omega_A)y^* &= -\omega_A N + \frac{\beta}{1-\alpha}\ ,
\end{aligned} \tag{9.38}$$

whose solution is

$$\frac{x^*}{N} = \frac{y^*}{N} = \frac{1}{2+u_D}\left(1 - \frac{\beta}{\Omega(1+\alpha)}\right) . \tag{9.39}$$

Interestingly, the fixed point does not depend on the charge exchange rate ω_X. Notice that this fixed point can only exist if $0 \leq x^*/N,\ y^*/N \leq 1$. Indeed, x^* and y^* of (9.39) always meet the second condition. The first condition, however, is only met for

$$\beta < \Omega(1+\alpha) . \tag{9.40}$$

Otherwise, the random walker is always biased towards the axis of the (x, y) plane which is closer to its position (see figure 9.7). In this case, $\Omega < \beta \to 0$, one recovers the toy model of [33] which yields a stable state of broken symmetry. One of the species then occupies most of the lattice, corresponding to the high-low asymmetric phase of the model.

Thus, the toy model yields two phases in the limit $\beta, \Omega \to 0$. For $\beta < \Omega(1+\alpha)$ one has a symmetric phase, with a dominating three-block configuration described by (9.39). This corresponds to a symmetric shock phase in the model, where the shock position of the positive particles is $x_s = 1 - x^*/N$, with x^* given by (9.39). Otherwise the system is in the high-low asymmetric phase, with the line $\beta = \Omega(1+\alpha)$ serving as the transition line between the two phases.

For the bulk-decoupled case, $\omega_A = \omega_X$ and $q = 1$, it is illuminating to compare these exact results with the ones obtained by mean field. The mean field analysis, performed in section 9.3, predicts in the limit $\beta, \Omega \to 0$ the two phases obtained in the toy model. The mean field transition line between the two phases (9.22) is identical, to first order in β, to the line $\beta = \Omega(1+\alpha)$ of the toy model. Also the shock position x_s calculated in the toy model is identical to first order in β to the one (9.23) calculated in mean field. This result also holds in the case $\omega_D \neq 0$. We thus conclude that the mean field solution is exact to first order in β.

9.11 Blockage picture

In this section we combine the mean field and stability analysis, the simulation results, and the toy model into a physical picture. Following [64] we term it the *blockage picture*.

Qualitatively, typical configurations in the asymmetric phases can be described in terms of blocks of the two species, which spread from the 'exit'

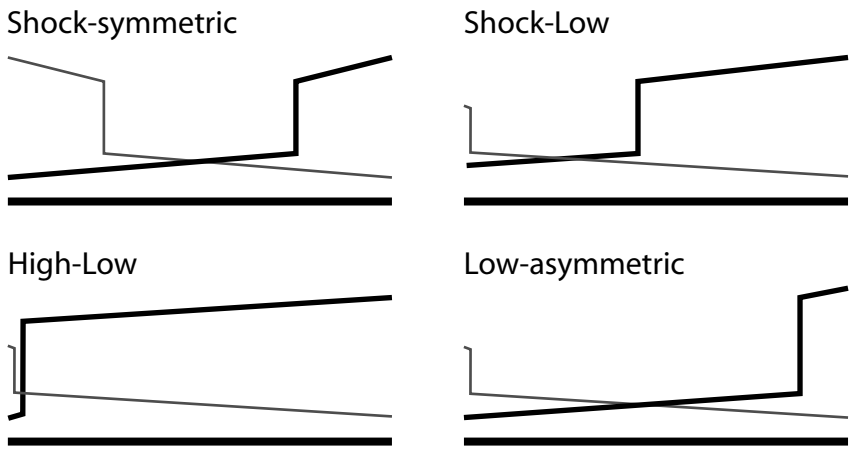

Figure 9.8: *Blockage picture.* Schematic picture of the instantaneous density profiles. Density profiles of positive particles are depicted by dark lines, negative particles by gray lines. Here, as in the text, we assume that the positive particles are the majority species.

boundary into the system (figure 9.8, and compare the toy model description in the previous section). The density profile within each block is not constant, but this feature is not relevant here. As mentioned above, a block of one species stalls the entry of particles of the other species through the boundaries, thus serving as a blockage. The possibility of particles to enter the system in the bulk serves to stabilize the domain size.

In the high-low phase the block of the majority species covers the entire system, while in the shock-low phase the block is limited to some part of the system. The fluctuations in the size of this block, corresponding to the width of the localized shock, are limited to an area of size $\sim N^{-1/2}$ [66]. The minority block in both phases is unstable in the sense that the domain wall between it and the bulk region drifts towards the boundary. Averaging over the positions of the domain wall results in the exponential decay of the mean field density profile from the left boundary.

In [64] it was observed that an instantaneous configuration in the low-density asymmetric phases comprises a small block of the majority phase, which is limited to the vicinity of the boundary. The formation of this block prevents particles of the other species from entering the system, thus leading to symmetry breaking. However, this block does not survive for times which are exponential in the system size.

The block picture is extended into the symmetric shock phase. Here the two blocks are covering equal distances from the 'exit' boundaries. The sizes

of the two blocks are again macroscopic and localized, in the sense that the size fluctuations vanish as $N^{-1/2}$.

We now turn to describe the different phases of the model in the language of block configurations. To this end we take a stroll along a line of constant α in the phase diagram, starting from the symmetric shock phase and going up in β. This line is chosen such that it cuts through all asymmetric phases.

In the shock symmetric phase, the two blocks inhibit, in a symmetric way, the inflow of particles of the opposite species. Increasing β decreases the sizes of the two blocks. However, as long as their size is macroscopic, the blocks keep their role of lessening the ability of particles of the other species to enter the system.

As the boundary line is approached, the size of the blocks is reduced to zero. Now the road is open for both species to enter the system. Due to fluctuations, the formation of a block is inevitable. As β is increased beyond the transition line into the shock-low phase, the possibility rises that this block will be stabilized by the non-conserving dynamics. A spontaneously created block of one species, which now has a stable macroscopic size, hinders particles of the other species and breaks the symmetry between the two species.

As β is increased from its value at the boundary line between the symmetric shock phase and the shock-low phase, the size of the block of the majority species increases. This is due to the coupling between the ejection rate β and the effective injection rates, which at this region of phase space serves to increase α^+ (in mean field this can be seen from eqs. (9.12), (9.24)). At some value of β, the block reaches the size of the entire system, and there it stays for some range of β. This, in fact, is the high-low phase of the system. As β is increased further the size of the majority block shrinks back, and the system is again in the shock-low phase. The transition from the shock-low phase to the high-low phase at some β, and the re-entrance to the shock-low phase at some higher β, occur at these points where the size of the majority blockage becomes identical with the size of the system.

Towards the boundary line between the shock-low phase and the low-density phase the size of the majority block vanishes. The existence of a reminiscent block which yields the asymmetric low phase, as discussed in [64], can be either attributed to fluctuations of the localized shock, or to an alternative mechanism.

To make the blockage picture more quantitative, we calculate the size of the majority block in each phase. This is done within mean field for the bulk-decoupled case. For simplicity we take $\omega_D = 0$, where the profiles of the blocks are linear. The block size is then just $1 - x_s$, where the shock position x_s is given in (9.23). In figure 9.9 (a) we plot the size of the block

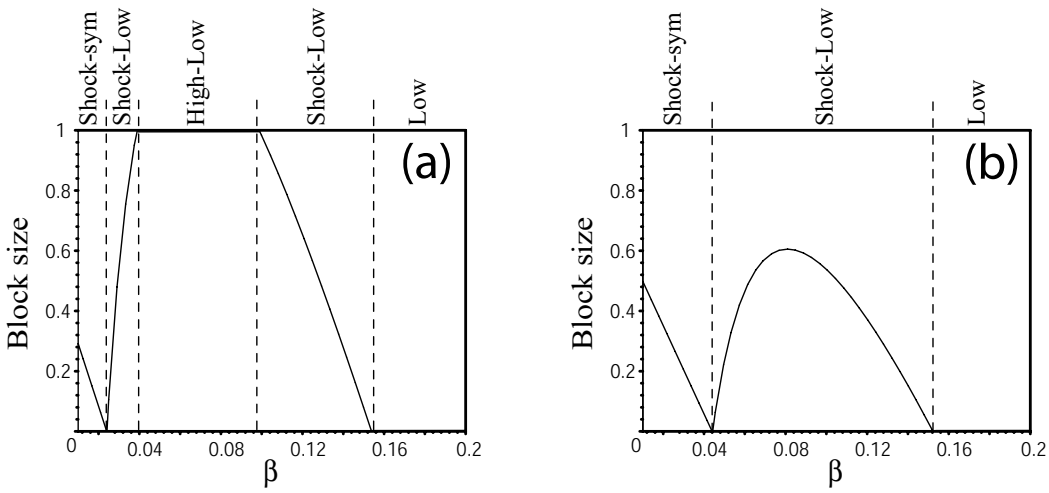

Figure 9.9: Blockage size as a function of β, as calculated in mean field for the bulk-decoupled case. Here $\alpha = 0.2, \omega_D = 0$ and (a) $\Omega = 0.02$, (b) $\Omega = 0.03$.

as a function of β at constant Ω and α. Using the picture described above, one can identify the phase boundaries. The value of β at which the blockage first disappears corresponds to the shock-symmetric to shock-low line. The two values between which the blockage spans the system are identified as the two lines between the shock-low and high-low phases. Finally, the higher β at which the blockage disappears completely corresponds to a transition into a low-density phase. It is easy to verify, by comparing with the mean field phase diagram, that these are indeed the transition points between the phases. Note that the low asymmetric phase escapes this picture.

It is also possible to describe in terms of the block size (or alternatively the shock position) the fact that asymmetric phases disappear as Ω is increased. The non-conserving dynamics in the bulk of the system serves to sustain the localized shock. Keeping α constant, for example, the increase in the amplitude of the non-conserving rates drives the position of the shock out of the system, thus decreasing the maximal size of the blockage. In terms of phases, this would decrease the segment on the β axis in which the shock is localized at the 'entry' boundary (*i.e.* the high-low phase), down to a point where the shock cannot get so far and the phase disappears. Beyond this point, as depicted in figure 9.9 (b), the position of the shock is driven back towards the 'exit' boundary, thus reducing the shock-low phase until it is finally gone.

9.12 Conclusion

In this chapter a two species one-dimensional model, with dynamics which is not conserving both at the boundaries and in the bulk, has been studied. The dynamics is symmetric under charge exchange and left-right reflection. By definition the non-conserving dynamics in the bulk of the system acts to diminish the difference between the densities of the two species. Nevertheless we have found that the symmetry between the two species can be broken even in the presence of bulk non-conserving processes.

The mean field phase diagram, obtained for the case where the bulk dynamics of the two species becomes decoupled, exhibits three phases in which the symmetry between the species is broken. One of these is unique to the case where the bulk dynamics is not conserving, and results from a localization of shocks in the density profiles. All asymmetric phases reside in regions of phase space where symmetric low-density profiles are another fixed point of the mean field dynamics. However, stability arguments shows that it is the asymmetric solution which should be expected to survive fluctuations. Indeed, comparing with Monte Carlo simulations, two asymmetric phases are confirmed. The third, in which the average density of both species is below $\frac{1}{2}$ is more difficult to determine.

In contrast to the bulk-conserving case, in this model the density profiles are generally not flat. In particular, localized shocks may be generated in the bulk of the system. In the general case, when the particle current of one species depends on the density of the other, a localized shock in the density profile of one species induces a shock in the other.

In the asymmetric phases, as well as in the shock symmetric phase, typical configurations can be described in terms three blocks. The leftmost block has a high density of negative particles, the middle block has a low density of particles of both species, and the right block is mainly occupied by positive particles. This observation serves to define a toy model which describes the dynamics of the system in terms of a two-dimensional random walker. Solving the toy-model yields an exact solution for the case where the exit rates and the non-conserving rates are taken to zero. The results coincide with the ones obtained in mean field at this limit. For the general case a more qualitative picture emerges, which serves to describe the phase transitions in the model in terms of the block sizes.

The bulk of this chapter, as well as of those works which studied the bridge model, has focused on the case in which the dynamics of the two species is decoupled in the bulk. The other, more general case, was studied only by numerical means, both on the mean field level and in Monte Carlo simulations. This enabled us to observe induced shocks. A more detailed study of

this case by analytical means should shed more light on this phenomenon.

The mean field phase diagram of the TASEP with LK is expected to be exact [7], while Monte Carlo results suggest that this is not the case here. Such is also the case in the bridge model. It should be interesting to study the correlations which build up in the system, taking it away from the mean field description.

9.13 Appendix: Mean field analysis of the case $\omega_D > 0$

In this Appendix we discuss the construction of the phase diagram for the bulk-decoupled case $q = 1,\ \omega_A = \omega_X$ with $\omega_D \neq 0$. This case corresponds to the TASEP with LK and non equal attachment and detachment rates (the case $K \neq 1$ in [7, 66, 74]). The phase diagram of the model in the case $\omega_D \neq 0$ exhibits two symmetric phases, symmetric low-density phase and shock symmetric one, and three asymmetric ones, high-low density phase, shock-low phase, and low-density asymmetric phase. The profiles do not have constant slopes as in the $\omega_D = 0$ case. Starting from left boundary density α, the density at the right boundary resulting from the left characteristic is given by

$$\rho_N^{(\ell)}(\alpha) = \frac{2 - uW_0\left(\frac{(2-4\alpha-2\alpha u)}{u}\exp\left(-\frac{4\,\alpha+2\,\alpha\,u+\Omega(2+u)^2-2}{u}\right)\right)}{2(2+u)}. \tag{9.41}$$

The respective expression for the density at the left boundary resulting from the right characteristics starting from density $1-\beta$ reads

$$\rho_1^{(r)}(\beta) = \frac{2 - uW_{-1}\left(\frac{(4\beta-2-2u+2\beta u)}{u}\exp\left(\frac{\Omega(2+u)^2-2(1+u)+2\beta(2+u))}{u}\right)\right)}{2(2+u)}\,. \tag{9.42}$$

Our aim is to use the known phase diagram of the TASEP with LK [66] to construct the phase diagram of the two species model, as it was done in section 9.4. To this end, let us define the two transition lines in this phase diagram. The first is the transition line between the high density phase and the localized shock phase,

$$\beta_{\rm HS}(\alpha) = \frac{2(1+u) + u\mathrm{W}_0\Big(\frac{(4\alpha-2-2u+2\alpha u)}{u}\exp\Big(\frac{-4\alpha+2+2u-2\alpha u+\Omega(2+u)^2}{u}\Big)\Big)}{2(2+u)}\,. \tag{9.43}$$

where $\mathrm{W}_k(z)$ is the Lambert-W function. This equation defines the line only for $\alpha < 1/2$. The second transition line separates the shock phase and the low density phase. This line is given, for $\alpha < 1/2$, by

$$\beta_{\mathrm{SL}}(\alpha) = \frac{2 - u\mathrm{W}_{-1}\Big(\frac{(2-4\alpha-2\alpha u)}{u}\exp\Big(-\frac{4\,\alpha+2\,\alpha\,u+\Omega(2+u)^2-2}{u}\Big)\Big)}{2(2+u)} \ . \tag{9.44}$$

Both boundary lines are continued for $\alpha > 1/2$ by $\beta_{\mathrm{HS}}(\frac{1}{2})$ and $\beta_{\mathrm{SL}}(\frac{1}{2})$, respectively.

Let us recall the procedure in which one obtains the phase diagram for the two species model. For each phase, one obtains from (9.12) the effective boundary rates, α^+ and α^-. This requires knowledge of the four boundary currents, $j_b^+ = p_b(1-p_b)$ and $j_b^- = m_b(1-m_b)$, where $b = 0, N$ for the left and right boundaries. The boundary lines are then obtained from comparing the effective boundary rates with the corresponding transition lines of the TASEP with LK.

We do not repeat the analysis here in such details as it was done for the case $\omega_D = 0$. Instead, we give for each phase the four boundary densities, needed to calculate the boundary currents and the effective rates. In addition the conditions on the effective rates, which define the phase boundaries, are given in terms of β_{HS} and β_{SL} of eqs. (9.43) and (9.44). The asymmetric low-density phase is omitted, as we could not obtain the boundary densities in this phase in a closed form. The boundary lines for this case were obtained numerically.

Low density symmetric phase. Here, $p_0 = m_N = \alpha^+$, $p_N = m_1 = \rho_N^{(\ell)}(\alpha^+)$ as in (9.41). The condition for the existence of this phase is

$$\beta < \beta_{\mathrm{SL}}(\alpha^+) \ . \tag{9.45}$$

Shock symmetric phase. The boundary densities are given by $p_0 = m_N = \alpha^+$, $p_N = m_1 = 1-\beta$. The conditions for this phases existence are

$$\beta_{\mathrm{SL}}(\alpha^+) < \beta < \beta_{\mathrm{HL}}(\alpha^+) \ . \tag{9.46}$$

Shock - Low asymmetric phase. Let the positive particles be in the shock phase. Then $p_0 = \alpha^+$, $p_N = 1-\beta$. The negative particles are in the low phase, where $m_N = \alpha^-$ and $m_1 = \rho_N^{(\ell)}(\alpha^-)$ as given by equation 9.41. The phase exists in a region in phase space where

$$\beta_{\mathrm{SL}}(\alpha^+) < \beta < \beta_{\mathrm{SL}}(\alpha^-) \ . \tag{9.47}$$

High - low asymmetric phase. As before it is assumed that the positive particles are in the majority phase: $p_0 = \rho_1^{(r)}(\beta)$ according to 9.42 and $p_N =$

$1-\beta$. The negative particles are in the low phase: $m_N = \alpha^-$ and $m_1 = \rho_N^{(\ell)}(\alpha^-)$. The high-low phase exists where

$$\beta_{\rm HL}(\alpha^+) < \beta < \beta_{\rm SL}(\alpha^-) \; . \tag{9.48}$$

Chapter 10

Directed percolation in an external field

10.1 Universal scaling behavior of directed percolation around the upper critical dimension

In this section we consider the universal scaling behavior of directed percolation in presence of an external field (see subsections 2.3 and 5.2) in various dimensions. Whereas most investigations on DP follow the seminal work ref. [112] and thus focus on activity spreading, we examine the steady state scaling behavior for $D \leq 5$. We determine the universal scaling functions of the order parameter (i.e. the equation of state) and its fluctuations. Furthermore we consider certain universal amplitude combinations which are related to the order parameter and its susceptibility. These amplitude combinations are immediately related to particular values of the universal scaling functions and are of great experimental interest [113]. We will see that the numerically obtained universal scaling functions and the related universal amplitude combinations allow a quantitative test of RG-results. The powerful and versatile ϵ-expansion provides estimates of almost all quantities of interest, e.g. the critical exponents and the scaling functions (see e.g. [114]). Unfortunately it is impossible to estimate within this approximation scheme the corresponding error-bars. Thus it is intriguing to compare our results with those of RG analysis [49, 50]. Furthermore we focus on the phase transition at the upper critical dimension $D_c = 4$. There the usual power-laws are modified by logarithmic corrections. These logarithmic corrections are well established in equilibrium critical phenomena [115, 116] but they have been largely ignored for non-equilibrium phase transitions. Due to the considerable numerical effort, sufficiently accurate simulation data for non-equilibrium systems became available only recently: Investigated systems include self-avoiding random walks [117, 118], self-organized critical systems [119, 120], depinning-transitions in disordered media [121], isotropic percolation [122], as well as absorbing phase transitions [123]. On the other hand, the numerical advance triggered further analytical RG calculations yielding estimates for the logarithmic correction exponents for the respective systems [50, 124–126]. The outline of the present section is as follows: The next subsection contains the model definition and a description of the method of numerical analysis. In subsection 10.1.2 we describe the scaling behavior at the critical point and introduce the critical exponents as well as the universal scaling functions. The numerical data of the order parameter and its fluctuations are analyzed in subsection 10.1.3 below ($D = 1, 2, 3$), above ($D = 5$), and at the upper critical dimension ($D = 4$). Several amplitude combinations are considered in subsection 10.1.4. Concluding remarks are given in subsection 10.1.5.

The results of this section were obtained in collaboration with S. Lübeck and published in ref. [11].

10.1.1 Model and simulations

In order to examine the scaling behavior of the D-dimensional DP universality class we consider the directed site percolation process using a generalized Domany-Kinzel automaton [127]. It is defined on a $D+1$-dimensional body centered cubic (bcc) lattice (where time corresponds to the $[0,0,\ldots,0,1]$ direction) and evolves by parallel update according to the following rules: A site at time t is occupied with probability p if at least one of its 2^D backward neighboring sites (time $t-1$) is occupied. Otherwise the site remains empty. Furthermore, spontaneous particle creation may take place at all sites with probability p_0 (see fig. 10.1). This spontaneous creation process can be viewed as unidirectional coupling to a bulk reservoir, as outlined in subsection 5.2. Directed site percolation corresponds to the choice $p_0 = 0$.

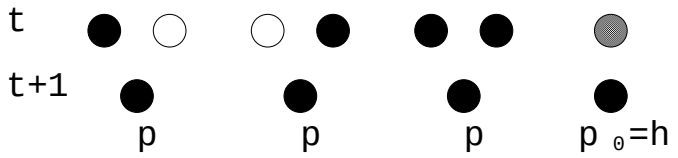

Figure 10.1: Generalized Domany-Kinzel automaton implementing directed site percolation with an external field. The propagation probability p is the control parameter of the phase transition, p_0 is the strength of the external field. Black circles symbolize occupied sites, open circles empty sites and grey ones either of the two.

The propagation probability p is the control parameter of the phase transition, i.e., below a critical value p_c the activity ceases and the system is trapped forever in the absorbing state (empty lattice). On the other hand a non-zero density of (active) particles ρ_a is found for $p > p_c$. The best estimates of the critical value of directed site percolation on bcc lattices are $p_c = 0.705489(4)$ [128] for $D = 1$ and $p_c = 0.34457(1)$ [129] for $D = 2$. The order parameter ρ_a of the absorbing phase transition vanishes at the critical point according to

$$\rho_a \propto \delta p^{\beta}, \tag{10.1}$$

with $\delta p = (p - p_c)/p_c$. Furthermore the order parameter fluctuations $\Delta\rho_a = L^D(\langle\rho_a^2\rangle - \langle\rho_a\rangle^2)$ diverge as (see fig. 10.2)

$$\Delta\rho_a \propto \delta p^{-\gamma'}. \tag{10.2}$$

The fluctuation exponent γ' obeys the scaling relation $\gamma' = D\nu_\perp - 2\beta$ [44],

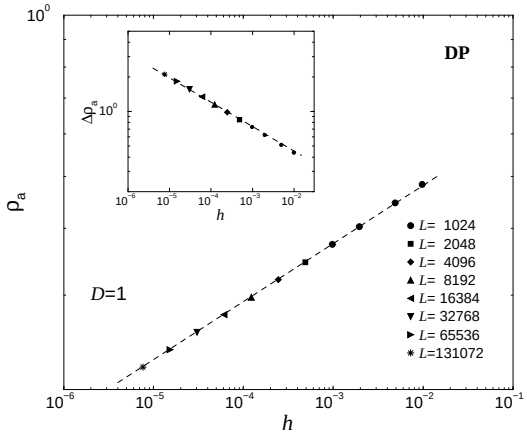

Figure 10.2: The field dependence of the order parameter and its fluctuations (inset) at the critical value p_c for one-dimensional directed percolation. The dashed lines correspond to the expected power-law behavior (10.9,10.10).

where $\nu_\perp$ describes the divergence of the spatial correlation length at the critical point. The critical behavior of the order parameter is shown in fig. 10.3 for $D = 1$ and in fig. 10.4 for $D = 2$. The data are obtained from numerical simulations of systems with periodic boundary conditions. Considering various system sizes L we take care that our results are not affected by finite-size effects. The system is started from a random initial configuration. After a certain transient regime a steady state is reached, which is characterized by the average particle density ρ_a and its fluctuations $\Delta\rho_a$. Similar to equilibrium phase transitions it is possible in DP to apply an external field h that is conjugated to the order parameter. Being a conjugated field it has to destroy the absorbing phase and the corresponding linear response function has to diverge at the critical point i.e.,

$$\chi_a = \frac{\partial \rho_a}{\partial h} \rightarrow \infty. \tag{10.3}$$

In DP the external field is implemented [5, 10] as a spontaneous creation of particles (i.e. $p_0 = h > 0$). Clearly, the absorbing state and thus the phase transition are destroyed. Figures 10.3 and 10.4 show how the external field results in a smoothening of the zero-field order parameter curve. The inset displays that the fluctuations are peaked for finite fields. Approaching the transition point ($h \rightarrow 0$) this peak becomes a divergence signaling the critical point.

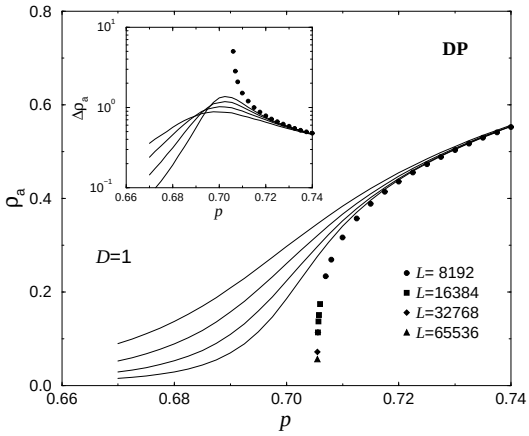

Figure 10.3: The one-dimensional directed percolation order parameter $\rho_{\rm a}$ as a function of the particle density for zero-field (symbols) and for various values of the external field ($h = 10^{-4}, 2 \cdot 10^{-4}, 5 \cdot 10^{-4}, 10^{-3}$) (lines). The inset displays the order parameter fluctuations $\Delta\rho_{\rm a}$ for zero field (symbols) and for various values of the external field h (lines).

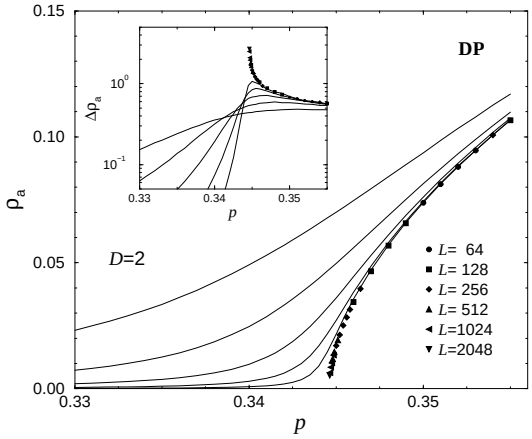

Figure 10.4: The two-dimensional directed percolation order parameter $\rho_{\rm a}$ as a function of the particle density for zero field (symbols) and for various values of the external field ($h = 3 \cdot 10^{-4},\ 10^{-4},\ 2 \cdot 10^{-5},\ 5 \cdot 10^{-6},\ 10^{-6}$) (lines). The inset displays the order parameter fluctuations $\Delta\rho_{\rm a}$ for zero field (symbols) and for various values of the external field h (lines).

10.1.2 Universal scaling forms

Sufficiently close to the critical point the order parameter, its fluctuations, as well as the order parameter susceptibility can be described by generalized

homogeneous functions

$$\rho_{\mathrm{a}}(\delta p, h) \quad \sim \quad \lambda^{-\beta}\ \tilde{R}(a_p \delta p\ \lambda, a_h h\ \lambda^{\sigma})\,, \tag{10.4}$$

$$a_\Delta\, \Delta\rho_{\mathrm{a}}(\delta p, h) \quad \sim \quad \lambda^{\gamma'}\ \tilde{D}(a_p \delta p\ \lambda, a_h h\ \lambda^{\sigma})\,, \tag{10.5}$$

$$a_\chi\, \chi_{\mathrm{a}}(\delta p, h) \quad \sim \quad \lambda^{\gamma}\ \tilde{C}(a_p \delta p\ \lambda, a_h h\ \lambda^{\sigma})\,. \tag{10.6}$$

Note that these scaling forms are valid for $D \neq D_{\mathrm{c}}$. At the upper critical dimension D_{c} they have to be modified by logarithmic corrections [123]. Taking into consideration that the susceptibility is defined as the derivative of the order parameter with respect to the conjugated field [eq. (10.3)] we find $\tilde{C}(x, y) = \partial_y \tilde{R}(x, y)$, $a_\chi = a_h^{-1}$, as well as the Widom scaling law

$$\gamma \ = \ \sigma \ - \ \beta\,. \tag{10.7}$$

The universal scaling functions $\tilde{R}$, $\tilde{D}$, and $\tilde{C}$ are identical for all models belonging to a given universality class whereas all non-universal system-dependent details (e.g. the lattice structure, range of interactions, the update scheme, etc.) are contained in the so-called non-universal metric factors a_p, a_h, and a_Δ [130]. The universal scaling functions can be normalized by the conditions $\tilde{R}(1, 0) = \tilde{R}(0, 1) = \tilde{D}(0, 1) = 1$. In that case the non-universal metric factors are determined by the amplitudes of the corresponding power-laws

$$\rho_{\mathrm{a}}(\delta p, h = 0) \quad \sim \quad (a_p\, \delta p)^{\beta}\,, \tag{10.8}$$

$$\rho_{\mathrm{a}}(\delta p = 0, h) \quad \sim \quad (a_h\, h)^{\beta/\sigma}\,, \tag{10.9}$$

$$a_\Delta\, \Delta\rho_{\mathrm{a}}(\delta p = 0, h) \quad \sim \quad (a_h\, h)^{-\gamma'/\sigma}\,. \tag{10.10}$$

Furthermore we just mention that $\tilde{C}(0, 1) = \beta/\sigma$, following trivially from the definition of the susceptibility. Usually, an analytical expression for the scaling functions is only known above D_{c}, where mean-field theories apply. The mean-field equation of state of DP can be easily derived from the corresponding Langevin equation

$$\partial_t \rho_{\mathrm{a}} \ = \ \delta p\, \rho_{\mathrm{a}} \ - \ \lambda \rho_{\mathrm{a}}^2 \ + \ \kappa\, h \ + \ D\, \nabla^2\, \rho_{\mathrm{a}} \ + \ \eta \tag{10.11}$$

which describes the order parameter field $\rho_{\mathrm{a}}(\underline{x}, t)$ on a mesoscopic scale (see [5] for a detailed discussion). Here D denotes the diffusion constant, η denotes a multiplicative noise term with the correlator

$$\langle\, \eta(\underline{x}, t)\, \eta(\underline{x}', t')\, \rangle \ = \ \Gamma\, \rho_{\mathrm{a}}(\underline{x}, t)\ \delta^d(\underline{x} - \underline{x}')\, \delta(t - t') \tag{10.12}$$

and $\lambda > 0$, $\kappa > 0$, and $\Gamma > 0$ are certain coupling constants. Neglecting spatial correlations and fluctuations ($D = 0$ and $\eta = 0$) one gets for the steady state behavior ($\partial_t \rho_\mathrm{a} = 0$)

$$\delta p\, \rho_\mathrm{a} \,-\, \lambda\, \rho_\mathrm{a}^2 \,+\, \kappa\, h \;=\; 0 \tag{10.13}$$

from which it is easy to derive the universal scaling function

$$\tilde{R}_\mathrm{MF}(x,y) = \frac{x}{2} \,+\, \sqrt{y \,+\, \left(\frac{x}{2}\right)^2}\,. \tag{10.14}$$

Similarly the remaining universal scaling functions are derived (see e.g. [131]).

$$\tilde{D}_\mathrm{MF}(x,y) \;=\; \frac{\tilde{R}_\mathrm{MF}(x,y)}{\sqrt{y \,+\, (x/2)^2}}\,, \tag{10.15}$$

$$\tilde{C}_\mathrm{MF}(x,y) \;=\; \frac{1}{2\,\sqrt{y \,+\, (x/2)^2}}\,. \tag{10.16}$$

Thus the mean-field exponents are $\beta_\mathrm{MF} = 1$, $\sigma_\mathrm{MF} = 2$, $\gamma_\mathrm{MF} = 1$, and $\gamma'_\mathrm{MF} = 0$ (corresponding to a finite jump of the fluctuations). Below D_c the universal scaling functions depend on dimensionality and are unknown due to a lack of analytical solutions. In this case the scaling functions have to be determined numerically or via approximation schemes, e.g. series expansions or ϵ-expansion of RG approaches. In case of the mean-field solution ($\gamma'_\mathrm{MF} = 0$) the scaling form of the fluctuations [eq. (10.5)] reduces to

$$a_\Delta\, \Delta\rho_\mathrm{a}(\delta p, h) \;\sim\; \tilde{D}(a_p \delta p\, \lambda, a_h h\, \lambda^\sigma). \tag{10.17}$$

Some interesting properties of the universal scaling function $\tilde{D}$ can be derived from this form. The non-universal metric factor a_Δ is determined by

$$a_\Delta \;=\; \frac{1}{\Delta\rho_\mathrm{a}(\delta p = 0, h)} \tag{10.18}$$

Table 10.1: The non-universal quantities for directed site percolation on a bcc lattice for various dimensions. The uncertainty of the metric factors is less than 7%.

D	p_c	a_a	a_p	a_h	a_Δ
1	0.705489 ± 0.000004		2.498	0.114	9.382
2	0.344575 ± 0.000015		0.795	0.186	9.016
3	0.160950 ± 0.000030		0.417	0.328	11.91
4	0.075582 ± 0.000017	14.70	3.055	59.80	19.19
5	0.035967 ± 0.000023		0.114	0.174	42.49

Table 10.2: The critical exponents of directed percolation for various dimensions D. The one-dimensional values were obtained in a famous series expansion by Jensen [48]. For $D = 2$ and $D = 3$ the authors investigated activity spreading and the presented exponents are derived via scaling relations. A complete list of all critical exponents of DP can be found in [5]. The symbol * denotes logarithmic corrections to the power-law behavior.

D	1 [48]	2 [132]	3 [133]	4	MF
β	0.276486(8)	0.584(4)	0.81(1)	1^*	1
σ	2.554216(13)	2.18(1)	2.04(2)	2^*	2
γ'	0.543882(16)	0.300(11)	0.123(25)	0^*	0

using that $\tilde{D}(0,1) = 1$. The value $\tilde{D}(1,0)$ is then given by

$$\tilde{D}(1,0) \;=\; \frac{\Delta\rho_{\mathrm{a}}(\delta p, h=0)}{\Delta\rho_{\mathrm{a}}(\delta p=0, h)}\,. \tag{10.19}$$

Finally, it is worth mentioning that the mean-field scaling function $\tilde{D}$ fulfills the symmetries

$$\tilde{D}(1,x) = \tilde{D}(x^{-1/\sigma},1) \tag{10.20}$$

$$\tilde{D}(x,1) = \tilde{D}(1,x^{-\sigma}) \tag{10.21}$$

for all positive x. In particular we obtain for $x \to 0$ $\tilde{D}(1,0) = \tilde{D}(\infty,1)$ and $\tilde{D}(0,1) = \tilde{D}(1,\infty)$, respectively.

10.1.3 Equation of state and fluctuations

Below the upper critical dimension

The scaling forms eqs. (10.4-10.6) imply that curves corresponding to different values of the conjugated field collapse to the universal functions $\tilde{R}(x,1)$, $\tilde{D}(x,1)$, $\tilde{C}(x,1)$, if $\rho_{\mathrm{a}}\,(a_h h)^{-\beta/\sigma}$, $a_\Delta \Delta\rho_{\mathrm{a}}\,(a_h h)^{\gamma'/\sigma}$, and $a_\chi \chi_{\mathrm{a}}\,(a_h h)^{\gamma/\sigma}$ are considered as functions of the rescaled control parameter $a_p \delta p\,(a_h h)^{-1/\sigma}$. In a first step, the non-universal metric factors a_p, a_h, a_Δ are obtained from measuring the power-laws eqs. (10.8-10.10) (see Table 10.1). Here, the best known estimates for critical exponents, as given in Table 10.2, are used. Subsequently, the rescaled order parameter and its fluctuations as a function of the rescaled control parameter are plotted for one, two- and three-dimensional DP (figs. 10.5, 10.6 and 10.7). A convincing data collapse is achieved, confirming the scaling ansatz as well as the values of the critical exponents. Besides the universal scaling function $\tilde{R}(x,1)$ the corresponding curve of

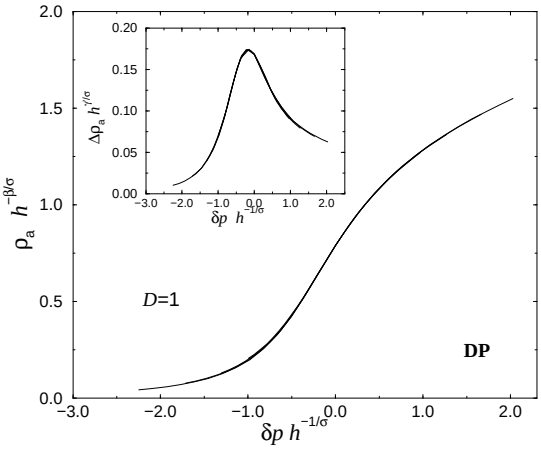

Figure 10.5: The scaling plot of the order parameter and its fluctuations (inset) for one-dimensional directed percolation.

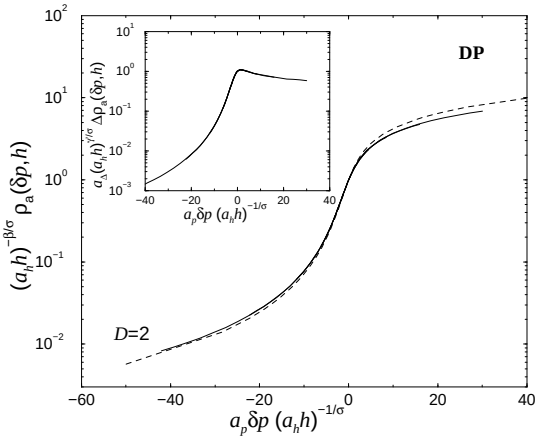

Figure 10.6: The universal scaling plots of the order parameter and its fluctuations (inset) for $D = 2$. The dashed line corresponds to an ϵ-expansion of a RG approach [49].

an ϵ-expansion obtained from a renormalization group analysis is shown in figs. 10.6 and 10.7. Using the parametric representation [134, 135] of the absorbing phase transition, Janssen *et al.* showed that the equation of state is given by the remarkably simple scaling function [49]

$$H(\theta) \;=\; \theta\,(2-\theta) + \mathcal{O}(\epsilon^3), \tag{10.22}$$

where ϵ denotes the distance to the upper critical dimension $D_c = 4$, i.e., $\epsilon = D_c - D$. Here the scaling behavior of the quantities ρ_a, δp, and h is transformed to the variables R and θ through the relations

$$b\,\delta p \;=\; R\,(1-\theta), \qquad\qquad \rho_a \;=\; R^{\beta}\,\frac{\theta}{2}. \tag{10.23}$$

The equation of state is given by

$$a\,h \;=\; \left(\frac{R^{\beta}}{2}\right)^{\delta} H(\theta) \tag{10.24}$$

with the metric factors a and b. The whole phase diagram is described by the parameter range $R \geq 0$ and $\theta \in [0, 2]$. In fig. 10.6 and 10.7 a comparison between the numerically obtained scaling functions and the analytical result of eqs. (10.22-10.24) is made. The RG-data differ slightly from the universal function. As expected the differences decrease with increasing dimension and are especially strong in $D = 1$ [10]. This point is discussed in detail below.

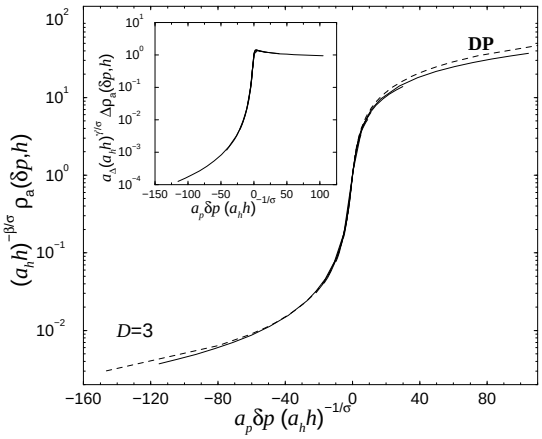

Figure 10.7: The universal scaling plots of the order parameter and its fluctuations (inset) for $D = 3$ and for various values of the external field ($h = 3 \cdot 10^{-4}$, 10^{-4}, $2 \cdot 10^{-5}$, $4 \cdot 10^{-6}$, $5 \cdot 10^{-7}$). The dashed line corresponds to an ϵ-expansion of a RG approach [49].

Above the upper critical dimension

Above the upper critical dimension the scaling behavior of a phase transition equals the scaling behavior of the corresponding mean-field solution

[eqs. (10.14-10.16)]. Plotting $\rho_{\rm a}/\sqrt{a_h h}$ as a function of $a_p \delta p/\sqrt{a_h h}$, the numerical data should collapse to the universal scaling function

$$\tilde{R}_{\rm MF}(x,1) \;=\; \frac{x}{2} + \sqrt{1 + \left(\frac{x}{2}\right)^2} \tag{10.25}$$

with the scaling variable $x = a_p\, \delta p \,/\, \sqrt{a_h\, h}$. In fig. 10.8 we plot the corresponding rescaled data of the five-dimensional model. A perfect collapse of the numerical data and $\tilde{R}(x,1)$ is obtained. This is a confirmation of the RG-result $D_{\rm c} = 4$ [136,137]. To the best of our knowledge no numerical evidence that five-dimensional DP exhibits mean-field scaling behavior was published so far. The rescaled fluctuation data is presented in fig. 10.8. As for the

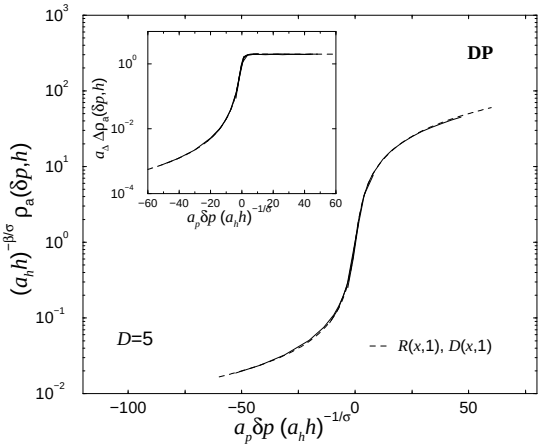

Figure 10.8: The universal scaling plots of the order parameter and its fluctuations (inset) for $D = 5$ and for various values of the external field ($h = 5 \cdot 10^{-5}$, $7 \cdot 10^{-5}$, 10^{-6}, $7 \cdot 10^{-7}$). The dashed lines correspond to the mean-field solutions $\tilde{R}_{\rm MF}(x,1)$ and $\tilde{D}_{\rm MF}(x,1)$ [see eqs. (10.25,10.26)].

universal order parameter, the data of the fluctuations are in agreement with the corresponding universal mean-field scaling function

$$\tilde{D}_{\rm MF}(x,1) \;=\; 1 + \frac{x}{2\sqrt{1 + (x/2)^2}}. \tag{10.26}$$

At the upper critical dimension

At the upper critical dimension $D_{\rm c} = 4$ the scaling behavior is governed by the mean-field exponents modified by logarithmic corrections. For instance

the order parameter obeys in leading order

$$\rho_{\mathrm{a}}(\delta p, h=0) \;\propto\; \delta p\,|\ln \delta p|^{\mathrm{B}}\,, \tag{10.27}$$

$$\rho_{\mathrm{a}}(\delta \rho=0, h) \;\propto\; \sqrt{h}\,|\ln h|^{\Sigma}\,. \tag{10.28}$$

The logarithmic correction exponents B and Σ are characteristic features of the whole universality class similar to the usual critical exponents. Numerous theoretical, numerical, as well as experimental investigations of critical systems at D_{c} have been performed (see for instance [50, 119–121, 125, 126, 138–142]). Logarithmic corrections make the data analysis quite difficult. Hence most investigations are focused on the determination of the correction exponents only, lacking the determination of the scaling functions at D_{c}. Recently, a method of analysis was developed to determine the universal scaling functions at the upper critical dimension [123]. In this work the authors use the phenomenological scaling ansatz (all terms in leading order)

$$a_{\mathrm{a}}\,\rho_{\mathrm{a}}(\delta p, h) \;\sim\; \lambda^{-\beta_{\mathrm{MF}}}\,|\ln\lambda|^{l}\;\tilde{R}(a_p \delta p\;\lambda\,|\ln\lambda|^{b}, a_h h\;\lambda^{\sigma_{\mathrm{MF}}}\,|\ln\lambda|^{s})\,, \tag{10.29}$$

with $\beta_{\mathrm{MF}} = 1$ and $\sigma_{\mathrm{MF}} = 2$. Therefore, the order parameter at zero field ($h = 0$) and at the critical density ($\delta\rho = 0$) are given in leading order by

$$a_{\mathrm{a}}\,\rho_{\mathrm{a}}(\delta p, h=0) \;\sim\; a_p \delta p\,|\ln a_p \delta\rho|^{\mathrm{B}}\;\tilde{R}(1,0), \tag{10.30}$$

$$a_{\mathrm{a}}\,\rho_{\mathrm{a}}(\delta p=0, h) \;\sim\; \sqrt{a_h h}\,|\ln\sqrt{a_h h}|^{\Sigma}\;\tilde{R}(0,1) \tag{10.31}$$

with $\mathrm{B} = b + l$ and $\Sigma = s/2 + l$. Similar to the case $D \neq D_{\mathrm{c}}$ the normalization $\tilde{R}(0,1) = \tilde{R}(1,0) = 1$ was used. According to the ansatz eq. (10.29) the scaling behavior of the equation of state is given in leading order by

$$a_{\mathrm{a}}\,\rho_{\mathrm{a}}(\delta\rho, h) \;\sim\; \sqrt{a_h h}\,|\ln\sqrt{a_h h}|^{\Sigma}\;\tilde{R}(x,1) \tag{10.32}$$

where the scaling argument is given by

$$x \;=\; a_\rho \delta\rho\,\sqrt{a_h h}^{\,-1}\,|\ln\sqrt{a_h h}\,|^{\Xi} \tag{10.33}$$

with $\Xi = b - s/2 = \mathrm{B} - \Sigma$. In case of directed percolation it is possible to confirm the scaling ansatz eq. (10.29) by a RG-approach [50]. In particular the logarithmic correction exponents are given by $l = 7/12$, $b = -1/4$, and $s = -1/2$. Thus the scaling behavior of the equation of state is determined by the logarithmic correction exponents [50]

$$\mathrm{B} \;=\; \Sigma \;=\; 1/3\,, \qquad \Xi = 0\,. \tag{10.34}$$

It is worth mentioning that in contrast to the RG results below the upper critical dimension the logarithmic correction exponents do not rely on approximation schemes like ϵ- or $1/n$-expansions. Within the RG theory they are exact results. Similarly to the order parameter the following form is used for its fluctuations [123]

$$a_\Delta \, \Delta\rho_{\rm a}(\delta\rho, h) \;\sim\; \lambda^{\gamma'} \, |\ln\lambda|^k \;\; \tilde{D}(a_\rho \delta\rho \, \lambda \, |\ln\lambda|^b, a_h h \, \lambda^{-\sigma} \, |\ln\lambda|^s) \, . \qquad (10.35)$$

Using the mean-field value $\gamma' = 0$ and taking into account that numerical simulations show that the fluctuations remain finite at the critical point (i.e. $k = 0$) the scaling function

$$a_\Delta \, \Delta\rho_{\rm a}(\delta\rho, h) \;\sim\; \tilde{D}(x, 1) \qquad (10.36)$$

is obtained, where the scaling argument x is given by eq. (10.33) with $\Xi = 0$. The non-universal metric factor a_Δ is determined again by the condition $\tilde{D}(0, 1) = 1$. Thus the scaling behavior of the order parameter and its fluc-

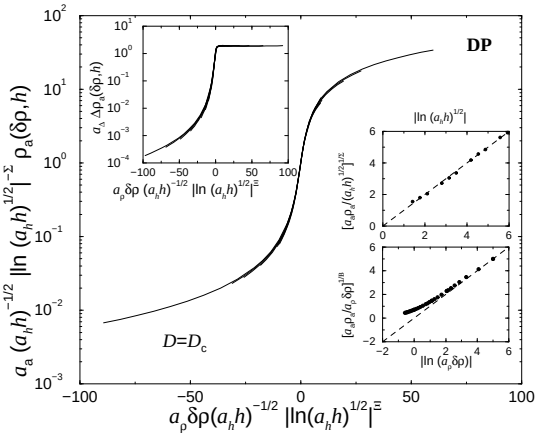

Figure 10.9: The universal scaling plots of the order parameter and its fluctuations (upper left inset) at the upper critical dimension $D_{\rm c} = 4$ for various values of the external field ($h = 5 \cdot 10^{-5}$, $2 \cdot 10^{-5}$, $8 \cdot 10^{-6}$, $4 \cdot 10^{-6}$, $2 \cdot 10^{-6}$). The logarithmic correction exponents are given by $\mathrm{B} = \Sigma = 1/3$ [50] and $\Xi = 0$. The right insets show the order parameter at the critical density and for zero field, respectively. The order parameter is rescaled according to eqs. (10.30,10.31). Approaching the transition point ($h \to 0$ and $\delta\rho \to 0$) the data tend to the function $f(x) = x$ (dashed lines) as required.

tuations at $D_{\rm c}$ is determined by two exponents ($\mathrm{B} = 1/3$ and $\Sigma = 1/3$) and four unknown non-universal metric factors ($a_{\rm a}, a_\rho, a_h, a_\Delta$). Following [123] we determine these values in our analysis by several conditions which are applied

simultaneously: first, both the rescaled equation of state and the rescaled order parameter fluctuations have to collapse to the universal functions $\tilde{R}(x,1)$ and $\tilde{D}(x,1)$. Second, the order parameter behavior at zero field and at the critical density are asymptotically given by the simple function $f(x) = x$ when plotting $[a_{\mathrm{a}}\rho_{\mathrm{a}}(\delta\rho,0)/a_{\rho}\delta\rho]^{1/\mathrm{B}}$ vs. $|\ln a_{\rho}\delta\rho|$ and $[a_{\mathrm{a}}\rho_{\mathrm{a}}(0,h)/\sqrt{a_h h}\,]^{1/\Sigma}$ vs. $|\ln\sqrt{a_h h}\,|$, respectively. Applying this analysis we observe convincing results for $\mathrm{B} = \Sigma = 1/3$, $\Xi = 0$, and for the values of the non-universal metric factors listed in Table 10.1. The corresponding plots are presented in fig. 10.9. In a very recent publication [143] the scaling behavior of directed site percolation at the upper critical dimension was investigated using spreading simulations. It was pointed out that next to leading order terms of the logarithmic corrections are needed to describe the obtained data in a satisfactory way.

10.1.4 Universal amplitude combinations

In the following we consider several universal amplitude combinations (see [113] for an excellent review). As pointed out in [113], these amplitude combinations are very useful in order to identify the universality class of a phase transition since the amplitude combinations vary more widely than the corresponding critical exponents. Furthermore, the measurement of amplitude combinations in experiments or simulations yields a reliable test for theoretical predictions. In particular, estimates of amplitude combinations are provided by RG approximation schemes like ϵ- or $1/n$-expansions. Usually numerical investigations focus on amplitude combinations arising from finite-size scaling analysis. A well known example is the value of Binder's fourth order cumulant at criticality (see e.g. [144]). Instead of those finite-size properties we continue to focus our attention to bulk critical behavior since bulk amplitude combinations are of great experimental interest. Furthermore, they can be compared to RG-results [49]. The susceptibility diverges as

$$\chi(\delta p > 0, h = 0) \sim a_{\chi,+}\,\delta p^{-\gamma}\,, \tag{10.37}$$

$$\chi(\delta p < 0, h = 0) \sim a_{\chi,-}\,(-\delta p)^{-\gamma}\,, \tag{10.38}$$

if the critical point is approached from above and below, respectively. The amplitude ratio

$$\frac{\chi(\delta p > 0, h = 0)}{\chi(\delta p < 0, h = 0)} = \frac{a_{\chi,+}}{a_{\chi,-}} \tag{10.39}$$

is a universal quantity similar to the critical exponents, i.e., all systems belonging to a given universality class are characterized by the same value

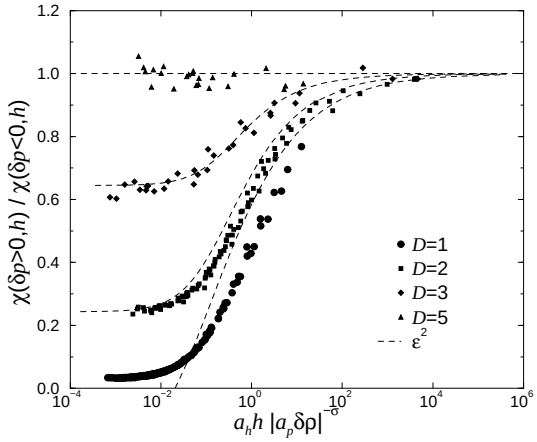

Figure 10.10: The universal scaling function $\tilde{C}(1,x)/\tilde{C}(-1,x)$ for various dimensions. The dashed lines correspond to an ϵ-expansion of a RG approach [49]. The universal amplitude $\tilde{C}(1,0)/\tilde{C}(-1,0)$ is obtained from the extrapolation $a_h h|a_p\,\delta p|^{-\sigma} \to 0$.

$a_{\chi,+}/a_{\chi,-}$. This can be seen from eq. (10.6). Setting $a_p|\delta p|\lambda = 1$ yields

$$\frac{\chi(\delta p > 0, h)}{\chi(\delta p < 0, h)} \;=\; \frac{\tilde{C}(+1,x)}{\tilde{C}(-1,x)} \tag{10.40}$$

with $x = a_h h|a_p\delta p|^{-\sigma}$. Obviously this is a universal quantity for all values of the scaling variable x. In particular it equals the ratio $a_{\chi,+}/a_{\chi,-}$ for $x \to 0$, i.e., vanishing external field. In general, universal amplitude combinations are related to particular values of the universal scaling functions. In fig. 10.10 the universal susceptibility ratio eq. (10.40) is shown for various dimensions. The corresponding data saturates for $x \to 0$. Our estimates for the amplitude ratios $\tilde{C}(+1,0)/\tilde{C}(-1,0)$ are 0.033 ± 0.004 for $D = 1$, 0.25 ± 0.01 for $D = 2$, as well as 0.65 ± 0.03 for $D = 3$. In case of five-dimensional DP the amplitude ratio is constant, as predicted from the mean-field behavior

$$\frac{\tilde{C}_{\mathrm{MF}}(+1,x)}{\tilde{C}_{\mathrm{MF}}(-1,x)} \;=\; 1 \tag{10.41}$$

for all x. The behavior of the ratio $\tilde{C}(+1,x)/\tilde{C}(-1,x)$ for $D < D_{\mathrm{c}}$ reflects the crossover from mean-field to non mean-field behavior. Far away from the transition point, the critical fluctuations are suppressed and the behavior of the system is well described by the mean-field solution [eq. (10.41)]. Approaching criticality the critical fluctuations increase and a crossover to the D-dimensional behavior takes place. In the already mentioned work [49],

Janssen *et al.* calculated the steady state scaling behavior of DP within a RG approach. In particular they obtained for the susceptibility amplitude ratio

$$\frac{\tilde{C}(+1,0)}{\tilde{C}(-1,0)} \;=\; 1 \;-\; \frac{\epsilon}{3}\left[1 \;-\; \left(\frac{11}{288} \;-\; \frac{53}{144}\,\ln\frac{4}{3}\right)\,\epsilon \;+\; \mathcal{O}(\epsilon^2)\right] \qquad (10.42)$$

leading to $-0.2030\ldots$ for $D = 1$, $0.2430\ldots$ for $D = 2$, $0.6441\ldots$ for $D = 3$. Except for the unphysical one-dimensional result these values agree well with our numerical estimates. Furthermore the parametric representation of the susceptibility was derived in [49] and it is straightforward to calculate the universal ratio eq. (10.40). The results are plotted for various dimensions in fig. 10.10. It is instructive to compare these results with the numerical data since the theoretical curve reflects the accuracy of the RG estimations of all three quantities, the exponent, the scaling function, as well as the non-universal metric factors. All quantities are well approximated for the three-dimensional model. In the two-dimensional case we observe a horizontal shift between the numerical data and the RG-estimates. Thus the RG-approach yields good estimates for the exponents and the scaling function but the metric factors are of significantly less quality. For $D = 1$ the ϵ^2-approximation does not provide appropriate estimates of the DP scaling behavior. Thus higher orders than $\mathcal{O}(\epsilon^2)$ are necessary to describe the scaling behavior of directed percolation in low dimensions. Analogous to the

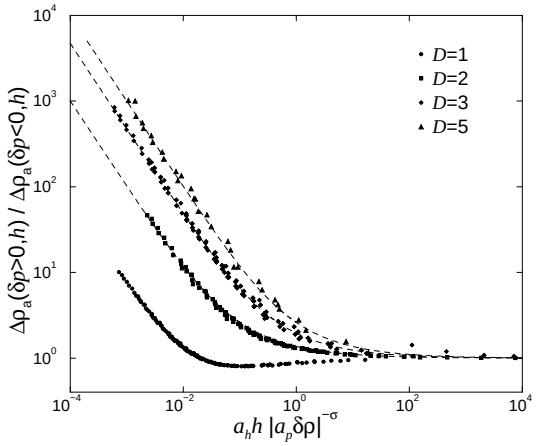

Figure 10.11: The universal scaling function $\tilde{D}(1,x)/\tilde{D}(-1,x)$ for various dimensions. The dashed line corresponds to the mean-field scaling behavior. For $D = 2$ and $D = 3$ the mean-field curves are shifted by the factors 9.56 and 2.12 to the left.

susceptibility the universal amplitude ratio of the fluctuations is given by

$$\frac{\Delta\rho_{\mathrm{a}}(\delta p > 0, h)}{\Delta\rho_{\mathrm{a}}(\delta p < 0, h)} \;=\; \frac{\tilde{D}(+1, x)}{\tilde{D}(-1, x)} \tag{10.43}$$

with $x = a_h h |a_p \delta p|^{-\sigma}$. In the case of absorbing phase transitions this ratio diverges for vanishing field. For $\delta p < 0$ the order parameter fluctuations are zero (absorbing state) for vanishing field whereas the fluctuations remain finite above the transition ($\delta p > 0$). Thus absorbing phase transitions are generally characterized by

$$\frac{\tilde{D}(+1, 0)}{\tilde{D}(-1, 0)} \;\to\; \infty. \tag{10.44}$$

In fig. 10.11 we plot the fluctuation ratio [eq. (10.43)] as a function of the scaling variable $a_h h |a_p \delta p|^{-\sigma}$ for various dimensions. We observe in all cases that the fluctuation ratios diverge for $x \to 0$. Only the one-dimensional system exhibits a particular behavior characterized by the minimum of the corresponding curve. The origin of this behavior is that for $D = 2, 3$ the universal scaling function $D(x, 1)$ exhibits a maximum for $x > 0$, whereas for $D = 1$ it is located at $x < 0$ (see fig. 8 in [123]). In the five-dimensional model we observe a perfect agreement with the mean-field behavior

$$\frac{\tilde{D}_{\mathrm{MF}}(+1, x)}{\tilde{D}_{\mathrm{MF}}(-1, x)} \;=\; \frac{1 \,+\, \sqrt{1 + 4x}}{-\,1 \,+\, \sqrt{1 + 4x}} \;\xrightarrow[x \to 0]{}\; \frac{1}{1 + 2x}\,. \tag{10.45}$$

Surprisingly, the two- and three-dimensional data are also well approximated by this formula provided that one performs a simple rescaling ($x \mapsto a_D x$) which results in fig. 10.11 in a horizontal shift of the data. We suppose that this behavior could be explained by a RG-analysis of the fluctuations. Similar to the universal amplitude ratios of the susceptibility and the fluctuations other universal combinations can be defined. Well known from equilibrium phase transitions is the quantity (see e.g. [113])

$$R_\chi \;=\; \Gamma\, d_{\mathrm{c}}\, B^{\delta - 1}\,, \tag{10.46}$$

which is also experimentally accessible, e.g. for magnetic systems. Here, Γ denotes the amplitude of the susceptibility χ in zero field ($\chi \sim \Gamma\, \delta T^{-\gamma}$) and B is the corresponding amplitude of the order parameter M ($M \sim B\, \delta T^{\beta}$). The factor d_{c} describes how the order parameter M depends on the conjugated field H at $\delta T = 0$ ($H \sim d_{\mathrm{c}}\, M^{\delta}$). In case of directed percolation these amplitudes correspond to the values $B = a_p^{\beta}\, \tilde{R}(1, 0)$, $\Gamma = a_p^{\gamma}\, a_h\, \tilde{C}(1, 0)$

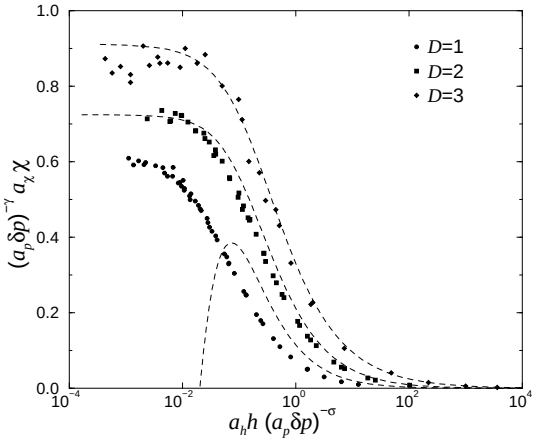

Figure 10.12: The universal scaling function $\tilde{C}(1,x)$ for various dimensions. The dashed lines correspond to an ϵ-expansion of an RG approach [49]. The universal amplitude R_χ is obtained from the extrapolation $a_h h(a_p\,\delta p)^{-\sigma} \to 0$.

as well as $d_c = a_h^{-1}\,\tilde{R}(0,1)^{-\delta}$ where $\delta = \sigma/\beta$. The normalizations $\tilde{R}(1,0) = \tilde{R}(0,1) = 1$ yield for the amplitude combination

$$R_\chi \;=\; \tilde{C}(1,0) \tag{10.47}$$

which is obviously a universal quantity. In fig. 10.12 the scaling function $\tilde{C}(1,x)$ is plotted as a function of $x = a_h h\,(a_p\,\delta p)^{-\sigma}$ for $D = 1,2,3$. The corresponding data saturates for $x \to 0$. Our estimates are $R_\chi = 0.60 \pm 0.04$ for $D = 1$, $R_\chi = 0.72 \pm 0.04$ for $D = 2$, and $R_\chi = 0.86 \pm 0.08$ for $D = 3$. Note that the error-bars reflect only the data scattering in fig. 10.12. In contrast to the amplitude $\tilde{C}(1,0)/\tilde{C}(-1,0)$ the data of R_χ are affected by the uncertainties of the exponent γ and the uncertainties of the metric factors a_p, a_h. These uncertainties increase the error-bars significantly. The two- and three-dimensional data agree quite well with the RG-results $R_\chi = 0.7244\ldots$ for $D = 2$ and $R_\chi = 0.9112\ldots$ for $D = 3$ [49]. In the one-dimensional model the ϵ^2-expansion yields again an unphysical result ($R_\chi = -3.927\ldots$).

10.1.5 Conclusion

We considered the universal steady state scaling behavior of directed percolation with an external field in $D \leq 5$ dimensions. Our data for D=5 coincide with the mean-field solution, confirming that $D_c = 4$ is the upper critical dimension. At D_c we presented for the first time a numerical scaling analysis of DP including logarithmic corrections. Our results agree well with those of a recently performed RG approach [50]. Apart from the scaling functions

we also considered amplitude ratios and combinations for the order parameter fluctuations and the susceptibility. A comparison with RG [49] results reveals that higher orders than $\mathcal{O}(\epsilon^2)$ are necessary to describe the scaling behavior in low dimensions.

10.2 The pair contact process

In this section we consider for the first time the one-dimensional pair contact process (PCP) in a conjugated field (which corresponds to a unidirectionally coupled bulk reservoir) and show that the scaling behavior is characterized by the DP critical exponents. The static universal scaling behavior of the PCP is presented in subsection 10.2.2. The obtained universal equation of state is compared to the results of a two loop renormalization group approach of the corresponding Langevin equation [49]. The dynamical scaling behavior of the PCP is compared to that of DP in subsection 10.2.3. Finally we derive the equation of state of the PCP within a mean-field approximation in subsection 10.2.4. Therefore we consider the PCP with particle creation at randomly selected sites. This random neighbor interaction suppresses long range correlations and the model is analytically tractable.
The results of this section were obtained in collaboration with S. Lübeck and published in ref. [10].

10.2.1 Model definition

The PCP as introduced by Jensen [145] is one of the simplest models with infinitely many absorbing states showing a continuous phase transition. At time t sites on a lattice of length L with periodic boundary conditions can either be occupied ($n_i(t) = 1$) or empty ($n_i(t) = 0$). Pairs of adjacent occupied sites $i, i+1$, linked by an active bond, annihilate each other with rate p or create an offspring with rate $1-p$ at either site $i-1$ or $i+2$ provided the target site is empty (see fig. 10.13). The density of active bonds ρ_{a} is the order parameter of a continuous phase transition from an active state for $p < p_{\mathrm{c}}$ to an inactive absorbing state without particle pairs. The behavior of the PCP order parameter and its fluctuations are plotted in figure 10.14. The data are obtained from simulations on various system sizes $L \leq 131072$ with periodic boundary conditions. Our analysis reveals that the critical value is $p_{\mathrm{c}} = 0.077093(3)$ which agrees with the value $p_{\mathrm{c}} = 0.077090(5)$ [146] obtained from a finite-size scaling analysis of the lifetime distribution. In contrast to DP there is no unique absorbing state (empty lattice) but infinitely many, as any configuration with only isolated inactive particles is absorbing. Thus

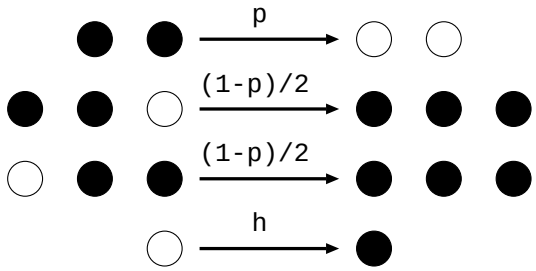

Figure 10.13: In the pair-contact process (PCP) sites can be empty or occupied. Adjacent pairs of particles are regarded as active and may either annihilate with rate p or create an offspring with rate $1-p$. Single particles without an occupied neighbor are inactive. Particles can be spontaneously created by an external field at rate h.

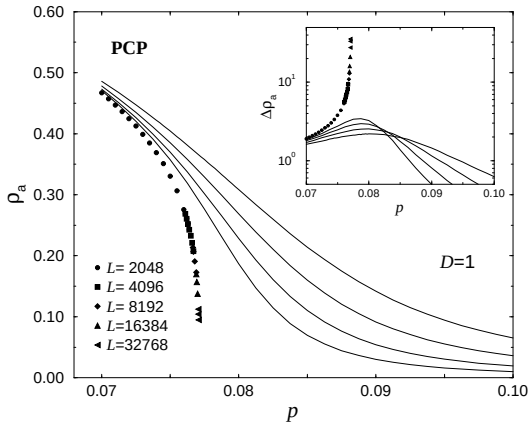

Figure 10.14: The one-dimensional pair contact process order parameter $\rho_{\rm a}$ as a function of the particle density for zero-field (symbols) and for various values of the external field from ($h = 10^{-4}, 2\cdot10^{-4}, 5\cdot10^{-4}, 10^{-3}$) (lines). The inset displays the order parameter fluctuations $\Delta\rho_{\rm a}$ for zero field (symbols) and for various values of the external field h (lines).

in the thermodynamic limit the system will be trapped in one of an infinite number of absorbing configurations for $p > p_{\rm c}$. Despite the different structure of the absorbing states the steady state scaling behavior of the PCP is believed to be characterized by the DP critical exponents β, γ', γ etc. On the other hand the dynamical scaling behavior, associated with activity spreading of a localized seed depends on the details of the system preparation [45]. Recently, Dickman et al. [147] considered the PCP with an external field

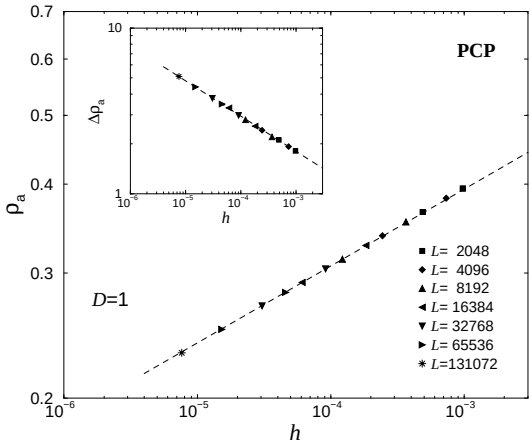

Figure 10.15: The field dependence of the order parameter and its fluctuations (inset) at the critical value p_c for the one-dimensional pair contact process. The dashed lines correspond to the expected power-law behavior of eqs. (10.8) and (10.10).

that randomly creates isolated particles. Thus the external field couples to the particle density but not to the order parameter itself, i.e., the external field is not conjugated to the order parameter. The authors observe that the external field shifts the critical values p_c continuously and that the critical exponents are unaffected by the presence of the particle source. In order to investigate the PCP in a conjugated field the implementation of the external field of [147] has to be modified. Several modifications of the external field are possible. For instance in absorbing phase transitions with particle conservation [41] the conjugated field triggers movements of inactive particles which can be activated in this way [148]. As shown below spontaneous particle creation with rate h acts as a conjugated field analogous to DP. Figure 10.14 shows how the spontaneous particle creation smoothens the critical zero field curves similar to the DP behavior (see figure 10.3). We simulated the PCP at the critical value p_c for various fields. The order parameter and its fluctuations as a function of the external field h are presented in figure 10.15. Approaching the transition point, ρ_a and $\Delta\rho_a$ scale according to the equations (10.8) and (10.10) where the exponents β/σ and γ'/σ agree with the DP values. Furthermore we assume that the order parameter and the order parameter fluctuations obey analogous to DP the scaling forms

$$\rho_a(\delta p, h) \sim \lambda\, \tilde{r}_{\mathrm{PCP}}(\delta p\, \lambda^{-1/\beta}, h\, \lambda^{-\sigma/\beta}), \tag{10.48}$$

$$\Delta\rho_a(\delta p, h) \sim \lambda^{\gamma'}\, \tilde{d}_{\mathrm{PCP}}(\delta p\, \lambda, h\, \lambda^{\sigma}), \tag{10.49}$$

where the distance to the critical point is now given by $\delta p = (p_c - p)/p_c$. Using the DP values of the critical exponents β, σ and γ' we get convincing data collapses (see figure 10.16). As pointed out above, the validity of the scaling ansatz (10.48) implies the singular behavior of the linear response function

$$\chi = \frac{\partial \rho_a}{\partial h} \rightarrow \infty, \tag{10.50}$$

i.e., the spontaneous particle creation in the PCP can be interpreted as an external field conjugated to the order parameter. The data collapse confirms again that the steady state scaling behavior of the PCP is characterized by the DP exponents.

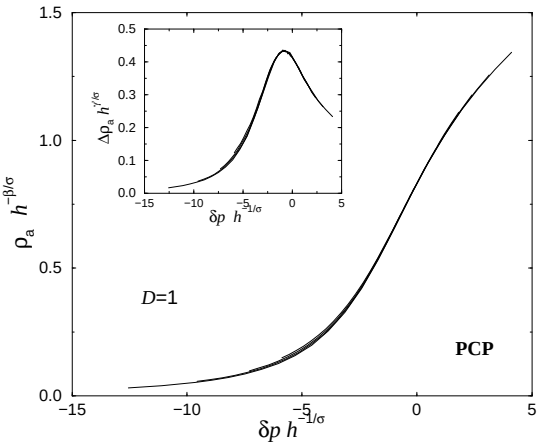

Figure 10.16: The scaling plot of the order parameter and its fluctuations (inset) for the one-dimensional pair contact process.

10.2.2 Universal steady-state scaling behavior

In the case of absorbing phase transitions the universality hypothesis states that systems exhibiting a continuous phase transition to a unique absorbing state generally belong to the universality class of directed percolation [39,40]. Following the concept of universality two models belong to the same universality class if the critical exponents and the universal scaling functions are identical. The universal scaling functions $\tilde{R}_{\rm DP}$ and $\tilde{D}_{\rm DP}$ of the one-dimensional DP universality class can be easily determined by measuring the non-universal metric factors a_p, a_h and a_Δ according to equations (10.8), (10.9) and (10.10).

In the case of one-dimensional directed site percolation in the Domany-

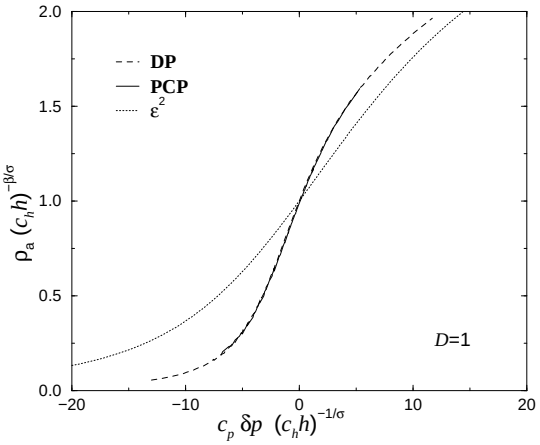

Figure 10.17: The universal order parameter scaling function $\tilde{R}_{\rm DP}(x,1)$ of the universality class of one-dimensional directed percolation. The dotted line corresponds to the result of a two loop renormalization group analysis of the Langevin equation [49].

Kinzel automaton we have obtained the values $a_p^{\rm sDP} = 2.489$, $a_h^{\rm sDP} = 0.114$, and $a_\Delta^{\rm sDP} = 9.382$ For the PCP on a square lattice we have determined the values $a_p^{\rm PCP} = 0.665$, $a_h^{\rm PCP} = 0.181$, and $a_\Delta^{\rm PCP} = 3.467$.
Analogous to the previous scaling analysis we set $a_p\, h\, \lambda^{-\sigma/\beta} = 1$ and consider for both models the rescaled order parameter $\rho_{\rm a}\,(a_h h)^{-\beta/\sigma}$ as a function of the rescaled control parameter $a_p \delta\rho\,(a_h h)^{-1/\sigma}$ as well as the rescaled order parameter fluctuations $(a_\Delta\, \Delta\rho_{\rm a}\,(a_h h)^{\gamma'/\sigma}$ as a function of $a_p \delta p\,(a_h h)^{-1/\sigma}$, respectively. The corresponding data are presented in figure 10.17 and figure 10.18. In both cases we get a perfect data collapse of the curves showing that the one-dimensional PCP steady state scaling behavior belongs to the universality class of directed percolation.

Additionally to the universal scaling function $\tilde{R}_{\rm DP}(x,1)$ we plot in figure 10.17 the corresponding curve of a second order ϵ-expansion obtained from the renormalization group analysis of a Langevin equation [49]. As can be seen the significant difference indicates that the $O(\epsilon^3)$ corrections to the scaling function are relevant, i.e., higher orders than $O(\epsilon^2)$ are necessary to describe the scaling behavior of directed percolation. As demonstrated in the previous subsection, this difference decreases with increasing dimension, i.e., for $\epsilon \to 0$.

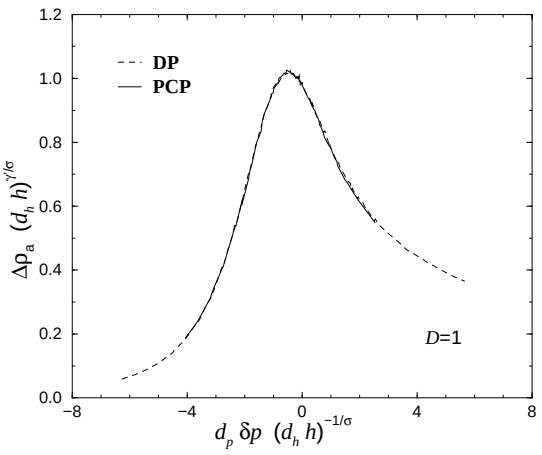

Figure 10.18: The universal scaling function $\tilde{D}_{\mathrm{DP}}(x, 1)$ of the order parameter fluctuations of the universality class of directed percolation.

10.2.3 Dynamical scaling behavior

In this subsection we show that the dynamical scaling behavior of the PCP belongs to the DP universality class too if the spreading of a localized seed is considered at the so-called natural particle density [44]. Examining spreading activity one usually considers the survival probability P_{a} of the activity as well as how the number of active particles $N_{\mathrm{a}} = L\rho_{\mathrm{a}}$ increases in time. In the case of DP the simulations are started with a single seed on an empty lattice. For the PCP an absorbing state at p_{c} is prepared to which a particle is added in order to create one seed (one active pair). At the critical point the following power-law behaviors are expected

$$N_{\mathrm{a}} \propto t^{\theta}, \qquad P_{\mathrm{a}} \propto t^{-\delta}. \tag{10.51}$$

Finite systems sizes limit these power-law behaviors and P_{a} and N_{a} obey the finite-size scaling ansatzes

$$N_{\mathrm{a}}(\delta p = 0, L) \sim \lambda\, \tilde{n}(\lambda^{-1/\theta} t, \lambda^{-1/\theta z} L) \tag{10.52}$$

$$P_{\mathrm{a}}(\delta \rho = 0, L) \sim \lambda\, \tilde{p}(\lambda^{1/\delta} t, \lambda^{1/\delta z} L) \tag{10.53}$$

where z denotes the dynamical exponent. Analogous to the above analysis the universal scaling curves $\tilde{N}$ and $\tilde{P}$ are obtained by introducing appropriate non-universal metric factors. Using the values $z = 1.580745$, $\theta = 0.313686$, and $\delta = 0.159464$ [48] we get convincing data collapses and the universal scaling functions are plotted in figure 10.19.

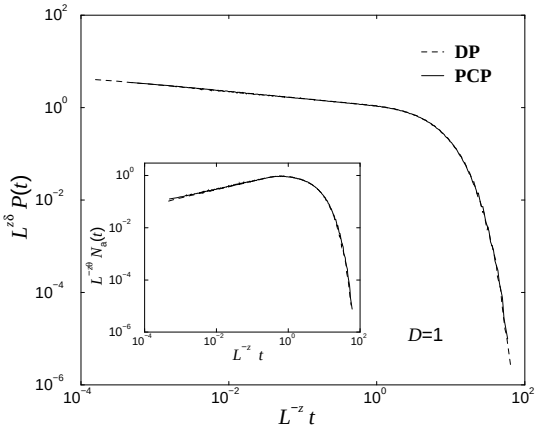

Figure 10.19: The DP universal finite-size scaling function $\tilde{P}$ and $\tilde{N}$. Both quantities describe the activity spreading of a localized seed (see text).

10.2.4 Mean-field scaling behavior

The mean-field equation of state of DP has already been derived from the corresponding Langevin equation in subsection 10.1.2.
Let us now consider the following modification of the PCP. An active bond produces an offspring with rate $(1-p)$ at an empty site selected at random. The rules for annihilation and action of the external field remain unchanged. This random neighbor interaction suppresses long range correlations and the model is therefore expected to be characterized by the mean-field scaling behavior. We denote the density of inactive bonds between an occupied and an empty site as $\rho_{\rm i}$. Bonds between empty sites are denoted as $\rho_{\rm e}$. Normalization requires $\rho_{\rm e} + \rho_{\rm i} + \rho_{\rm a} = 1$. Depending on the sites adjacent to the target site the number of active bonds $n_{\rm a}$, inactive bonds $n_{\rm i}$ or empty bonds $n_{\rm e}$ is changed. For instance if the adjacent sites are empty, for which the probability in absence of correlations is $\rho_{\rm e}^2$, the number of empty bonds decreases by two ($\Delta n_{\rm e} = -2$). On the other hand there are two new inactive bonds ($\Delta n_{\rm i} = +2$). The total probability for this event is $(1-p)\rho_{\rm a}\rho_{\rm e}^2$. A list of all possible processes and their mean-field probabilities is given in table 10.3. Thus we obtain rate equations for the expectation values $E[\Delta n_x]$ of the changes in active, inactive and empty bond numbers. These expectation values are zero in the steady state, i.e.,

$$E[\Delta n_x] \;=\; \sum_{\Delta n_x} \Delta n_x \; p(\Delta n_x) \;=\; 0 \qquad (10.54)$$

with $x \in \{a, i, e\}$. In the case of $E[\Delta n_a]$ we get

$$\begin{aligned} E[\Delta n_a] &= -3p\rho_{\mathrm{a}}^3 - 4p\rho_{\mathrm{a}}^2\rho_{\mathrm{i}} - p\rho_{\mathrm{a}}\rho_{\mathrm{i}}^2 + 2(1-p)\rho_{\mathrm{a}}\rho_{\mathrm{i}}^2 \\ &\quad +2(1-p)\rho_{\mathrm{a}}\rho_{\mathrm{i}}\rho_{\mathrm{e}} + 2h\rho_{\mathrm{i}}^2 + 2h\rho_{\mathrm{i}}\rho_{\mathrm{e}} \;=\; 0, \end{aligned} \tag{10.55}$$

whereas we get for the for inactive bonds

$$\begin{aligned} E[\Delta n_i] &= -2(1-p)\rho_{\mathrm{a}}\rho_{\mathrm{i}}^2 + 2(1-p)\rho_{\mathrm{a}}\rho_{\mathrm{e}}^2 + 2p\rho_{\mathrm{a}}^3 \\ &\quad -2p\rho_{\mathrm{a}}\rho_{\mathrm{i}}^2 - 2h\rho_{\mathrm{i}}^2 + 2h\rho_{\mathrm{e}}^2 \;=\; 0. \end{aligned} \tag{10.56}$$

Using this equations together with the normalization allows for calculating the order parameter for zero-field ($h = 0$) which yields the non-trivial ($\rho_{\mathrm{a}} > 0$) solution

$$\rho_{\mathrm{a}} \;=\; \frac{8 - 3p^2 - 5p - 2\sqrt{2p(1-p)(3p-4)^2}}{9p^2 - 9p + 8}. \tag{10.57}$$

This solution is valid below the mean-field critical point $p_{\mathrm{c}} = 8/9$ whereas the trivial solution $\rho_{\mathrm{a}} = 0$ is valid for all p but unstable above p_{c}. Expanding (10.57) around the critical point leads to

$$\rho_{\mathrm{a}} \;=\; \frac{3}{8}\delta p \,+\, O(\delta p^2) \tag{10.58}$$

with $\delta p = (p_{\mathrm{c}} - p)/p_{\mathrm{c}}$. Thus the mean-field exponent of the PCP is $\beta = 1$ and the non-universal metric factor $c_1^{\mathrm{PCP}} = 3/8$. In order to obtain the order parameter in presence of an external field h equations (10.55) and (10.56) are solved for ρ_{i} which yields

$$\begin{aligned} &4h + 4\rho_{\mathrm{a}} - 4h\rho_{\mathrm{a}} - 4p\rho_{\mathrm{a}} - 4\rho_{\mathrm{a}}^2 \\ &+\left\{-12p^2\rho_{\mathrm{a}}^2 + (2h + 2\rho_{\mathrm{a}} - 2h\rho_{\mathrm{a}} - 2p\rho_{\mathrm{a}} - 2\rho_{\mathrm{a}}^2 - 2p\rho_{\mathrm{a}}^2)^2\right\}^{1/2} \\ &\quad -\left\{(-2h - 2\rho_{\mathrm{a}} + 2p\rho_{\mathrm{a}} + 2\rho_{\mathrm{a}}^2 - 2p\rho_{\mathrm{a}}^2)^2 + \ldots\right. \\ &\ldots + \left. 4p\rho_{\mathrm{a}}(h + \rho_{\mathrm{a}} - 2h\rho_{\mathrm{a}} - p\rho_{\mathrm{a}} - 2\rho_{\mathrm{a}}^2 + h\rho_{\mathrm{a}}^2 + 2p\rho_{\mathrm{a}}^2 + \rho_{\mathrm{a}}^3)\right\}^{1/2} \;=\; 0. \end{aligned} \tag{10.59}$$

To obtain the field dependence of the order parameter a series expansion around $h = 0$ at $p_{\mathrm{c}} = 8/9$ is performed which results in leading order

$$\rho_{\mathrm{a}} \;=\; \sqrt{\frac{3}{8}\,h}, \tag{10.60}$$

i.e., the mean-field values of the PCP are given by $c_2^{\mathrm{PCP}} = \sqrt{3/8}$ and $\sigma = 2$. Finally we derive the mean-field universal scaling function $\tilde{R}$ of the PCP. Therefore we write (10.59) as a function of the reduced control parameter δp

Table 10.3: The configuration of a PCP lattice before ($\mathcal{C}$) and after ($\mathcal{C}'$) an event. Only the sites left and right of those changed by particle creation (top), pair annihilation (middle) or particle creation due to the the external field (bottom) are shown. Empty sites are marked by ∘, and occupied sites by •. Here, Δn_a denotes the change of the number of active bonds, Δn_i the respective change of inactive bonds, Δn_e that of empty bonds and P is the corresponding probability of the event if spatial correlations are neglected.

$\mathcal{C}$	$\mathcal{C}'$	Δn_a	Δn_i	Δn_e	$p(\mathcal{C} \to \mathcal{C}')$
• ∘ •	• • •	+2	−2	0	$(1-p)\rho_\mathrm{a}\rho_\mathrm{i}^2$
• ∘ ∘	• • ∘	+1	0	-1	$(1-p)\rho_\mathrm{a}\rho_\mathrm{i}\rho_\mathrm{e}$
∘ ∘ •	∘ • •	+1	0	-1	$(1-p)\rho_\mathrm{a}\rho_\mathrm{i}\rho_\mathrm{e}$
∘ ∘ ∘	∘ • ∘	0	+2	-2	$(1-p)\rho_\mathrm{a}\rho_\mathrm{e}^2$
• • • •	• ∘ ∘ •	-3	+2	+1	$p\rho_\mathrm{a}^3$
∘ • • •	∘ ∘ ∘ •	-2	0	+2	$p\rho_\mathrm{a}^2\rho_\mathrm{i}$
• • • ∘	• ∘ ∘ ∘	-2	0	+2	$p\rho_\mathrm{a}^2\rho_\mathrm{i}$
∘ • • ∘	∘ ∘ ∘ ∘	-1	−2	+3	$p\rho_\mathrm{a}\rho_\mathrm{i}^2$
• ∘ •	• • •	+2	−2	0	$h\rho_\mathrm{i}^2$
• ∘ ∘	• • ∘	+1	0	-1	$h\rho_\mathrm{i}\rho_\mathrm{e}$
∘ ∘ •	∘ • •	+1	0	-1	$h\rho_\mathrm{i}\rho_\mathrm{e}$
∘ ∘ ∘	∘ • ∘	0	+2	-2	$h\rho_\mathrm{e}^2$

and perform the limits $\rho_\mathrm{a} \to 0$, $\delta\rho \to 0$ and $h \to 0$ with the constraint that $\rho_\mathrm{a}/\sqrt{h}$ and $\rho_\mathrm{a}/\delta p$ are finite. Thus we remain in leading order with

$$\frac{3}{8}\,\delta p\,\rho_\mathrm{a} \;-\; \rho_\mathrm{a}^2 \;+\; \frac{3}{8}\,h \;=\; 0. \tag{10.61}$$

Solving this equation yields

$$\rho_\mathrm{a} \;=\; \frac{1}{2}\,\frac{3}{8}\,\delta p \;+\; \sqrt{\frac{3}{8}\,h \;+\; \left(\frac{1}{2}\,\frac{3}{8}\,\delta p\right)^2} \;=\; \tilde{R}_\mathrm{DP}(a_p^\mathrm{PCP}\,\delta p, a_h^\mathrm{PCP}\,h). \tag{10.62}$$

This functional form is up to non-universal metrical factors identical to the solution for DP (see eq. (10.14)).

10.2.5 Conclusion

In this section we have investigated the critical exponents and universal scaling functions for the pair contact process in an external field in $D = 1$ and above the upper critical dimension. We have shown that both DP and the

PCP are characterized by the same critical exponents and scaling functions. Thus the PCP belongs in $D = 1$ and above the upper critical dimension to the universality class of directed percolation.
This is an explicit demonstration that the DP conjecture due to Janssen and Grassberger (see subsection 2.3), which demands a unique absorbing state, does not uniquely define the DP universality class.

Bibliography

[1] M. Plischke and B. Bergersen. *Equilibrium Statistical Physics*. World Scientific, 1989.

[2] J. M. Yeomans. *Statistical mechanics of phase transitions*. Oxford University Press, 1995.

[3] G. M. Schütz. *Phase Transitions and Critical Phenomena*, volume 19. Academic, 2000.

[4] G. M. Schütz. *J. Phys. A*, 36:R339, 2003.

[5] H. Hinrichsen. *Adv. Phys.*, 49:815, 2000.

[6] Y. Kafri, E. Levine, D. Mukamel, G. M. Schütz, and R. D. Willmann. *Phys. Rev. E*, 68:035101, 2003.

[7] V. Popkov, A. Rakos, R. D. Willmann, A. B. Kolomeisky, and G. M. Schütz. *Phys. Rev. E*, 67:066117, 2003.

[8] R. D. Willmann, G. M. Schütz, and D. Challet. *Physica A*, 316:430, 2002.

[9] E. Levine and R. D. Willmann. *J. Phys. A*, 37:3333, 2004.

[10] S. Lübeck and R. D. Willmann. *J. Phys. A*, 35:10205, 2002.

[11] S. Lübeck and R. D. Willmann. *J. Stat. Phys*, 115:1231, 2004.

[12] J. T. MacDonald and J. H. Gibbs. *Biopolymers*, 6:1, 1968.

[13] K. Nagel and M. Schreckenberg. *J. Phys. I France*, 2:2221, 1992.

[14] V. Popkov, L. Santen, A. Schadschneider, and G. M. Schütz. *J. Phys. A*, 34:L1, 2001.

[15] T. Halpin-Healy and Y.-C. Zhang. *Physics Reports*, 254:215, 1995.

[16] T. M. Liggett. *Trans. Amer. Math. Soc.*, 179:433, 1975.

[17] G. Schütz and E. Domany. *J. Stat. Phys.*, 72:277, 1993.

[18] B. Derrida, M. R. Evans, V. Hakim, and V. Pasquier. *J. Phys. A*, 26:1493, 1993.

[19] S. Katz, J. L. Lebowitz, and H. Spohn. *J. Stat. Phys.*, 34:497, 1984.

[20] J. S. Hager, J. Krug, V. Popkov, and G. M. Schütz. *Phys. Rev. E*, 63:056110, 2001.

[21] B. Schmittmann and R. K. P. Zia. *Phase Transitions and Critical Phenomena*, volume 17. Academic, 1995.

[22] A. Kolomeisky, G. M. Schütz, E. B. Kolomeisky, and J. P. Straley. *J. Phys. A*, 31:6911, 1998.

[23] V. Popkov and G. M. Schütz. *Europhys. Lett.*, 48:257, 1999.

[24] P. F. Arndt, T. Heinzel, and V. Rittenberg. *J. Phys. A*, 31:L45, 1998.

[25] N. Rajewsky, T. Sasamoto, and E. R. Speer. *Physica A*, 279:123, 2000.

[26] T. Sasamoto and D. Zagier. *J. Phys. A*, 34:5033, 2001.

[27] Y. Kafri, E. Levine, D. Mukamel, G. M. Schütz, and J. Török. *Phys. Rev. Lett.*, 89:035702, 2002.

[28] G. Korniss, B. Schmittmann, and R. K. P. Zia. *Europhys. Lett.*, 45:431, 1999.

[29] I. J. Aitchison and A. J. Hey. *Gauge theories in particle physics*. Hilger, 1982.

[30] M. R. Evans, D. P. Foster, C. Godrèche, and D. Mukamel. *Phys. Rev. Lett*, 74:208, 1995.

[31] M. R. Evans, D. P. Foster, C. Godrèche, and D. Mukamel. *J. Stat. Phys.*, 80:69, 1995.

[32] V. Popkov and G. M. Schütz. 2004.

[33] C. Godrèche, J. M. Luck, M. R. Evans, D. Mukamel, S. Sandow, and E. R. Speer. *J. Phys. A*, 28:6, 1995.

[34] P. F. Arndt, T. Heinzel, and V. Rittenberg. *J. Stat. Phys.*, 90:783, 1998.

[35] D. Stauffer and A. Aharony. *Introduction to Percolation theory*. Taylor and Francis, 1992.

[36] H. E. Stanley. *Rev. Mod. Phys.*, 71:S358, 1999.

[37] K. G. Wilson. *Phys. Rev. B*, 4:3184, 1971.

[38] K. G. Wilson. *Phys. Rev. B*, 4:3174, 1971.

[39] H. K. Janssen. *Z. Phys. B*, 42:151, 1981.

[40] P. Grassberger. *Z. Phys. B*, 47:365, 1982.

[41] M. Rossi, R. Pastor-Satorras, and A. Vespignani. *Phys. Rev. Lett.*, 85:1803, 2000.

[42] J. W. Essam. *J. Phys. A*, 22:4927, 1989.

[43] J. L. Cardy and U. C. Täuber. *Phys. Rev. Lett.*, 13:4780, 1996.

[44] I. Jensen and R. Dickman. *Phys. Rev. E*, 48:1710, 1993.

[45] I. Jensen. *Phys. Rev. Lett.*, 70:1465, 1993.

[46] M. A. Munoz, G. Grinstein, R. Dickman, and R. Livi. *Phys. Rev. Lett.*, 76:451, 1996.

[47] F. van Wijland. *Phys. Rev. Lett.*, 89:190602, 2002.

[48] I. Jensen. *J. Phys. A*, 32:5233, 1999.

[49] H. K. Janssen, Ü. Kutbay, and K. Oerding. *J. Phys. A*, 32:1809, 1999.

[50] H. K. Janssen and O. Stenull. *Phys. Rev. E*, 69:026118, 2004.

[51] M. R. Evans, Y. Kafri, H. M. Koduvely, and D. Mukamel. *Phys. Rev. Lett.*, 80:425, 1998.

[52] M. R. Evans, Y. Kafri, H. M. Koduvely, and D. Mukamel. *Phys. Rev. E*, 58:2764, 1998.

[53] P. F. Arndt, T. Heinzel, and V. Rittenberg. *J. Stat. Phys.*, 97:1, 1999.

[54] R. Lahiri and S. Ramaswamy. *Phys. Rev. Lett.*, 79:1150, 1997.

[55] R. Lahiri, M. Barma, and S. Ramaswamy. *Phys. Rev. E*, 61:1648, 2000.

[56] J. T. Mettetal, B. Schmittmann, and R. K. P. Zia. *Europhys. Lett.*, 58:653, 2002.

[57] M. R. Evans. *Braz. J. Phys.*, 30:42, 2000.

[58] Y. Kafri, E. Levine, D. Mukamel, and J. Török. *J. Phys. A*, 35:L459, 2002.

[59] J. Krug and P. Meakin. *J. Phys. A*, 23:L987, 1990.

[60] J. Krug and L. Tang. *Phys. Rev. E*, 50:104, 1990.

[61] J. Krug. *Adv. Phys.*, 46:139, 1997.

[62] H. van Beijeren, R. Kutner, and H. Spohn. *Phys. Rev. Lett.*, 54:2026, 1985.

[63] Y. Kafri, D. Mukamel, and L. Peliti. *Eur. Phys. J. B.*, 27:135, 2002.

[64] M. Clincy, M. R. Evans, and D. Mukamel. *J. Phys. A*, 44:9923, 2001.

[65] R. D. Willmann, G. M. Schütz, and S. Grosskinsky. 2004.

[66] A. Parmeggiani, T. Franosch, and E. Frey. *Phys. Rev. Lett.*, 90:811, 2003.

[67] R. Lipowsky, S. Klumpp, and T. M. Nieuwenhuizen. *Phys. Rev. Lett.*, 87:108101, 2001.

[68] J. Howard. *35. Spring School 2004: Physics meets Biology*. Forschungszentrum Jülich, 2004.

[69] A. Alberts. *Molecular Biology of the Cell*. Garland, 1994.

[70] S. Klumpp and R. Lipowsky. *J. Stat. Phys.*, 113:233, 2003.

[71] S. Klumpp and R. Lipowsky. *Europhys. Lett.*, 66:90, 2004.

[72] R. H. Fowler. *Statistical Mechanics*. Cambridge University Press, 1936.

[73] R. Juhasz and L. Santen. *J. Phys. A*, 37:3933, 2004.

[74] M. R. Evans, R. Juhász, and L. Santen. *Phys. Rev. E*, 68:026117, 2003.

[75] A. Rákos, M. Paessens, and G. M. Schütz. *Phys. Rev. Lett.*, 91:238302, 2003.

[76] F. Rezakhanlou. *Comm. Math. Phys.*, 140:417, 1991.

[77] P.-M. Binder, M. Paczuski, and M. Barma. *Phys. Rev. E*, 49:1174, 1994.

[78] R. D. Willmann. 2003.

[79] K. P. N. Murthy and G. M. Schütz. *Phys. Rev. E*, 57:1388, 1992.

[80] K. Krebs, F. H. Jafarpour, and G. M. Schütz. *New Journal of Physics*, 5:145, 2003.

[81] F. Lutscher and A. Stevens. *J. Nonlinear Sci*, 12:619, 2002.

[82] V. Popkov and G. M. Schütz. *J. Stat. Phys.*, 112:523, 2003.

[83] R. Mantegna and H. E. Stanley. *An Introduction to Econophysics*. Cambridge University Press, 2000.

[84] J.-P. Bouchaud and M.Potters. *Theory of Financial Risks*. Cambridge University Press, 2000.

[85] J. D. Farmer. *Computing in Science and Engineering*, 11/12:26, 1999.

[86] M. M. Dacorogna, R. Gençay, U. Müller, and R. B. Olsen. *An Introduction to High-Frequency Finance*. Academic Press, 2001.

[87] R. Cont and J.-P. Bouchaud. *Macroecon. Dyn*, 4:170, 2000.

[88] T. Lux and M. Marchesi. *Nature*, 397:498, 1999.

[89] P. Jefferies, M.L. Hart, P.M. Hui, and N.F. Johnson. *cond-mat*, 9910072, 1999.

[90] D. Challet *et al. Quant. Fin.*, 1:168.CMZ01, 2001.

[91] D. Challet, M. Marsili, and Y.-C. Zhang. *Physica A*, 294:514, 2001.

[92] I. Giardina, J.-P. Bouchaud, and M. Mézard. *Physica A*, 299:28, 2001.

[93] J. D. Farmer. Santa Fe Institute working paper 98-12-117, 2002.

[94] P. Jefferies, M.L. Hart, P.M. Hui, and N.F. Johnson. *Eur. Phys. J. B*, 20:493, 2001.

[95] D. Helbing and D. Kern. *Physica A*, 287:259, 2000.

[96] P. Bak, M. Paczuski, and M. Shubik. *Physica A*, 246:430, 1997.

[97] S. Maslov. *Physica A*, 278:571, 2000.

[98] D. Challet and R. Stinchcombe. *Physica A*, 300:285, 2001.

[99] M. G. Daniels, J. D. Farmer, G. Iori, and E. Smith. *cond-mat*, 0112422, 2002.

[100] J.-P. Bouchaud and M. Mézard. *cond-mat*, 0203511, 2002.

[101] J. Krug. *Solids far from equilibrium*. Cambridge University Press, 1991.

[102] M. Kardar, G. Parisi, and Y.-C. Zhang. *Phys. Rev. Lett.*, 56:889, 1986.

[103] L.-H. Tang and G.-S. Tian. *Physica A*, 264:543, 1999.

[104] S. Maslov and M. Mills. *Physica A*, 299:234, 2001.

[105] G. T. Barkema, M. J. Howard, and J. L. Cardy. *Phys. Rev. E*, 92:2017, 1996.

[106] D. Challet and R. Stinchcombe. *cond-mat*, 2002.

[107] P. A. Ferrari, C. Kipnis, and E. Saada. *Ann. Prob.*, 19:226, 1991.

[108] L. H. Gwa and H. Spohn. *Phys. Rev. Lett*, 68:725, 1992.

[109] M. Prähofer and H. Spohn. *In and out of equilibrium, Progress in Probability*. Birkhauser, 2002.

[110] H. Spohn. private communication.

[111] B. Derrida ans E. Domany E and D. Mukamel. *J. Stat. Phys.*, 69:667, 1992.

[112] P. Grassberger and A. de la Torre. *Ann. Phys. (NY)*, 122:373, 1979.

[113] V. Privman, P. C. Hohenberg, and A. Aharony. *Phase Transitions and Critical Phenomena*, volume 14, chapter 1. Academic, 1991.

[114] P. Pfeuty and G. Toulouse. *Introduction to the renormalization group and critical phenomena*. John Wiley, 1994.

[115] F. J. Wegner and E. K. Riedel. *Phys. Rev. B*, 7:248, 1973.

[116] K. G. Wilson and J. Kogut. *Phys. Rep.*, 12C:75, 1974.

[117] P. Grassberger. *Phys. Rev. E*, 56:3682, 1997.

[118] P. Grassberger, R. Hegger, and L. Schäfer. *J. Phys. A*, 27:7265, 1994.

[119] S. Lübeck. *Phys. Rev. E*, 58:2957, 1998.

[120] D. V. Ktitarev, S. Lübeck, P. Grassberger, and V. B. Priezzhev. *Phys. Rev. E*, 61:81, 2000.

[121] L. Roters, S. Lübeck, and K. U. Usadel. *Phys. Rev. E*, 66:069901, 2002.

[122] P. Grassberger. *Phys. Rev. E*, 67:036101, 03.

[123] S. Lübeck and P. C. Heger. *Phys. Rev. Lett.*, 90:230601, 2003.

[124] A. A. Fedorenko and S. Stepanow. *Phys. Rev. E*, 67:057104, 2003.

[125] H. K. Janssen and O. Stenull. *Phys. Rev. E*, 68:036131, 2003.

[126] O. Stenull and H. K. Janssen. *Phys. Rev. E*, 68:036129, 2003.

[127] E. Domany and W. Kinzel. *Phys. Rev. Lett.*, 53:311, 1984.

[128] A. Y. Tretyakov and N Inui. *J. Phys. A*, 28:3985, 1995.

[129] P. Grassberger and Y. C. Zhang. *Physica A*, 224:169, 1996.

[130] V. Privman and M. E. Fisher. *Phys. Rev. B*, 30:322, 1984.

[131] H. Mori and K. J. McNeil. *Prog. Theor. Phys.*, 57:770, 1977.

[132] C. A. Voigt and R. M. Ziff. *Phys. Rev. E*, 56:R6241, 1997.

[133] I. Jensen. *Phys. Rev. A*, 45:R563, 1992.

[134] P. Schofield. *Phys. Rev. Lett.*, 22:606, 1969.

[135] D. Josephson. *J. Phys. C*, 2:1113, 1969.

[136] S. P. Obukhov. *Physica A*, 101:145, 1980.

[137] J. L. Cardy and R. L. Sugar. *J. Phys. A*, 13:L423, 1980.

[138] A. I. Larkin and D. E. Khmel'nitski. *JETP*, 29:1123, 1969.

[139] A. Aharony. *Phys. Rev. B*, 8:3363, 1973.

[140] J. A. Griffiths, J. D. Litster, and A. Linz. *Phys. Rev. Lett.*, 38:251, 1977.

[141] J. Bringmann, R. Courths, and H. J. Guggenheim. *Phys. Rev. Lett.*, 40:1286, 1978.

[142] N. Aktekin. *J. Stat. Phys.*, 104:1397, 2001.

[143] P. Grassberger. 2004.

[144] K. Binder and D. W. Heermann. *Monte Carlo Simulation in Statistical Physics*. Springer, 1997.

[145] I. Jensen. *J. Phys. A*, 29:7013, 1996.

[146] R. Dickman and J. Kamphorst Leal da Silva. *Phys. Rev. E*, 58:4266, 1998.

[147] R. Dickman, W. Rabelo, and G. Odor. *Phys. Rev. E*, 65:016118, 2001.

[148] S. Lübeck. *Phys. Rev. E*, 65:046150, 2002.

Acknowledgements

First and foremost I wish to thank my supervisor PD Dr. Gunter M. Schütz for many helpful discussions, interesting common projects, the international experiences that are part of his education and the freedom to pursue my own ideas and collaborations.
Prof. Ulf.-G. Meißner be thanked for his willingness to be the second referee for this work.
My time at the Weizmann Institute of Science was for sure one of the most interesting experiences during my PhD. I wish to thank Prof. David Mukamel for accepting me as a visiting student and many interesting discussions. Furthermore, I learned a lot from sharing ideas with Yarif Kafri and especially from Erel Levine.
Dr. Sven Lübeck deserves thanks for introducing me into the physics of absorbing phase transitions and being a good companion both in Israel and Germany.
During the past three years, my office mate Matthias Paeßens was the person I could share with all ideas on physics and beyond. His help and good company deserve my gratitude.
Attila Rakos and Vladislav Popkov be thanked for many interesting discussions on the physics of driven diffusive systems.
Thanks also go to Helga Paffen for helping a lot with the intricacies of administration and providing the vital morning coffee.
Finally, I wish to thank my wife Stana for supporting me during the last three years in all my physics projects and during my stays abroad.

Summary / Zusammenfassung

Summary

In this work the influence of bulk reservoirs on lattice models for many-particle systems far from equilibrium is studied.
A hydrodynamic equation is presented that allows to compute the steady state density profile for single species driven diffusive systems with open boundaries and a coupling of the bulk reservoir scaling with the inverse system size. Furthermore, a related model for a limit order market as well as the case of periodic single species driven models with a weak coupling to the reservoir are treated.
New results on driven systems with two particle species are presented both for the cases with and without coupling to a bulk reservoir. For a two species model with periodic boundaries and conserving dynamics a novel type of phase transition is observed that is formally similar to Bose-Einstein condensation.
In absence of a bulk reservoir, the existence of a spontaneously symmetry broken phase in a two species model with open boundaries and deterministic bulk behavior is demonstrated by regarding the dynamics of the system. For a related model with non-conserving bulk dynamics a rich phase diagram is found.
In systems with an absorbing phase transition the action of the reservoir is that of an external field. For the universality class of directed percolation the scaling functions are determined in several dimensions.

Zusammenfassung

Gegenstand der vorliegenden Arbeit ist das Studium des Einflusses von Teilchenreservoirs, die unabhängig an jeden Platz von Vielteilchen-Gittermodellen fern des Gleichgewichtes koppeln.
Für eindimensionale getrieben diffusive Systeme mit einer Teilchensorte wird für den Fall einer Skalierung der Kopplungsstärke mit der inversen Systemgröße eine hydrodynamische Gleichung zur Berechnung des stationären Dichteprofiles eines Systems mit offenen Rändern eingeführt. Ferner werden ein verwandtes Modell für einen Limit-Order-Markt sowie getrieben diffusive Systeme mit einer Teilchensorte und periodischen Randbedingungen bei schwacher Kopplung an ein Reservoir betrachtet.
Getrieben diffusive Systeme mit zwei Teilchensorten werden sowohl mit als auch ohne Teilchenzahlerhaltung im Inneren des Systems behandelt. Für ein periodisches System mit zwei erhaltenen Teilchensorten wird eine neue Art von Phasenübergang demonstriert, die mathematisch analog zur Bose-

Einstein Kondensation ist.
In einem offenen System mit zwei erhaltenen Teilchensorten wird durch Betrachtung der Dynamik die Existenz einer Phase mit spontan gebrochener Symmetrie nachgewiesen. Ein ähnliches Modell ohne Teilchenzahlerhaltung zeigt ein reichhaltiges Phasendiagramm.
Für Systeme mit einem absorbierenden Phasenübergang wirkt die platzweise Kopplung an ein Teilchreservoir wie ein externes Feld. Für die Universalitätsklasse der gerichteten Perkolation werden die Skalenfunktionen um den kritischen Punkt in verschiedenen Dimensionen bestimmt.